

GRADUATE PROGRAM IN PHYSICS
UNIVERSIDADE FEDERAL DO RIO GRANDE DO SUL

Computational study of the effects of
the confinement and the interacting
solutes on the properties of the
water-like models. †

Alexandre Penteado Furlan

Thesis submitted to the Universidade Federal do Rio Grande do Sul, Brazil as a partial requirement to obtain the degree of Doctor in Sciences, under the supervision of Profa. Dra. Marcia C. B. Barbosa (Institute of Physics - UFRGS) and co-supervision of Prof. Dr. Carlos E. Fiore dos Santos (Institute of Physics - USP).

2017

†Project financed by the Coodenação de Aperfeiçoamento de Pessoal de Nível Superior (CAPES).

“If I have seen a little further it is by standing on the shoulders of Giants.”

Isaac Newton

Aos gigantes Roberto e Teresinha Furlan

Agradecimentos

- À minha orientadora Marcia Barbosa, pela orientação, dedicação e pelo exemplo de profissionalismo.
- Ao Carlos Fiore pela co-orientação e disposição em ajudar nas simulações.
- À minha família pelo apoio incondicional que me permitiram realizar este trabalho.
- Aos professores do IF-UFRGS e Dpto. de Física UFPR, pela formação.
- Ao Centro de Física Computacional - IF (CFCIF - UFRGS) pelo suporte computacional.
- Aos meus amigos, que mesmo longe, nunca me abandonaram.
- Aos colegas do grupo de fluidos complexos e da sala M205, pela ajuda, e pelas risadas.
- A CAPES pelo apoio financeiro.
- A todos que direta ou indiretamente, colaboraram de alguma maneira para a conclusão deste trabalho.

Abstract

FURLAN, A. P. - **Computational study of the effects of the confinement and the interacting solutes on the properties of the simplified water-like models**

Although the familiarity and simplicity, the water show a set of thermodynamic, dynamics and structural properties which are still subject to intense research. The increase of density as the temperature, of diffusion as the density, or even of ordering with the temperature are examples of some of its unusual behavior. In order to better understand these properties numerous approaches have been used, such as the use of confinement geometries, simplified models, or even mixtures. Among the confinement geometries used, are those, nanopores, parallel plates and porous media. The porous media are formed by fixed obstacles that impose the additional excluded volume effects to the system. In the case of mixtures, when they occur between liquids able to form hydrogen-bonds, the unusual behavior of water give rise to a set even higher anomalous properties. The water-methanol mixture, for example, has a set of excess properties unable to be described by usual theories. Some examples are the maximum in the specific heat and minimum in excess volume and enthalpy. In this Ph.D. project, we study by numerical simulations, the confinement of water by porous media(or under quenched disorder) and the mixture of water with interacting solutes. The first study is performed using a 2D lattice model which is widely known in the literature. In a second stage, we study the influence of interacting solutes on the properties of lattice and continuous models. For the lattice model, we develop a solute model and a technique to simulate mixtures of lattice models at constant pressure. Using this technique, we study the excess properties of the mixture. For the continuous model we study the influence of a dimeric solute on the TMD of a water-like model and posteriorly we study the excess properties of this type of mixture.

Keywords: Water confinement, water anomalies, porous media, lattice models, mixtures, Monte Carlos simulations.

Resumo

FURLAN, A. P. - **Estudo computacional dos efeitos de confinamento e de solutos interagentes nas propriedades de modelos simplificados tipo-água**

Apesar de sua familiaridade e simplicidade, a água apresenta um conjunto propriedades termodinâmicas, dinâmicas e estruturais que são ainda objeto de intensa pesquisa. O aumento da densidade com a temperatura, da difusão com a densidade, ou ainda do ordenamento com a temperatura são exemplos de alguns de seus comportamentos não usuais. Com a finalidade de melhor compreender tais propriedades inúmeras abordagens têm sido utilizadas, tais como o uso geometrias de confinamento, modelos simplificados ou até mesmo misturas. Dentre as geometrias confinantes frequentemente usadas, encontra-se, nanoporos, placas paralelas e meio porosos. Os meios porosos são formados por obstáculos fixos que impõem efeitos de volume excluído adicionais ao sistema. Já no caso de misturas quando elas ocorrem entre líquidos capazes de formar ligações de hidrogênio, o comportamento não usual da água dá origem a um conjunto ainda maior de propriedades anômalas. A mistura água-metanol por exemplo, é munida de um conjunto propriedades de excesso incapazes de serem descritas pelas teorias usuais. São alguns exemplos, o máximo no calor específico e o mínimo no volume e entalpia de excesso. Neste projeto de doutoramento, nós estudamos por simulações numéricas o confinamento por meio poroso (*desordem queched*) e misturas de água com solutos interagentes. O primeiro estudo é realizado usando um modelo 2D tipo-água que é largamente conhecido na literatura. No segundo estágio, estamos a influência de solutos interagentes nas propriedades de modelos em rede e contínuos. Para o modelo em rede, nós desenvolvemos um modelo de soluto e posteriormente uma técnica capaz de simular misturas de modelos em rede a pressão constante. De posse desta técnica estudamos as propriedades de excesso da mistura.

Palavras-chave: Confinamento de água, anomalias da água, meios porosos, modelo de rede, misturas, metanol, simulação de Monte Carlo

Contents

List of Acronyms	ix
1 Introduction	1
1.1 The Water	1
1.2 Water confined	11
1.2.1 Porous media	12
1.3 Mixtures of associating fluids	15
1.4 Objectives and organization of the thesis	23
2 Influence of disordered porous media on the anomalous properties of a simple water model	25
2.1 The Model	25
2.2 The Methods and Simulation Details	29
2.3 Results	31
2.3.1 Structural and thermodynamic behavior	31
2.3.2 Diffusion and dynamic anomaly	37
2.4 Conclusion	38
3 Lattice Model for water-solute mixtures	39
3.1 The Model	40
3.2 Simulation and Numerical Details	44
3.2.1 Computation of isobars for pure components	45
3.2.2 The properties of mixtures at fixed T and p	46
3.3 Numerical Results	47
3.3.1 The phase diagram for pure components	47
3.3.2 Critical lines and order parameters	48
3.3.3 The excess properties of the water-solute mixtures	55
3.4 Conclusions	60
4 Temperature of maximum density and excess properties of short-chain alcohol aqueous solutions: A simplified model simulation study	63
4.1 The Model	64
4.2 Simulation details	65

4.3	Results	66
4.3.1	The temperature of maximum density (TMD)	67
4.3.2	Excess thermodynamic properties	72
4.4	Conclusions	74
5	General Conclusions	76
6	Published articles	78
A	Computation of the residual entropy	79

List of Figures

1.1	The water phase diagram shown in reference [1]. Solid thick lines represent first-order phase transition between phases as solid-liquid, liquid-vapour, vapour-solid. The thin solid lines represent the limit of structures in the solid phase. The roman numbers represent the different structures of Ice. The black dashed line represents the second-order phase transition. The circles represent the end, critical and tricritical points and are described on the figure. The gray dashed lines work as a guide of eyes.	2
1.2	Temperature <i>versus</i> pressure phase diagram of water. LDA and HDA represent the low density and high-density amorphous phases respectively [2] observed experimentally. The LDL and the HDL represent the low density and high density liquid phases observed only in simulations [3]. The solid line separated by a first-order phase transition these phases. The dotted lines separate the stable water from supercooled and the supercooled from “no man’s land” and this from the amorphous region. The dotted lines are not real phase transitions.	3
1.3	Tetrahedral structure of water. The white spheres represent the hydrogen and the gray spheres are oxygens. Dashed lines represent the hydrogen bonds at distance 1.88Å.	5
1.4	Two possible configurations for the octamer. (A) Shows a close structure in which the tetramers are non-bonded; (B) shows open structures and with bonded tetramers [1].	5
1.5	Experimental data water. Figure shows the maximum in density as function of temperature $T = 4^{\circ}\text{C}$ at pressure of 1 atm. The figure was taken from [4].	6
1.6	Diffusion coefficient versus pressure for different temperatures. The large circles represent the maximum in diffusion and the dashed line connects these points [5].	7
1.7	At figure (A) the dependence of specific heat at constant pressure and on inset the same property at supercooled temperatures [1]. At (B) the thermal compressibility against temperature and on inset is shown the peak in this property [1].	7
1.8	At (A) a two length scales potential purely repulsive [6]. At (B) two length scales potential but with an attractive part [7].	9
1.9	At (A) potential proposed by de Oliveira <i>et. al.</i> [8]. On inset is presented the force. At (B) is represented a continuous potential with energy barrier more pronounced. This potential was proposed by Franzese <i>et.al.</i> [9].	10

1.10	(A) A hypothetical phase diagram. The negatively sloped liquid–liquid coexistence line generates a Widom line that extends beyond the critical point (filled circle), suggesting that water may exhibit a fragile-to-strong transition for $P < P_c$ (path α). (B) A sketch of the pressure-temperature phase diagram for the two-scale Jagla model. Upon cooling at constant pressure above the critical point (path α), the liquid changes, as the path crosses the Widom line, from a low-density state (LDL - non-Arrhenius dynamics) to a high-density state (HDL - Arrhenius dynamics) as the path crosses the Widom line. [10].	12
1.11	At DIST is shown a porous matrix in which the position of obstacles are obtained by Gaussian distortion of a cubic lattice. At RND the position of obstacle are chosen randomly [11].	13
1.12	Image taken from [12]. Gray large spheres represent the particles of the matrix and black spheres represent the fluid. Two configurations of porous media were explored in this work. At (A) is shown an FCC and at (B) a disordered configuration is shown.	14
1.13	Figure taken from reference [13]. At (a) snapshot of the region occupied by the obstacle/repulsive nanoparticle. The small cyan spheres represent water particles and the colors on the bonds represent the possible state of the water particle.(b) Snapshot of the system with 2.4% of its volume occupied by obstacles (large golden spheres) randomly placed. (c) and (d) are fluctuations of volume and compressibility K_T for different concentrations of the obstacles respectively.	15
1.14	Experimental result displayed in reference [14]. The figure shows the variation in temperature of maximum density as function of the solute fraction.	16
1.15	(A) Excess enthalpy versus alcohol fraction. The squares and the circles are experimental data for ethanol and methanol respectively [15]. At (B) Excess volume as function of methanol fraction. Circles are experimental data [16].	17
1.16	Experimental data of excess specific heat at constant pressure in function of methanol fraction. The blue circles are experimental data and solid line works as a guide for eyes.	18
1.17	At (A) the gray lobes represent the spherical distribution function of water molecules around a central water molecule at $r_{Ow...Ow} \leq 3.5$. The cases I,II,III and IV represent methanol fractions of $x_m = 0, 0.1, 0.5$ and 0.9 respectively [17]. At (B) is shown a water-methanol mixture with methanol fraction of 0.70. The blue spheres represent the water oxygen atoms and sticks represent the methanol molecules. Dashed blue lines indicate the hydrogen-bonding [18].	19
1.18	(Left) excess enthalpy for the water methanol mixture and (Right) excess isobaric molar heat capacity c_p^E . Filled squares correspond to simulations with the Lorentz-Berthelot combining rules for the water-methanol interactions and empty squares are results obtained with the model developed in this reference [19]. Full line represent experimental data in both figures. . .	20

1.19	Difference ΔT between the TMD of the mixture and that of pure water plotted as a function of methanol mole fraction x_2 . Simulation results for the OPLS+TIP4P/2005, the L2+TIP4P/2005, and the OPLS/2016+TIP4P/2005.	20
1.20	At (A) The excess volume versus methanol volume fraction. Symbols represent simulation data and solid lines are guides of eyes. At (B) variation of TMD versus the methanol fraction at different pressures. Methanol fraction of mixture, at different pressures.	22
1.21	(A) V_p^E and (B) H_p^E . Filled markers and solid lines represent $T = 90\text{K}$ and $p = 0\text{MPa}$. Open markers and dashed lines represent $T = 100\text{K}$ and $p = 0\text{MPa}$. Blue circles represent association (A), green diamonds represent Lorentz-Berthelot (LB), blue squares represent quasi-ideal(ID) and red triangles solvation(S).	23
2.1	The occupational and orientational states of a molecule at the site i . The arms variables are: $\tau_i^{(1)} = 0, \tau_i^{(2)} = 1, \tau_i^{(3)} = 1, \tau_i^{(4)} = 0, \tau_i^{(5)} = 1, \tau_i^{(6)} = 1$	26
2.2	Examples of a configuration for the HDL (a) and LDL (b) phases for the Associating Lattice Gas (ALG) model. The solid and dashed lines indicate the bonding and inert arms, respectively.	27
2.3	For the ALG model, panel (a) shows the phase diagram μ^* vs T^* , illustrating the gas-LDL (empty circles) and the LDL-HDL (filled circles) phase transitions, the λ -line (empty squares) and the TMD line (filled triangles). In panel (b) we plot the c_V^* versus T^* for $\mu^* = -0.80$ (circles), $\mu^* = 0.60$ (diamonds) and $\mu^* = 1.20$ (squares). In (c) the system density ρ versus T^* for fixed μ^* along the TMD line (dashed line).	28
2.4	(a) shows a lattice configuration where the solid gray, the solid black and the dashed circles describe water molecules, obstacles and empty sites respectively. For clarity, the bonds are not shown. (b) shows a lattice configuration with the subdivision in four sublattices.	29
2.5	ρ vs μ^* for distinct porous densities ρ_o for $T^* = 0.40$	32
2.6	For $\rho_o = 0.08$: (a) Chemical potential μ^* versus reduced temperature T^* phase diagram showing the Gas-LDL (empty circles), the LDL-HDL (filled circles) phase transitions, the λ -line (empty squares) and the TMD line (filled triangles). (b) Specific heat at constant volume c_V versus T^* for the system with obstacles (filled squares) and system with no obstacles (empty circles) at $\mu^* = -1.00$. Panel (c) ρ versus T^* for $\mu^* = 0.0, \dots, 2.2$ showing the TMD line (dashed line).	33
2.7	For $\rho_o = 0.24$: (a) Chemical potential μ^* versus reduced temperature T^* phase diagram showing the Gas-LDL (empty circles), the LDL-HDL (filled circles) phase transitions, the λ -line (empty squares) and the TMD line (filled triangles). (b) Specific heat at constant volume c_V versus T^* for the system with obstacles (filled squares) and system with no obstacles (empty circles) at $\mu^* = -1.00$. Panel (c) ρ versus T^* for $\mu^* = 0.0, \dots, 2.0$ showing the TMD line (dashed line).	34

2.8	For $\rho_o = 0.40$: (a) Chemical potential μ^* versus reduced temperature T^* phase diagram showing the Gas-LDL (empty circles), the LDL-HDL (filled circles) phase transitions, the λ -line (empty squares) and the TMD line (filled triangles). (b) Specific heat at constant volume c_V versus T^* for the system with obstacles (filled squares) and system with no obstacles (empty circles) at $\mu^* = -1.00$. Panel (c) ρ versus T^* for $\mu^* = 0.0, \dots, 2.0$ showing the TMD line (dashed line).	35
2.9	Spatial snapshot (35×35 sites) of triangular lattice. Each site is represented by hexagon, with its six nearest-neighbor sites. White hexagons represent vacancies, black represent obstacles and gray represent water-like particles. The snapshots exhibit character configurations of system with chemical potential $\mu^* = -0.5$ and temperature $T^* = 0.3$. In (a) we present the unconfined system. In (b) the system submitted at low degree of confinement $\rho_o = 0.08$ and the blue rectangles denote the regions where the characteristic geometry of LDL of ALG is preserved. In (c), intermediate degree of confinement $\rho = 0.24$, and green rectangles denote the LDL structure. The highest degree of confinement $\rho = 0.40$ is shown in (d). . . .	36
2.10	Chemical potential versus temperature illustrating (a) the TMD lines (b) the gas-LDL tricritical point (c) the LDL-HDL critical point values for the unconfined (circles) and the system with different concentrations of obstacles. The symbols squares, triangles and diamonds correspond to the $\rho_o = 0.08, 0.24$ and 0.40 , respectively.	36
2.11	Diffusion coefficient versus density at fixed temperatures for: (A) $\rho_o = 0.08$, (B) $\rho_o = 0.24$ and (C) $\rho_o = 0.40$. The solid gray lines are the values of the diffusion coefficient for $T^* = 0.30 \dots 1.00$ with $\Delta T^* = 0.05$ (from bottom to top), the blue dashed and dot-dashed lines connect the minimum and maximum in D respectively.	37
3.1	Representation of lattice for pure components. The blue sphere represents the water and the patches A and B represent the donors and acceptors arms respectively. The red sphere represent the solute particle and the arms A and B represent the donor and acceptors, and the patch C represents the anisotropic group	41
3.2	Representation of lattice. S_i and S_j represent particle on its respective positions i and j . Blue sphere represent a water and red, a solute particle. B_W and B_S represent the patches B of water and solute respectively. The patch D is not represented here for the clarity of the image.	41
3.3	(A) LDL (B) HDL phases. At (B), the colors blue and red are used to facilitate the visualization.	43
3.4	Reduced chemical potential versus reduced temperature phase diagram for (up) pure water (down) pure solute. Solid thick lines represent first-order phase transitions, liquid-gas (LGT) and liquid-liquid (LLT). Thin lines represent continuous (second-order) transition, the empty circles show the λ -line and the filled circles are the τ -line. The big patterned circles represent the multi-critical points of the model. (See the text for details).	49

3.5	In (A) $u^* = U/L^3$ vs chemical potential for (A) water model for three different temperatures $T^* = 0.30, 0.50, 0.80$. and (B) for the solute model. In (C) the energy per site for the different models at $T^* = 0.5$ are compared.	50
3.6	In (A) we plot the density $\rho^* = N/L^3$ vs chemical potential for water model for three different temperatures $T^* = 0.30, 0.50, 0.80$. In (B) the same plot of (A) for the methanol model. In (C) the density for the different models for $T^* = 0.5$ are computed.	50
3.7	Order parameter θ_λ versus reduced temperature for (A) water and (B) solute for various chemical potentials. Average density of the empty (red) and full (blue) sublattices for (C) water and for (D) the solute.	51
3.8	Location of the continuous LDL-HDL transitions for the water model at $T^* = 0.80$ and different system sizes: $N_L = 2L^3$. At (A) Total reduced density and partial densities, ρ_α as functions of μ . (B) Order parameter O_λ and (C) $g_{4\lambda}$ as a function of μ .	53
3.9	Heat capacity versus reduced temperature for the reduced chemical potentials (A) $\mu^* = 1.0$ and (B) $\mu^* = 1.6$ for water and solute respectively for different L values for the λ -line. The same for $\mu^* = 1.2$ showing both the λ and the τ -lines.	53
3.10	O_τ versus reduced temperature for different systems sizes at chemical potential $\mu = 2.0$ for water (A) and solute (B) models. $g_{4\tau}$ versus reduced temperature for different systems sizes at chemical potential $\mu = 2.0$ for water (C) and solute (D) models.	54
3.11	(A) excess volume and (B) excess enthalpy per particle as a function of solute concentration for $\lambda_S = 0.25, \lambda_W = 0.25, p^* = 0.10$ and several temperatures.	57
3.12	The snapshot of system for $\lambda_W = 0.25$ and $T^* = 0.350$. The blue and red spheres represent the water and solute respectively. At (A)- $x_2 = 0.024105$, (B)- $x_2 = 0.704341$ and (C)- $x_2 = 1$.	58
3.13	(A) Excess volume and (B) Excess enthalpy <i>versus</i> fraction of solute for various temperatures, $\lambda_W = 0, \lambda_M = 0.25$ and $p^* = 0.10$.	58
3.14	(A) Excess volume and (B) excess enthalpy <i>versus</i> fraction of methanol for various temperatures. $\lambda_W = -0.25, \lambda_M = 0.25$ and $p^* = 0.10$.	59
4.1	Interaction potential <i>versus</i> distance. The solid blue line represents the softened-core interaction potential U_{sc} (equation 4.1) between OH-OH, OH-water and water-water sites. The dashed red line and green dot-dashed line represent the R-R, R-OH and R-water repulsive interactions.	65
4.2	Temperature dependence of the density for various solute compositions along isobars with increasing pressure from bottom to top ($P^* = 2.3, \dots, 27.6$). Open circles correspond to simulation data and a dotted line denotes a polynomial fit. (A) $x_{ROH} = 0.0$ (pure water), (B) $x_{ROH} = 0.01$, (C) $x_{ROH} = 0.02$ and (D) $x_{ROH} = 0.03$. The TMD is represented by filled symbols, which are connected with a dashed curve that correspond to a polynomial fit, to represent the TMD curve. Pressure increases from bottom to top.	68

4.3	Density values at the temperature of maximum density of the heteronuclear alcohol model, for various mole fractions, $x_{ROH} = 0.00$ (black solid lines and filled circles), $x_{ROH} = 0.002$ (red dashed and filled squares) and $x_{ROH} = 0.003$ (green dot-dashed line and filled triangles). In all cases the points are simulation data, and lines correspond to polynomial fits. State points at the same pressure are connected with dotted lines.	69
4.4	Change in the temperature of maximum density with respect to the bulk solvent value vs. alcohol mole fraction for various pressures for the heteronuclear alcohol model.	69
4.5	Same as Figure 4.3 for the homonuclear alcohol model	70
4.6	Change in the temperature of maximum density with respect to the bulk solvent value vs. alcohol mole fraction for various pressures for the homonuclear alcohol model.	71
4.7	Water-water (left) and Water-OH (right) radial distribution functions for $P^* = 6.8$ and $T^* = 0.4$ for various solute concentrations. The insets show zoom of the regions around the first two maxima.	72
4.8	Excess thermodynamics of our water-ROH mixture model (heteronuclear model). (A) Excess volume; (B) excess enthalpy; (C) excess specific heat. In all figures the symbols are data obtained from MD simulations. In graphs (A) and (B) lines are drawn as a guide to the eyes. In graph (C), to compensate the dispersion of the simulated data, the curve is a least squares fit. All calculations were done at pressure $P^* = 18$	73

List of Acronyms

LLCP - Liquid-liquid critical point

LGCP - Liquid-gas critical point

SCPH - Second critical point hypothesis

LDL - Low density liquid

HDL - High density liquid

HDA - High density amorphous phase

LDA - Low density amorphous phase

TMD - Temperature of maximum density

FS - Fragil-Strong

ALG - Associating lattice gas

CS - Core-softened

BCC - Body-centered cubic

Chapter 1

Introduction

1.1 The Water

The water is a substance of fundamental importance for the creation and maintenance of life. In the body it works diluting solids, transporting nutrients and controlling the temperature. The water is also employed in the control of temperature in thermal machines, in the production of food, in the energy generation, among others. Even though abundant and quite common in nature water is not a simple liquid, instead it exhibits a number of unusual properties. Actually it has 74 anomalies known to this date [1].

The peculiarities present on the thermodynamic, dynamic and structural properties of water makes it one of the main representative of the selected group known as anomalous liquids. Such substances exhibit non-usual properties such as the increase of the density with the temperature, the increase of the diffusion coefficient with the increase of the density [4, 5, 20] and others. The collective interactions between water molecules plus the effect of the temperature gives rise to the complex phase diagram illustrated in the figure 1.1.

In the pressure *versus* temperature phase diagram illustrated in the figure 1.1, it is possible to observe three main phases: solid, liquid and gas, separated by first-order phase transition lines (thick lines). The three lines end in a triple point located at $T_t = 273.26K$ and $P_t = 611.69Pa$. At higher temperatures and pressures, the gas-liquid coexistence line ends in a critical point, located at $T_c = 647K$ and $P_c = 2.30 \times 10^7 Pa$. For the temperature above the critical point no liquid-gas phase transition is observed. At low-temperatures many crystalline structures coexist and they are represented by roman numbers in the figure 1.1. For example, the regions VIII and I_h represent the ice-eight and hexagonal ice

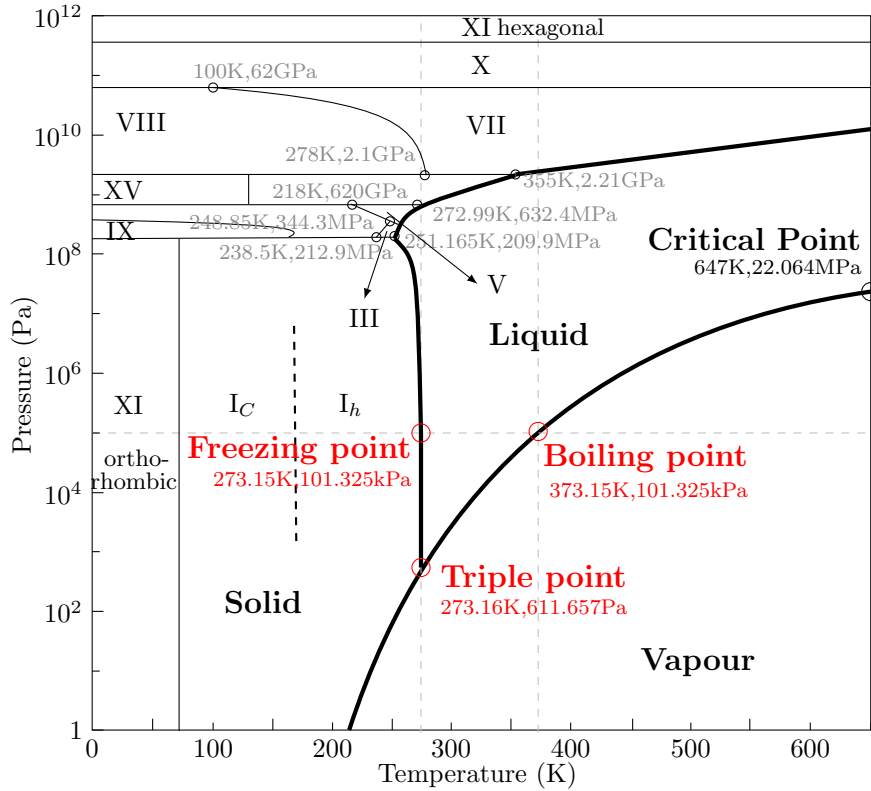


Figure 1.1 The water phase diagram shown in reference [1]. Solid thick lines represent first-order phase transition between phases as solid-liquid, liquid-vapour, vapour-solid. The thin solid lines represent the limit of structures in the solid phase. The roman numbers represent the different structures of Ice. The black dashed line represents the second-order phase transition. The circles represent the end, critical and tricritical points and are described on the figure. The gray dashed lines work as a guide of eyes.

respectively. The hexagonal ice form is the most popular ice structure. It is the form of ice found in the nature, and give the origin to the hexagonal structure observed in the six-fold symmetry in ice crystals [1].

Despite the richness of the water phase diagram, a region close to 220 K and 200MPa, has received particular attention. This region is located at supercooled temperature, between $T_H = 232\text{K}$ (the temperature of cubic ice crystallization) and $T_X = 150\text{K}$ (the temperature of homogeneous nucleation) [21]. It receives the name of “no man’s land” [3,22–25] because system coming from the liquid phases, immediately crystallizes and no liquid phase is observed. The large increase in the response function in temperatures surrounding the no man’s land it was assumed the possibility of the presence of two metastable liquids. This theory received the name of the second critical point hypothesis (SCPH) [3]. The SPCH [3] was originally formulated based on the experimental results [26] that showed the existence of two amorphous phases, a high-density amorphous phase (HDA) and a low-density amorphous phase (LDA), at very low temperatures [26]. The SCPH conjectures, as illustrated in the Figure 1.2, that the increase of the temperature would lead, continuously, the HDA

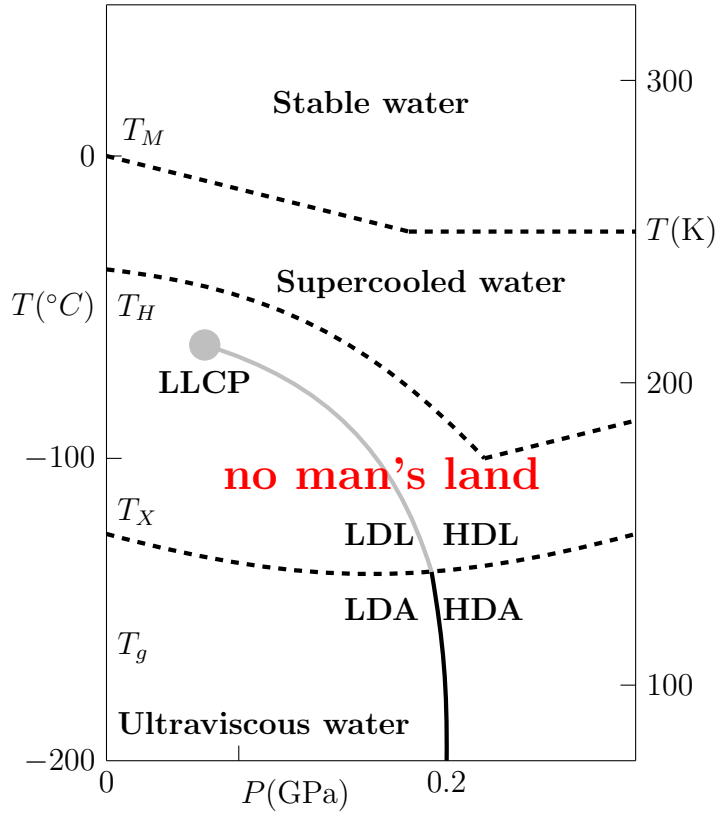


Figure 1.2 Temperature *versus* pressure phase diagram of water. LDA and HDA represent the low density and high-density amorphous phases respectively [2] observed experimentally. The LDL and the HDL represent the low density and high density liquid phases observed only in simulations [3]. The solid line separated by a first-order phase transition these phases. The dotted lines separate the stable water from supercooled and the supercooled from “no man’s land” and this from the amorphous region. The dotted lines are not real phase transitions.

and LDA phases, to the liquid phases called low-density liquid (LDL) and high-density liquid (HDL). These liquid phases would be separated by the same first order transition which divides the amorphous phase (see figure 1.2), however the liquid-liquid transition would end in a critical point known by liquid-liquid critical point (LLCP) or the, second critical point (SCP). The critical fluctuations in the vicinity of the liquid-liquid critical points would explain the anomalies present in water. Unfortunately this critical point is located in a region of pressures and temperatures in which liquid water is inaccessible to the experiments. Water freezes for these pressures and temperatures and the region is called “no man’s land” or homogeneous nucleation region.

Among the different anomalies present in water, the large increase of the response functions are the properties more closely related with the hypothesis of the second critical point. The specific heat at constant pressure, c_p , and the isothermal compressibility, κ_T , are example of these functions. Both c_p and κ_T show a large increase in the vicinity of the LLCP temperature. This increase never becomes a divergence (which is a requirement for a critical point) because the system crystallizes before reaching the hypothetical critical temperature.

Although of apparent agreement of LLC scenario and experimental results, other scenarios have been proposed for describing the behavior of water in the supercooled region. The stability limit/critical point free scenario (SL/CPF) [27,28], for example, claims that no critical point exists and suggests that an order-disorder transition extends until regions of the limit of stability of liquid-water. In a similar way, the singularity-free scenario [29] defends that the increase in the response function of water in supercooled regions is just a sharp increase but is not related to any critical point. Independently of scenario, the different hypothesis states that, at low temperatures the water is composed by two different metastable liquids, a low-density liquid (LDL) and high degree of local tetrahedral order [30,31], and a high-density liquid (HDL) with structure more disordered and higher coordination number [32].

Independent of which scenario is correct, or even, which of them have more experimental evidences, it is well known that the water exhibits a considerable amount of unusual behavior popularly, regarded as anomalies. The best known is certainly the anomaly in the density. For normal liquids the density increases with the decrease of the temperature. Water has a maximum in the density [4,5,20]. Other examples of water anomalies are the anomaly in the diffusion, in the translational order parameter, in the orientational order parameter, in the viscosity, in the specific heat, in the surface tension, in the compressibility, the relative permittivity, in the dielectric constant and in the solubility. In fact, the literature reports more than 74 different water anomalies [1].

The existence of the anomalies can not be explained by a simple mechanism as van der Waals theory. In the case of the anomalous liquids and in the particular case of water two length scales are needed. The origin of these two length scales is the presence of the hydrogen bonds in addition to the van der Waals interactions. But, what are the hydrogen-bonds [1,8] ? These structures appear (see figure 1.3) as a consequence of the bonds between the oxygen and the hydrogen of distinct molecules. The figure 1.3 exhibits a water molecule and its four hydrogen bonds with the neighboring water molecules. The hydrogen of the upper and left molecules shares electrons of its valence shell with the oxygen of central molecule, forming two bonds. In a similar way, each hydrogen of central molecule shares its electron with the oxygen of the molecule below. In this sense, a central molecule makes four hydrogen bonds, two as a donor and two as a receptor.

The set of four molecules of water receives the name of tetramers and as mentioned previously, the arrangement between them is fundamental for understanding the origin of water anomalies. These structures, show two distinct arrangements (see Figure 1.4 (A)),

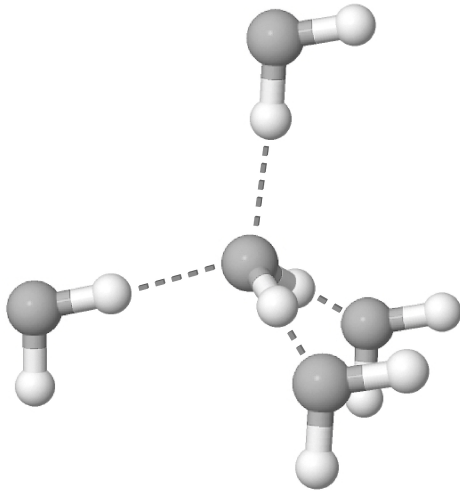


Figure 1.3 Tetrahedral structure of water. The white spheres represent the hydrogen and the gray spheres are oxygens. Dashed lines represent the hydrogen bonds at distance 1.88\AA .

one more dense, with high configurational entropy, in which the tetramers tend to be closer to each other, and other forming a less dense structure, more organized and with the tetramers more distant (see Figure 1.4 (B)).

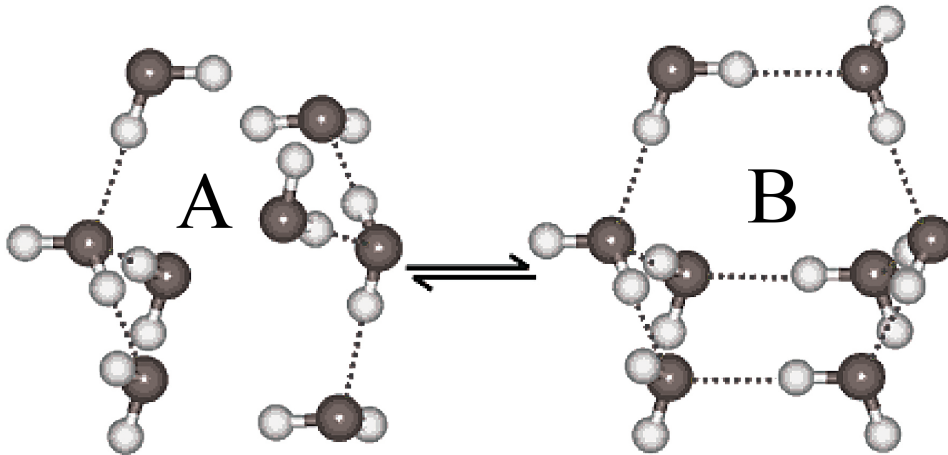


Figure 1.4 Two possible configurations for the octamer. (A) Shows a close structure in which the tetramers are non-bonded; (B) shows open structures and with bonded tetramers [1].

The competition of these two structures as the temperature is increased leads to the appearance of the density anomaly. At low temperatures, the tetrahedral structure remains stable forming all the hydrogen bonds. However, the increase of the temperature distorts its tetrahedral geometry sharing and breaking of the hydrogen bonds and as consequence, approximating a fraction of neighbor water molecules. This phenomenon of the approximation of water particles, or in other words, increasing of the density with respect to the

temperature receives the name of the anomaly in the density [4, 5, 20] and its behavior is illustrated in the Figure 1.5. As the temperature increases even further entropic effects dominates and the molecules become more appart, decreasing the density.

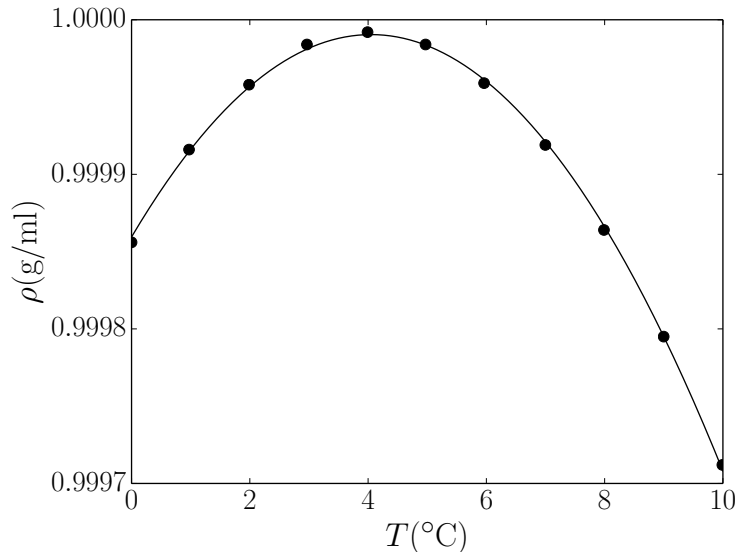


Figure 1.5 Experimental data water. Figure shows the maximum in density as function of temperature $T = 4^\circ\text{C}$ at pressure of 1 atm. The figure was taken from [4].

While the density anomaly assumes a central role in the thermodynamic anomalies group, the diffusion represents a very important dynamic anomalous behavior. As illustrated in the figure 1.6, for low temperatures the diffusion coefficient increases with the increase of pressure [5] while in normal materials the diffusion coefficient is a monotonic decreasing function with the density (or pressure). The diffusion anomaly belongs to the dynamical anomalies group and its origin is in sharing of the hydrogen-bonds. The increasing of the pressure induces a partial approaching of water molecules by disrupting hydrogen-bonds, increasing the displacement of the molecules.

As mentioned previously, in addition to density anomaly reported in the Figure 1.5, the water also shows an anomalous behavior on its response functions, such as, specific heat at constant pressure c_p and isothermal compressibility κ_T . While usual liquids increase monotonically their response functions with the increase of the temperature, the water decreases its values until a specific temperature, $T \sim 35^\circ\text{C}$ for c_p (see figure 1.7 (A)) and $T \sim 46^\circ\text{C}$ for κ_T (see figure 1.7 (B)), and only after these temperatures, it acquires an usual behavior in which they increase as the temperature goes up.

In addition the anomalies mentioned above, for the temperatures above the supercooled ($T > T_M$) regions, the response functions present a “divergent” behavior as shown on the inset of Figure 1.7 (A) [1, 33] and Figure 1.7 (B) [1, 27] for specific heat and compressibility

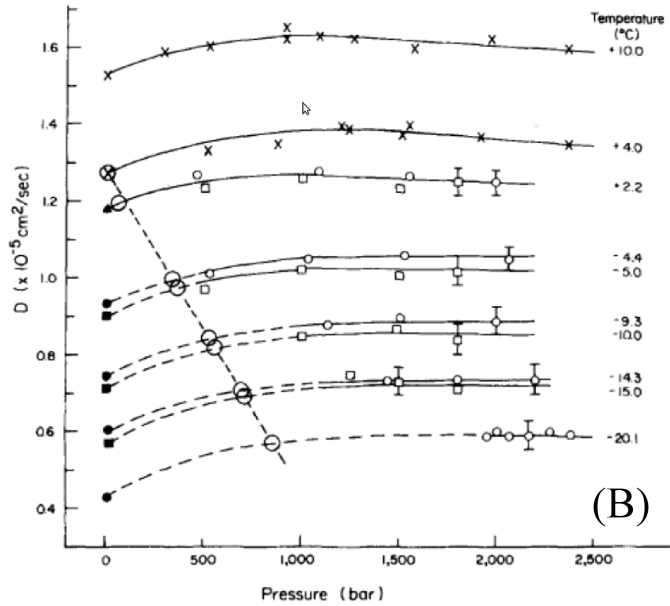


Figure 1.6 Diffusion coefficient versus pressure for different temperatures. The large circles represent the maximum in diffusion and the dashed line connects these points [5].

respectively. The “divergent” behavior of c_p and κ_T (see inset figure 1.7 (A) and (B)) are

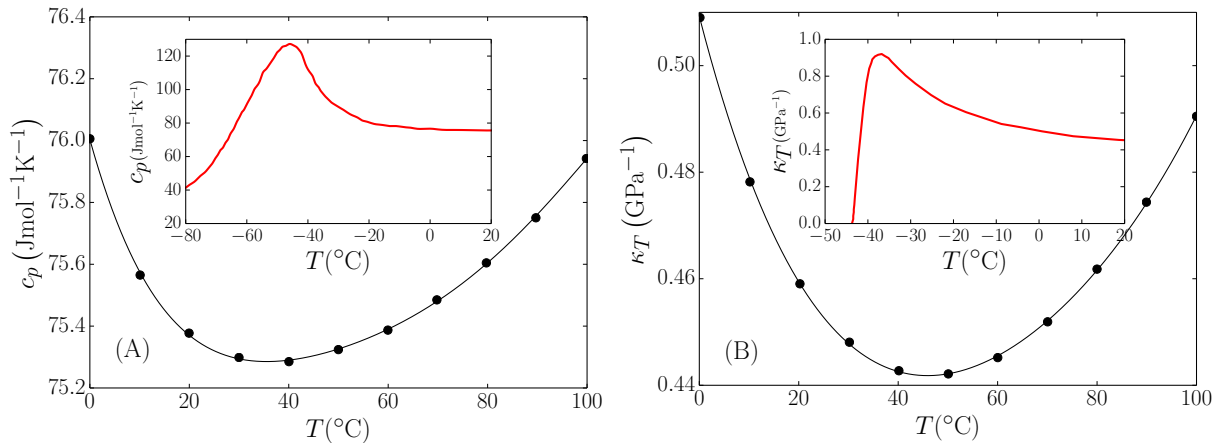


Figure 1.7 At figure (A) the dependence of specific heat at constant pressure and on inset the same property at supercooled temperatures [1]. At (B) the thermal compressibility against temperature and on inset is shown the peak in this property [1].

usually associated with the presence of criticality in this region, and for this reason is in complete agreement with the SCPH.

Due to the difficulties of keeping water liquid in the “no man’s land”, computer simulations have shown to be a powerful tool for the accessing this region. In this way, several classical models of water have been proposed, for example, ST2, SPC, SPC/E, TIP3P, TIP5P and SPC/Fw [34–38]. These models are commonly known as atomistic models

since they are built atom by atom. In the SPC (Simple Point Charge) model for example, the water molecule has three centers of concentrated charge, being the atoms H positive and atom O negative. These sites are positioned in a trigonal geometry with O-H distance equal to 95.48 pm and H-O-H angle equal to 109.42 degrees. The SPC/E, extended simple point charge model is a slight reparameterisation of the SPC model of water, in which the oxygen and the hydrogen charges present a modified value. Independently on the model chosen, both of them show a good agreement with experimental results of the supercooled water and water anomalies, being frequently used to analyze the thermodynamic, dynamic and structural anomalous behavior of water. The ST2 model [34,39] not only shows liquid-liquid coexistence as well as, it presents an incredible agreement with experimental results in relation to the changes in response function at vapor-liquid coexistence [40] and pressure-density phase diagram.

Even though atomistic models are a very interesting tool to reproduce the anomalies of water, they are not able to identify its origin. They exhibit many parameters and the complexity of these atomistic models hinders the detecting the main aspects responsible to anomalous behavior. In order to explore the mechanism behind the presence of anomalies and of the second critical point, the development of coarse-graining models has been an interesting strategy.

These models are based on the idea that under the influence of the temperature, tetramers of water move from opened structures to closed structures as shown in the figure 1.4. This mechanism suggests that the interaction between the tetramers could be represented by potentials with two scales. A given scale of the potential is identified as a minimum on the potential curve. Consequently, a potential with two scales presents a local minimum and a global minimum. The location and the characteristic values of different scales of the potential, define the emergence of the competitive nature present in liquid water [8,41,42].

The first two length scale potential was proposed by Stell and Hemmer [6]. They developed a ramp like spherical symmetric potential as shown in the figure 1.8(A). Subsequently, Jagla showed that this potential in three dimensions lead to the presence of double criticality and anomalies similar to the water [7]. On basis of the assumption of Stell and Hemmer, a number of spherical (symmetric) two length scales potential have been proposed [8,42-45]. Unfortunately, not all the two length scale potentials show the presence of anomalies. If any of the two of the length scale potentials is too attractive (see figure 1.8(B)) the anomalies will not be present. On the contrary, the cases in which the

attractive scale is present, the double criticality appears. In addition, if the potential is not smooth, the anomalies will also not be present, but double criticality appears [9, 43].

The success of the Jagla model led the development of more realistic smooth potentials. Such models are also represented by two length scales potentials and are known as the core-softened potential (CS). They do not represent a water molecule but clusters of molecules, for example, the tetramers shown in figure 1.3. These potentials show a repulsive core with a softening region when particles are very close and an attractive region particles are more distant as shown in figure 1.9. In figure 1.9(A) is shown a two length scale potential with a very weak attractive part in the spirit of the work of Bell [46] and Jagla [7]. Oliveira *et. al.* [41, 43] proposed a two length scale potential formed by a Lennard-Jones potential plus a Gaussian. This combination results in a repulsive shoulder at short distances and an attractive part at long distances being able to reproduce many features observed in liquid water, such as anomaly in density, diffusion, translation order parameter and cascade structure between the classes of anomalies. Following the well potential [9, 47] a smooth version was proposed and analyzed by Franzese [9] and both are illustrated in the figure 4.1. This potential, despite presenting a rather complex structure, it is able to reproduce the anomalous behavior of water and also LGCP and LLC.

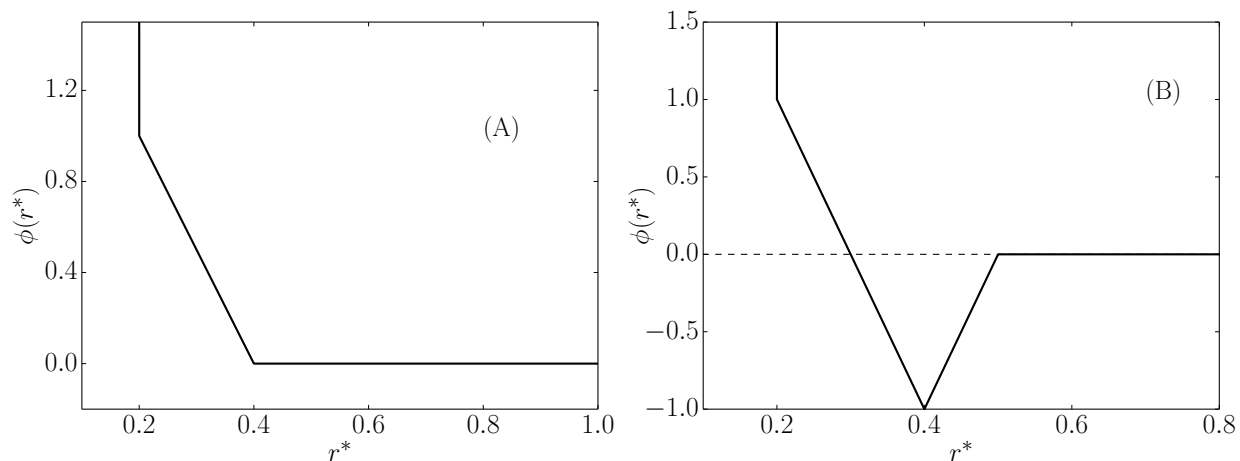


Figure 1.8 At (A) a two length scales potential purely repulsive [6]. At (B) two length scales potential but with an attractive part [7].

Notwithstanding the relevance of the findings obtained with of the spherical symmetric effective potential, they all do not exhibit the anisotropy present in the tetrahedral structure of water. In order to circumvent this difficulty, a number of lattice models in which the spherical symmetry is broken were developed. The pioneer model in this approach is the

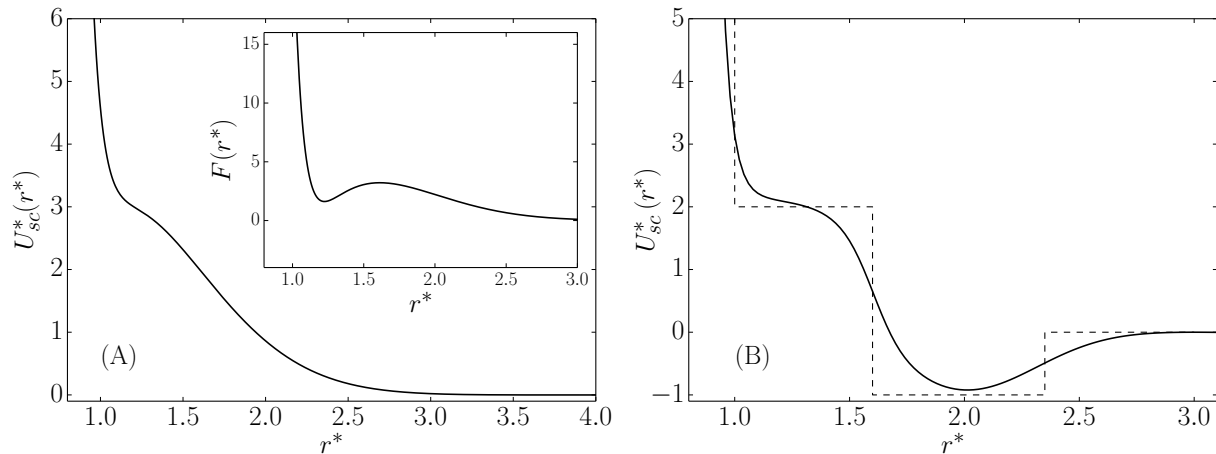


Figure 1.9 At (A) potential proposed by de Oliveira *et. al.* [8]. On inset is presented the force. At (B) is represented a continuous potential with energy barrier more pronounced. This potential was proposed by Franzese *et.al.* [9].

Bell-Lavis model [46,48]. This model and its variations are in two dimensions, the structure of water is represented by two states variable. The interactions between water molecules can be of two ways: van der Waals energy and a hydrogen-bond energy. Although of simplicity and low number of adjustable parameters, this model is able to capture the anomalous behavior of density and diffusion and also liquid phases [49,50].

Following the ideas of Bell-Lavis [46], more recently was proposed the Associating Lattice Gas (ALG) model. This model combines the occupational variables capable to produce liquid-gas coexistence with arm variables that also lead to the density and the diffusion anomalies [51–53] and in contrast to the Bell-Lavis, liquid-liquid phase coexistence. It is a good example of two length scales potential in a lattice system where directionality is an intrinsic ingredient. The inclusion of directionality adds orientational entropy and frustration, not present in the spherical symmetric systems. Therefore, when the properties of water depend on the two aspects, the lattice model becomes a good tool for describing the system. The similar idea gave rise to others directional water-like models [46]. An interesting aspect of this class of the models is that due to excess of the symmetries and the degree of freedom intrinsic these models move the second critical point predicted for water into critical lines. Over time, other water lattice models were proposed, among them should be mention the model proposed by Franzese and Stanley [54] and the Ciach *et.al* [55]. The model of the Ciach [55] is an extension of the well known Blume-Emery-Griffiths model [56] where the opened and closed structures of the tetramers of water are represented by two different states. Through the mean-field approximation, they showed that the model repro-

duce the TMD of water with quantitative agreement and predicts the liquid-liquid critical point.

1.2 Water confined

As mentioned previously, liquid water can not be experimentally observed in the “no man’s land” due to the homogeneous nucleation phenomena and therefore, the existence of the liquid-liquid phase transition can not be tested. In order to circumvent this difficulty, experiments with confined water have been proposed [57, 58]. The idea behind the use of confinement is that a wall disrupts the hydrogen-bonds, in which the formation of ice is disturbed and then moving the crystallization to lower temperatures in such a way that liquid-liquid transition can be detected.

Then, experimental studies and computer simulations of confined water [11, 57, 59–61] have shown that the water remains liquid in supercooled regions. This fact suggests the possibility of detection of criticality. Even though confinement moves the melting temperature it does not move it low enough to make possible to observe the LLC. The indirect measures are necessary. The experimental studies measure the diffusion coefficient and observe a fragile to strong transition¹ on crossing the Widom line [10] (the analytic continuation of the coexistence line beyond the critical point) as illustrated in figure 1.10. In addition to the possibility to test the LLC hypothesis, the study of confined water also has been used to modeling biological environment [62] and develop new nanomaterials [63].

Simulation studies of water confined between parallel plates are widely used in literature to represent both biological and nanoconfined systems [60, 64, 65]. In these cases, the temperature of maximum density (TMD) moves to lower temperatures when compared with the bulk temperature, and the system is structured in layers depending on the distance of plates. Another type of confinement widely used in literature is the porous media². It is an interesting alternative to represent the confined structure of the inner rocks on the earth and in the cellulose in plants. In addition, the nanopores are the confined structures used for testing the double criticality hypothesis [66].

¹A fragile to strong, or just, fragile-strong transition, is characterized by a change in the diffusion coefficient, from Arrhenius ($D \propto e^{1/T}$) to non-Arrhenius.

²Along this text we will use synonyms of random porous media, such as porous matrix, nanoporous matrices, disordered porous, disordered media etc.

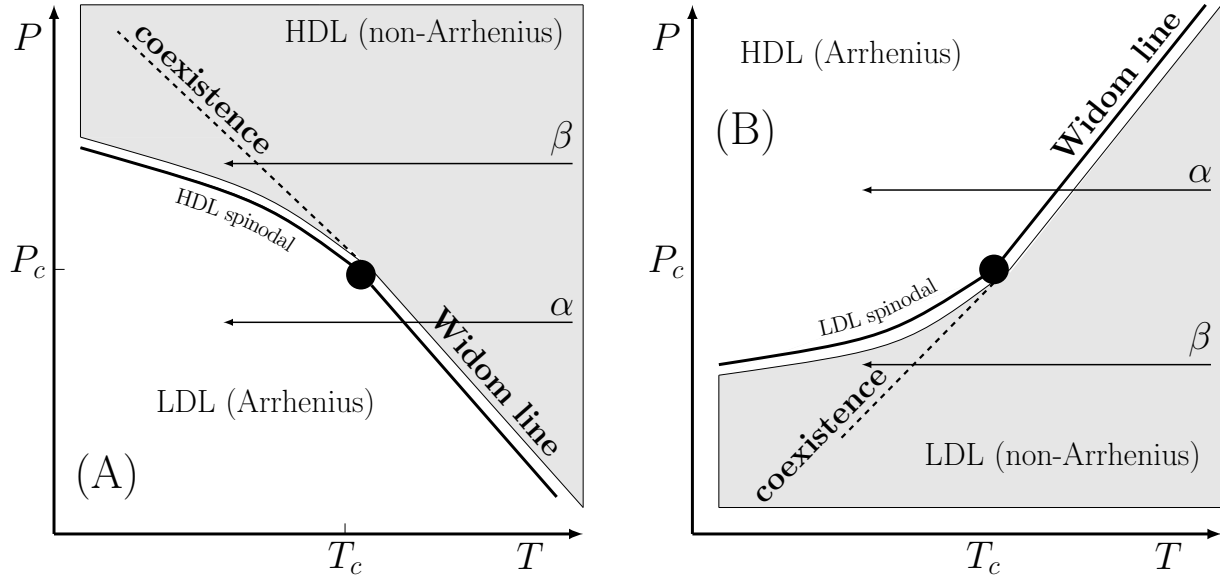


Figure 1.10 (A) A hypothetical phase diagram. The negatively sloped liquid–liquid coexistence line generates a Widom line that extends beyond the critical point (filled circle), suggesting that water may exhibit a fragile-to-strong transition for $P < P_c$ (path α). (B) A sketch of the pressure-temperature phase diagram for the two-scale Jagla model. Upon cooling at constant pressure above the critical point (path α), the liquid changes, as the path crosses the Widom line, from a low-density state (LDL - non-Arrhenius dynamics) to a high-density state (HDL - Arrhenius dynamics) as the path crosses the Widom line. [10].

1.2.1 Porous media

Porous media also have shown an alternative not only to study confined water but also to technological applications, such as gas storage, heterogeneous catalysis, activated carbon fibers and silica gels. Computer simulations of fluids confined in disordered porous structure are still a very difficult task. In general, the adsorption properties of this kind of systems are exclusive to a given distribution of obstacles that compose the porous media [67]. For this reason, the full understanding of the behavior of fluid adsorbed is necessary realize an average over a representative sample of the disorder. The literature reports many different techniques to generate the porous media. The most used technique consists in simulating a gas with number of particles equal to number of obstacles of the porous media and after a given number of simulation steps, the particles suffer a quench, in which they held fixed on their positions. The simulation box is filled using a grand canonical simulation. This procedure is then repeted in order to obtain different distribution of obstacles and therefore, perform an average over the replicas. Another possibility is simulate a gas with number

of particles equal to the number of obstacles plus number of particles of fluid. After a given number of the simulation steps the obstacles are fixed on their positions, while the particles of fluid are free to move in the porous media. In this case, the procedure also be repeated to obtain more samples of porous media. Although of easy implementation, the relaxation process and the average over replicas demand a very high computational cost, and in some cases an unworkable task.

Computer simulations show that the effects of adsorption are strongly related to the geometry of matrix [68]. Strelakova *et.al.* [11] studied a water-like model confined in nanoporous matrices of different geometries as shown in the figure 1.11: a ordered (DIST) and random distribution of obstacles (RND). In this work, they studied the influence of

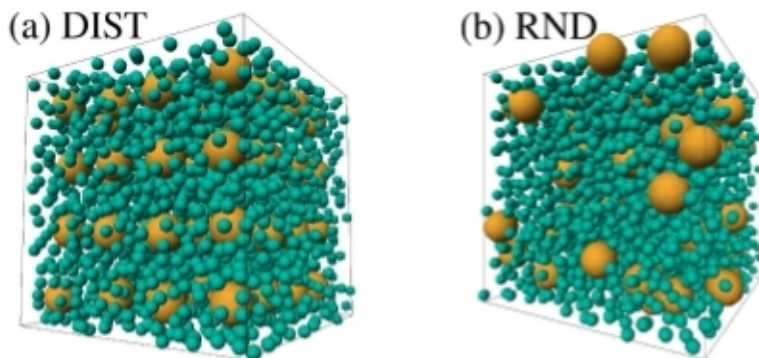


Figure 1.11 At DIST is shown a porous matrix in which the position of obstacles are obtained by Gaussian distortion of a cubic lattice. At RND the position of obstacle are chosen randomly [11].

geometry of porous matrix in a water-like model. They employed two different water-like models for the interaction potential, a Jagla potential [7] as illustrated in the figure 1.8(B) and a CS potential [9] as shown in the figure 4.1(B).

They show that the influence of obstacles on the TMD and LLCPC of the fluid is strongly related to the geometry of the system. In both cases the LLCPC shifts to lower temperatures and higher densities and pressures. However, in the disordered confining matrix case, the shift of temperature is more pronounced than the density and pressure ones. They also show that DIST geometry preserves the liquid-liquid coexistence, whereas the RND case shrinks the region.

A similar idea was explored by Dominguez *et.al* [69]. Using molecular dynamics simulation, they studied the changes in the anomalous behavior of a water-like model [41], illustrated in figure 4.1(A) due to confinement in disordered porous media. The interaction between obstacles (matrix) and fluid was modelled through the Lennard-Jones potential. They showed that the anomalous behavior is suppressed by the influence of media, mainly the diffusion anomaly. They also claim that is expected that all anomalies disappear if the

density of the porous matrix is high enough.

Page *et.al* [12] performed Monte Carlo simulation for studying the effects of porous media at vapor-liquid transition in Kaminsky-Monson molecular model [70]. They used two types of porous media: disordered and face-centered cubic (FCC), as shown figure 1.12. In accordance with other authors [11,69], they showed that the critical temperature moves to lower temperatures when compared with the bulk temperature, but this effect is also influenced by the geometry of matrix. As result the interaction between fluid-obstacles,

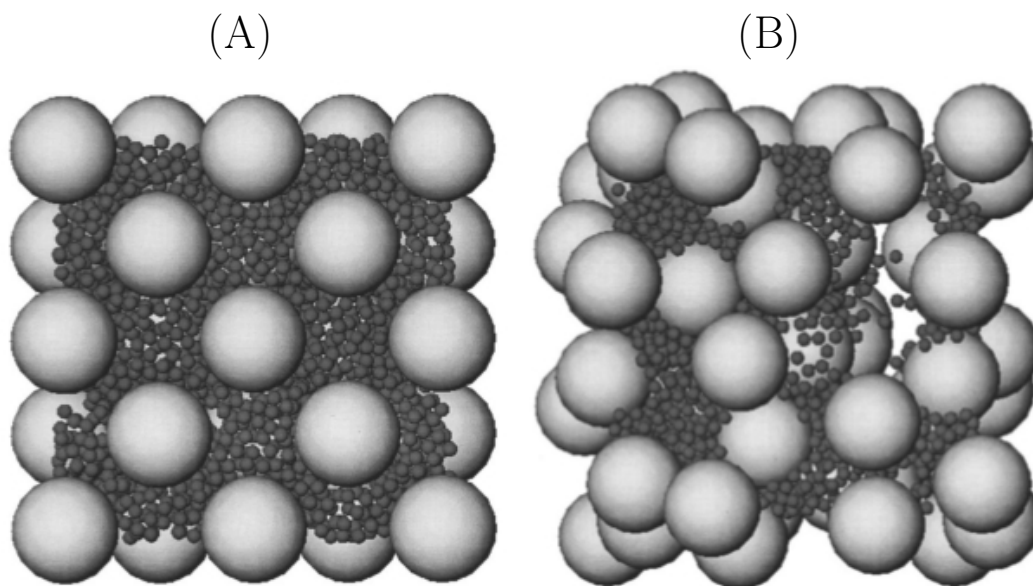


Figure 1.12 Image taken from [12]. Gray large spheres represent the particles of the matrix and black spheres represent the fluid. Two configurations of porous media were explored in this work. At (A) is shown an FCC and at (B) a disordered configuration is shown.

they showed that the temperature-density phase diagram is considerable changed, given origin to a new phase and a new critical point, not present in the bulk might appear.

The effects of confinement of the porous matrix in water-like models are not a exclusivity only of the continuous models. The study of this type of confinement is also used in lattice models. In these cases, the obstacles are modeled as sites of lattice where the particles can not assume. An example of this approach is reported in Ref. [13], for different fraction of obstacles. The figure 1.13(a) and (b) illustrate the implementation of the matrix. They observed that the disruption of the bonds, motivated by the placement of the obstacle, decreasing the liquid-liquid coexistence and give origin to a second critical point, different of the LLCPP. This behavior is due to the suppression of the fluctuations of the system. The

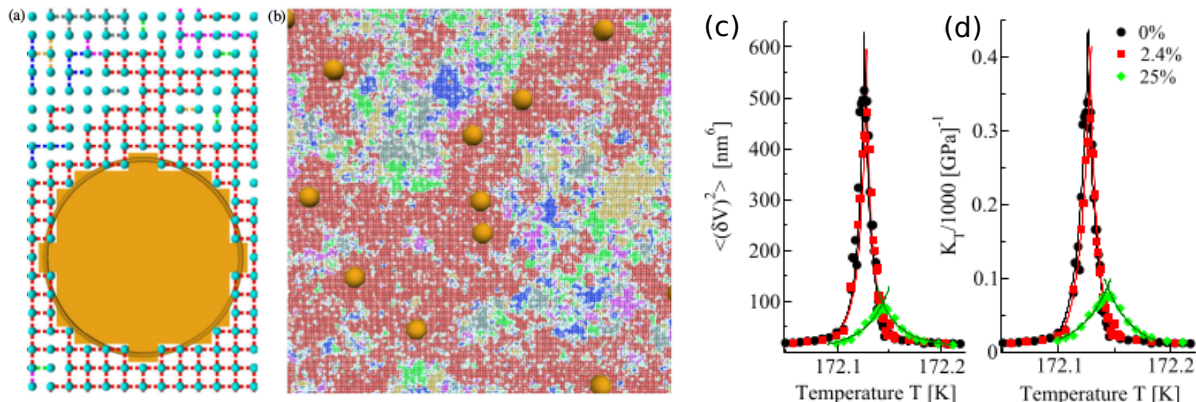


Figure 1.13 Figure taken from reference [13]. At (a) snapshot of the region occupied by the obstacle/repulsive nanoparticle. The small cyan spheres represent water particles and the colors on the bonds represent the possible state of the water particle. (b) Snapshot of the system with 2.4% of its volume occupied by obstacles (large golden spheres) randomly placed. (c) and (d) are fluctuations of volume and compressibility K_T for different concentrations of the obstacles respectively.

placement of obstacles in the system gives origin a different local ordering, since that the domain of boundaries increase with the concentration and then decrease the fluctuations in the response functions. The same is not true in the bulk system when a small variations in the temperature induces a rapid change from ordered to a disordered configuration, given rise a first-order phase transition.

1.3 Mixtures of associating fluids

Associating fluids is the nomenclature referred to the fluids composed of molecules presenting associative interactions. An associative interaction in turn, is an attractive interaction between two molecules which is both short ranged and highly directional. Interaction of this nature shows a saturation phenomena originated by the attractive and repulsive parts of a particle. Hydrogen-bonded fluids, like water, ionic and organic liquids are common examples of this group of fluid. Contained in the group of association fluids, the mixture of water and organic molecules corresponds to a very emblematic example of the real mixture. In this context, and motivated by its fundamental and technological reason, the mixtures of water and methanol have been intensively studied.

Wada and Umeda [14] showed that the variation of the temperature of maximum density of water moves to higher temperatures as the including of the solute, as shown in the

figure 1.14. The variations in the TMD (ΔT_{MD}) are obtained by relation $\Delta T_{MD} = T_M - T_W$ where T_M represents temperature of mixture and T_W temperature of water. For this reason, the regions where $\Delta T_{MD} > 0$ represent the regions where the TMD increase front of the insertion of the solute.

This behavior is quite unexpected, since the standard behavior of mixtures is decrease the value TMD. In addition to this conclusion, they showed that the variation of the temperature is strongly dependent on the size of the methyl group of the alcohol. In this

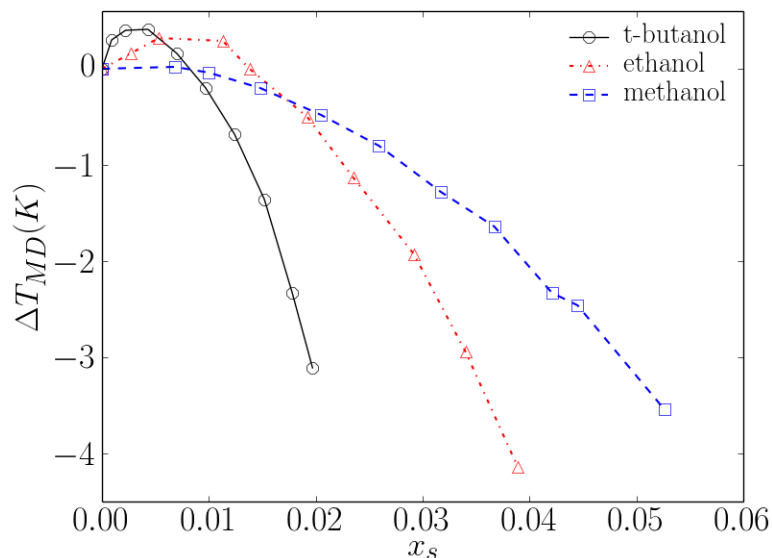


Figure 1.14 Experimental result displayed in reference [14]. The figure shows the variation in temperature of maximum density as function of the solute fraction.

case, as higher the size of the methyl group, higher is the variation in the temperature of maximum density. It is also possible to verify that the range in which the variation in TMD is positive is equally affected by the size of the methyl group. In the figure 1.14 the curve corresponding to the t-butanol shows the higher variations and the behavior persists only for very low solute fractions. For the ethanol (red dash-dotted curve), in which the methyl group is considerably lower than the t-butanol, the amplitude of the ΔT is lower, but the positive values in ΔT persist for higher solute fraction when compared to the t-butanol.

The excess properties are also widely studied in this context. A given excess property A^E of a mixture can be obtained by

$$A^E(x_2, p, T) = A(x_2, p, T) - [x_2 A_2^0(p, T) + (1 - x_2) A_1^0(p, T)], \quad (1.1)$$

where $A(x_2)$ is the value of the property A in the real mixture at solute fraction x_2 , pressure p and temperature T and A_2^0 and A_1^0 are the value of property A of the solute and solvent in an ideal mixture respectively. A solution is called ideal if each component of the mixture

fulfills a relation like, $A_i = x_i A_i^0$ ³. Although there is not, actually, ideal mixtures, some mixtures presents a behavior very close to that described by Raoult’s law. Unfortunately, mixtures of the associating liquids can not be, in general, described by this law. The interactions intermediated by short-range attractive potentials and strong directionality (e.g. hydrogen-bonds) confer a particular unusual feature to the mixture.

Experimental results for this mixture show that the excess enthalpy [15] and excess volume [16] present a non-monotonic behavior in relation to the solute fraction. The excess enthalpy for example, decreases until methanol fraction close to $x_{Me} = 0.35$ and from this value, increase until become an ideal mixture (see figure 1.15(A)). The excess volume in turn, shows a minimum for methanol fractions close to $x_{Me} = 0.52$ [16] (see figure 1.15(B)).

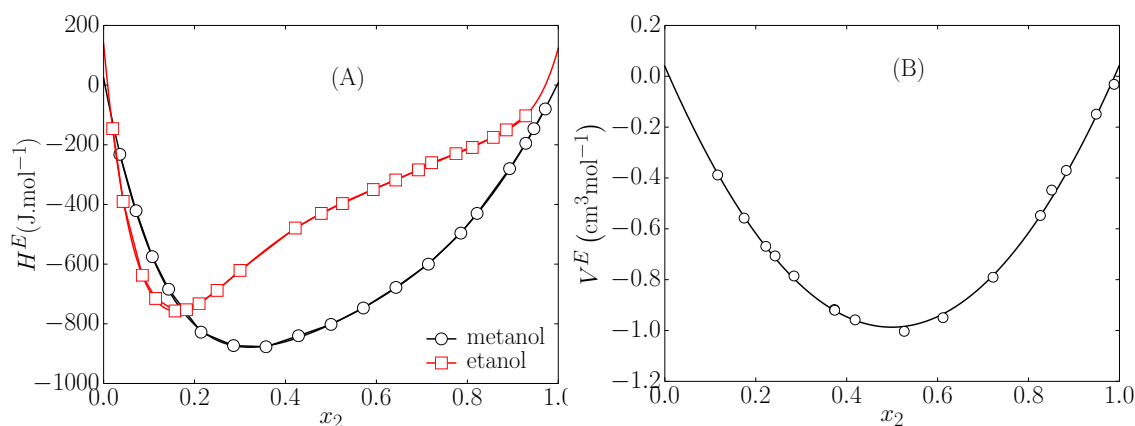


Figure 1.15 (A) Excess enthalpy versus alcohol fraction. The squares and the circles are experimental data for ethanol and methanol respectively [15]. At (B) Excess volume as function of methanol fraction. Circles are experimental data [16].

Similar to reported in excess enthalpy and volume, the specific heat also presents a nonideal behavior in relation to methanol fraction. The excess specific heat at constant pressure presents a maximum for low methanol fractions, $x_2 \sim 0.16$ [71, 72] as shown in figure 1.16. Is possible to list several properties that in a mixture of associating fluids exhibit an unusual behavior, the excess free-energy for example also belongs to this group. This property presents a harmonic dependence in relation to the methanol fraction [73].

In the last years, distinct approaches have been used to study the properties of this kind of mixtures. The statistical associating fluid theory (SAFT) and computer simulations have been shown a powerful tool to describe the liquid structure of the associating fluid. In

³Initially the Raoult’s law was written in terms of the pressure, $p_i = p_i^0 x_i$

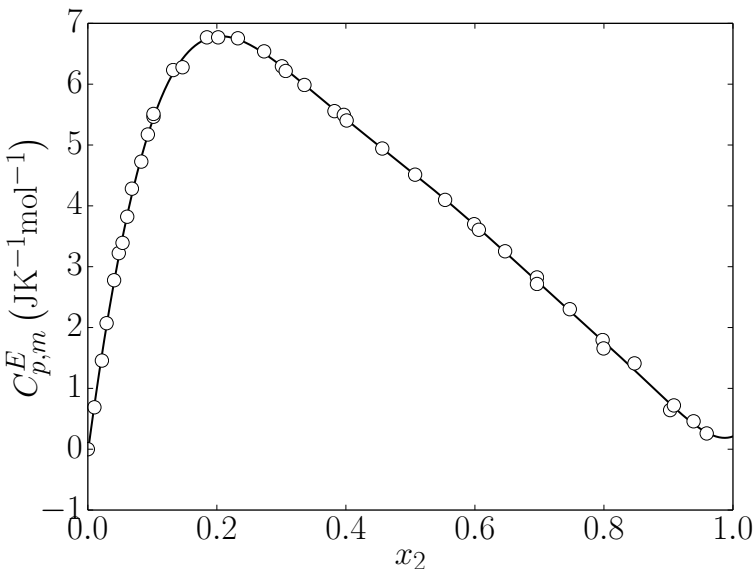


Figure 1.16 Experimental data of excess specific heat at constant pressure in function of methanol fraction. The blue circles are experimental data and solid line works as a guide for eyes.

this context of the SAFT theory, the Helmholtz free energy is expressed as an appropriate functions of the parameters and number of different segments representing the chemical groups that make up the molecules. Despite applicability and accuracy of this theory in the description of the phase equilibrium of the associating fluids and their mixtures, in general for a good accuracy of thermodynamic behavior of these systems is necessary to use the experimental or/and simulation data.

Traditionally, these type of problems are performed through sophisticated computational molecular models. To represent the water several models are used, among then SPC/E [36], ST4 [74] and TIP5P [37], on the other hand, to represent the organic molecule, in general, are used force fields such as OPLS (Optimized Potential for Liquid State) and TraPPE (Transferable Potentials for Phase Equilibria). In this direction Bakó *et.al.* [17] showed that with the increasing of alcohol fraction, the structure of water maintain its tetrahedral structure, however, the number of hydrogen-bonds is substantially reduced. (see figure 1.17). In a similar way, using classical MD simulations, Allison *et.al* [18] showed that not only the hydrogen-bonds decreases, but the water molecules are divided into rings and cluster, as well as reported experimentally by Dixit *et.al* [75].

Analysis of spatial distribution function [76] showed that the system is highly structured around of hydroxyl group and the methanol molecules are solvated by water molecules. Face of the difficulty to describe the behavior of water-methanol mixtures by the standard atomistic models, González *et.al* [19] proposed a new force field based on TIP4P/2005 + OPLS/2016 to describe the excess properties and the variations on the TMD of the

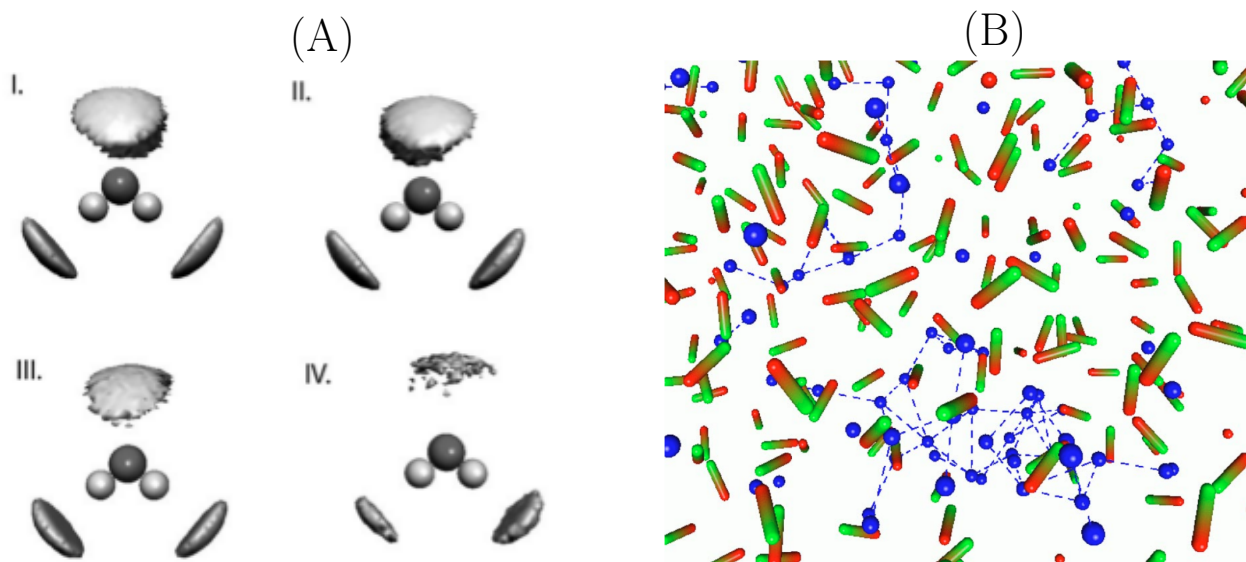


Figure 1.17 At (A) the gray lobes represent the spherical distribution function of water molecules around a central water molecule at $r_{Ow...Ow} \leq 3.5$. The cases I,II,III and IV represent methanol fractions of $x_m = 0, 0.1, 0.5$ and 0.9 respectively [17]. At (B) is shown a water-methanol mixture with methanol fraction of 0.70 . The blue spheres represent the water oxygen atoms and sticks represent the methanol molecules. Dashed blue lines indicate the hydrogen-bonding [18].

mixture. In general terms, the model proposed in the reference [19] is based on the fit the cross interaction parameters from the experimental excess properties over the whole composition range. The fit procedure was made expressing the dependence of the h^E and v^E with the composition through the Taylor expansion. With these values, they develop a force-field that can precisely reproduce the thermodynamic properties of the methanol-water system for any composition. The results of this model can be shown in the figure 1.18. The mixture rules added with the new force-field reproduce quantitatively well the excess enthalpy and volume (for volume see the reference [16]), while the excess isobaric molar heat capacity exhibits a quantitative agreement only for low solute fractions. Based on the success of their model on the describing the excess thermodynamic of the mixture, they studied the variations in the TMD (see figure 1.19). In the figure 1.19 we observe that the model has not the same success on the description the shift in the TMD. In all models studied by then, the shift in the TMD ΔT , are in disagreement with experimental behavior in the temperature, exhibiting deviations amounting to about 300% at $x_2 = 0.05$.

Front of the difficult to reproduce the excess thermodynamic and the variations in the TMD of water by the classical atomistic models and added to this, the high computational

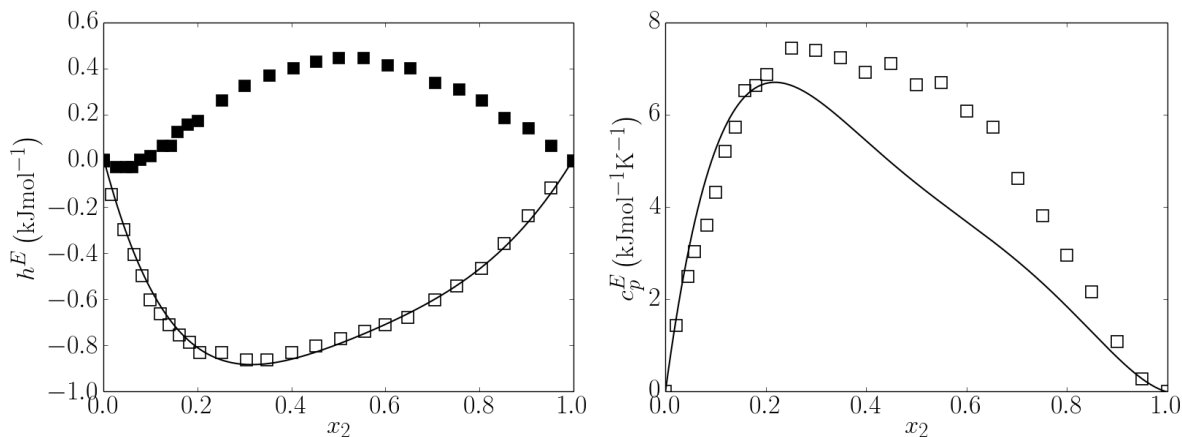


Figure 1.18 (Left) excess enthalpy for the water methanol mixture and (Right) excess isobaric molar heat capacity c_p^E . Filled squares correspond to simulations with the Lorentz-Berthelot combining rules for the water-methanol interactions and empty squares are results obtained with the model developed in this reference [19]. Full line represent experimental data in both figures.

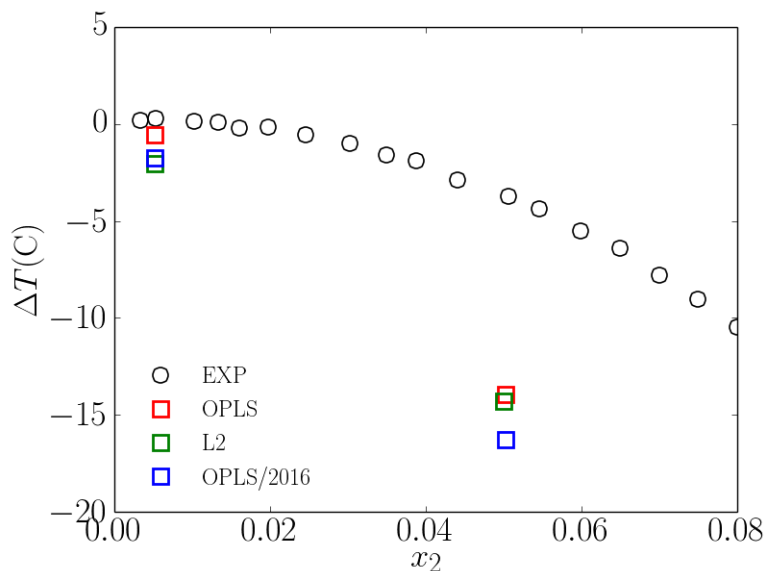


Figure 1.19 Difference ΔT between the TMD of the mixture and that of pure water plotted as a function of methanol mole fraction x_2 . Simulation results for the OPLS+TIP4P/2005, the L2+TIP4P/2005, and the OPLS/2016+TIP4P/2005.

cost of these models, different alternative have been proposed, among them, the simplified models with effective potentials assume an essential role. In this approach, the water is frequently represented by the potentials mentioned in the Section 1.1, whereas the alcohol particle are represented by a chain formed by attractive and repulsive sites. For the methanol for example (the most simple alcohol molecule) the molecule is frequently represented by a dimer, in which one of the particle of dimer represent the methyl group and other represent the hydroxyl group. In this approach different combinations of hydroxyl-methyl potentials have been proposed. Using a Jagla [7] like potentials for the hydroxyl group and a hard sphere potential for methyl group, Su *et. al.* [77] obtain, for a set of parameters studied, a good agreement of excess volume with experimental (see figure 1.20) however, for TMD, their results diverge of the behavior expected for water-methanol mixture [14]. Some of the discrepancies, the authors attribute to the potential used to methanol-like particles, was the same of water particles.

In a similar direction, Su *et.al* studied the mixture of water and alcohol where the alcohol is represented by an amphiphilic dimer. The idea of this paper is to reproduce the methyl group of an alcohol by a repulsive particle of the dimer and the hydroxyl group of by an attractive particle of the dimer. The water particles are modeled by a sphere represented by a Jagla potential [7]. In this approach different combinations of hydroxyl-methyl potentials have been proposed. Using a Jagla [7] like potentials for the hydroxyl group and a hard sphere potential for methyl group, Su *et. al.* [77] obtain, for a given set of parameters studied, a good agreement of excess volume with experimental result (see figure 1.20), where the excess volume exhibits a minimum at fractions of $\varphi = x_2 = 0.5$ as shown also in the figure 1.15(B). This result reflects that despite the simplicity, the universal ingredients that give origin to the minimum in the excess volume are captured by the model. The same thing does not happen with the TMD. The variations ΔT in relation to the pure water show negative values, diverging of the behavior expected for water-methanol. The authors attribute the discrepancies between experiment and model to the similarities between potential used to represent the distinct species of the system. Similar idea was explored by Hus *et. al.* [78,79], where the hydroxyl group and water particles are modeled by CS potentials and the methyl group is represented by Lennard-Jones potential. They observe a good agreement with the excess volume but the for enthalpy, the behavior of the model is somewhat different of experimental data. They also studied the effects of methanol on TMD of the model, and differently of reference [77], they obtain a qualitative behavior, similar to experimental results [14].

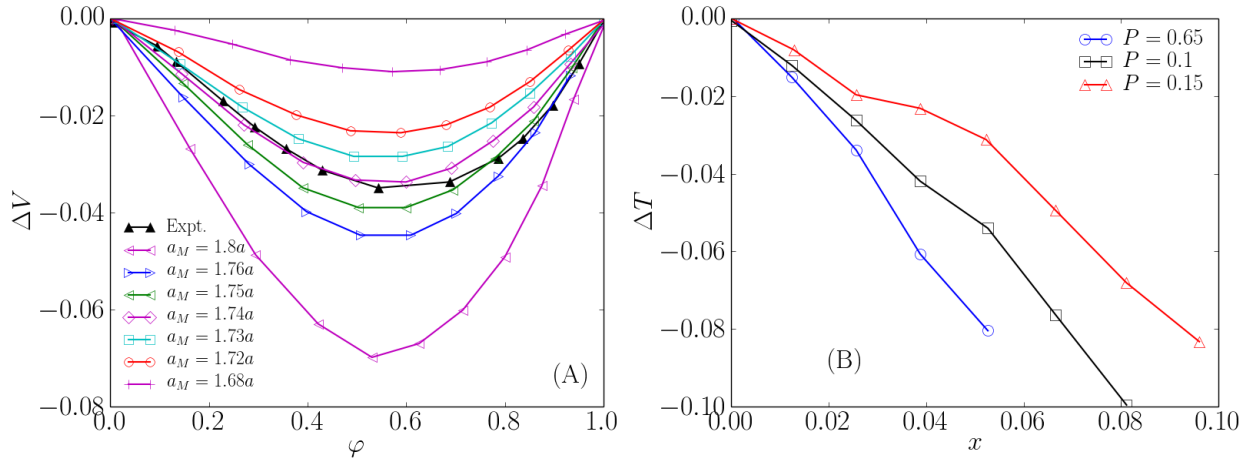


Figure 1.20 At (A) The excess volume versus methanol volume fraction. Symbols represent simulation data and solid lines are guides of eyes. At (B) variation of TMD versus the methanol fraction at different pressures. Methanol fraction of mixture, at different pressures.

Given the impossibility to obtain a universal argument that connect the changes in the excess thermodynamic and the shape of the interaction parameters, Fujihara *et. al.* [80] studied the excess thermodynamic behavior for a mixture of LJ particles subject to different mixture rules. They adopted four distinct cases given by

$$\epsilon_{12}^A = \epsilon_{11} \quad \text{A(association)} \quad (1.2)$$

$$\epsilon_{12}^{LB} = (\epsilon_{11} \times \epsilon_{22})^{1/2} \quad \text{LB(Lorentz - Berthelot)} \quad (1.3)$$

$$\epsilon_{12}^{ID} = \frac{(\epsilon_{11} + \epsilon_{22})}{2} \quad \text{ID(quasi - ideal)} \quad (1.4)$$

$$\epsilon_{12}^S = \epsilon_{22} \quad \text{S(solvation)} \quad (1.5)$$

$$(1.6)$$

where the subindex 1 and 2 represent the specie of the particle involved in the mixture and $\epsilon_{12}^A < \epsilon_{12}^{LB} < \epsilon_{12}^{ID} < \epsilon_{12}^S$. In the Figure 1.21(A) is shown the excess volume. Just the case A the excess volume is able to assume positive values, but its absolute value is four times lower than that of the case S for example. The excess volume curves are so negative the higher the cross interactions. It can be understood through the argument that with more strong cross-interactions, particles of different types will be more close, reducing the volume of the mixture in relation to the ideal mixture. In relation to the excess enthalpy, the effects of the temperature are more modest and the cases LB and ID have a behavior

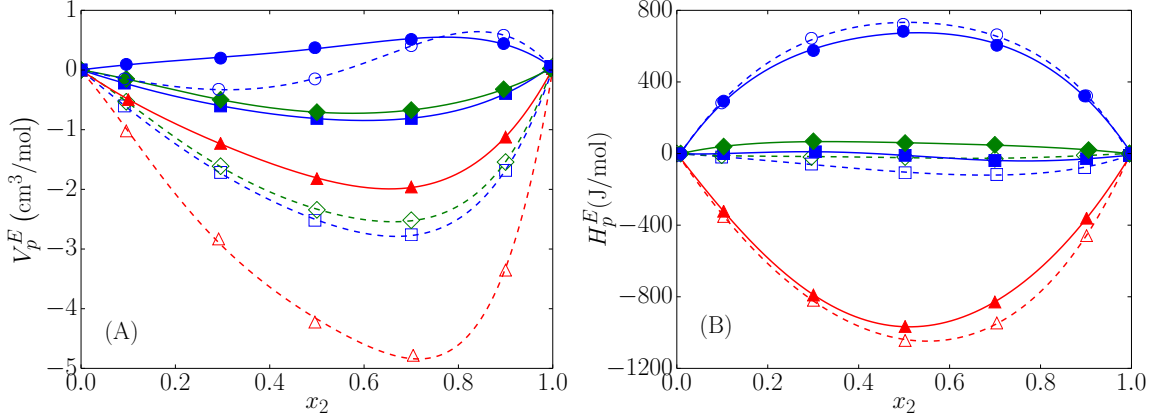


Figure 1.21 (A) V_p^E and (B) H_p^E . Filled markers and solid lines represent $T = 90\text{K}$ and $p = 0\text{MPa}$. Open markers and dashed lines represent $T = 100\text{K}$ and $p = 0\text{MPa}$. Blue circles represent association (A), green diamonds represent Lorentz-Berthelot (LB), blue squares represent quasi-ideal(ID) and red triangles solvation(S).

almost ideal. The maximum value assumed in these cases is 66J/mol . For the cases A and S the system show a strong non-ideal behavior, assuming a parabolic behavior. Although of very generic, the results showed above show a tendency of how the excess properties of a binary mixtures changes as function of the attractive part of interaction potential.

1.4 Objectives and organization of the thesis

This thesis is divided in two parts characterized by two distinct problems. In the first part we dedicate to understand the changes in the thermodynamic, dynamic and structural properties of a lattice water-like model when it is subject to a disorder. The disorder adopted here is a random quenched disorder, commonly referenced by porous media. In this part we obtain the phase diagram of system and study the critical, dynamical and thermodynamical properties of system for different densities of the disorder/obstacles. The details and results of this work can be seen in the Chapter 2 and were published in the reference [81].

The second part we studied the properties of mixture of water models and different solutes. In this part we divided in two different approaches, for the first we studied the effect of the attractive and repulsive interactions in the excess properties of a water-solute mixture. Here, both water and solute, are represented by a three-dimensional lattice model. The details and results for this part of work can be seen in the Chapter 3 and were published in the reference [82]

The third part of this thesis and then the third Chapter, we extend our study about the aqueous mixtures studying the effects of size of solute in the excess properties of the system. In this work use a two length scale potential to model the water and dimers represented by a repulsive particle and CS particle. We studied here, two solutes, one with a big hydrophobic particle and other with a small hydrophobic particle. The details and results for this part of work can be seen in the Chapter 4 and are submitted to publication on the Journal Chemical Physics.

After these three chapters we ends this thesis with the general conclusions shown in the Chapter 5 and one appendices for explain with more details some thecniques used in this thesis.

Chapter 2

Influence of disordered porous media on the anomalous properties of a simple water model

The thermodynamic, dynamic and structural behavior of a water-like system confined in a matrix is analyzed for increasing confining geometries. The liquid is modeled by a two dimensional associating lattice gas model that exhibits density and diffusion anomalies, in similarity to the anomalies present in liquid water. The matrix is a triangular lattice in which fixed obstacles impose restrictions to the occupation of the particles. We show that obstacles shortens all lines, including the phase coexistence, the critical and the anomalous lines. The inclusion of a very dense matrix not only suppress the anomalies but also the liquid-liquid critical point.

2.1 The Model

The ALG model is defined in a triangular lattice, in which each accessible site i can be empty or occupied by a water molecule. Empty sites have $\sigma_i = 0$ while occupied sites have $\sigma_i = 1$. Each water molecule has orientational states represented by the variable τ that presents six arms, being two inert arms with $\tau_i = 0$ and four active arms with $\tau_i = 1$. They represent the possibility of a molecule to form hydrogen bonds with up to four neighbor

molecules. The two inert arms are diametrically positioned, in such a way that there are just three different orientational states. Fig. 2.1 exemplifies the geometry of the model.

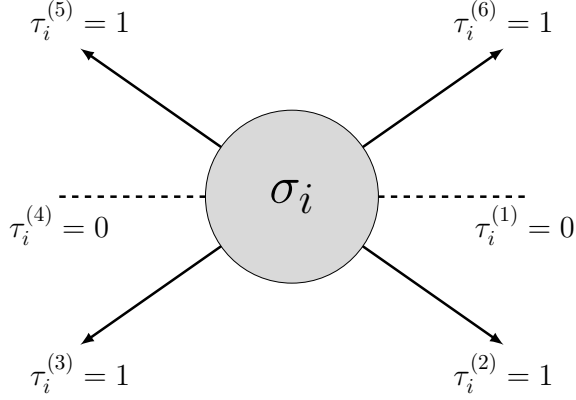


Figure 2.1 The occupational and orientational states of a molecule at the site i . The arms variables are: $\tau_i^{(1)} = 0$, $\tau_i^{(2)} = 1$, $\tau_i^{(3)} = 1$, $\tau_i^{(4)} = 0$, $\tau_i^{(5)} = 1$, $\tau_i^{(6)} = 1$.

A bond is formed only when the active arms of two neighbor molecules point out to each other, namely $\tau_i \tau_j = 1$. In this case, the interaction energy between two bonded arms reads $-v$ while non bonded arms contribute with a higher energy of $-v + 2u$ (punishment for non forming hydrogen bonds). The Hamiltonian of the system is given by

$$\mathcal{H} = 2u \sum_{\langle i,j \rangle} \sigma_i \sigma_j \left[\left(1 - \frac{v}{2u} \right) - \tau_i \tau_j \right] - \mu \sum_i \sigma_i . \quad (2.1)$$

The phase behavior of the system in the absence of obstacles was already analyzed in a previous publication [51] and it is reviewed as follows. At ground state, $T^* \equiv T/v = 0$, the grand potential per site is $\Phi = e - \mu N$ where $e = \langle \mathcal{H} \rangle / L^2$. At low chemical potentials, the lattice is empty and the system is constrained in gas phase, $\rho = 0$. In this phase the grand potential is $\Phi_{GAS} = 0$. Increasing the chemical potential the system reaches a point at which the gas phase coexists with a low density liquid phase (LDL). In this phase, the density is $\rho = 3/4$ and each particle forms four hydrogen bonds with its neighbors, resulting in a grand potential per site $\Phi_{LDL}/L^2 = -(3/2)v - (3/4)\mu$ and consequently in a gas-LDL coexistence chemical potential $\mu_{G-LDL}^* = \mu_{G-LDL}/v = -2$. For high chemical potentials, all sites of lattice are occupied by particles, resulting in a density $\rho = 1$ and grand potential per site $\Phi_{HDL}/L^2 = -3v + 2u - \mu$. The coexistence between the LDL phase and the HDL phase occurs at $\mu_{LDL-HDL}^* = \mu_{LDL-HDL}/v = 8u/v - 6$. The main features of LDL and HDL phases are exemplified in Fig. 2.2 for two possible configurations at $T^* = 0$.

At temperatures $T^* \equiv T/k_B v > 0$, the model was also already analyzed by Monte Carlo simulations [51]. The chemical potential versus temperature phase diagram is shown in the Fig. 2.3(a).

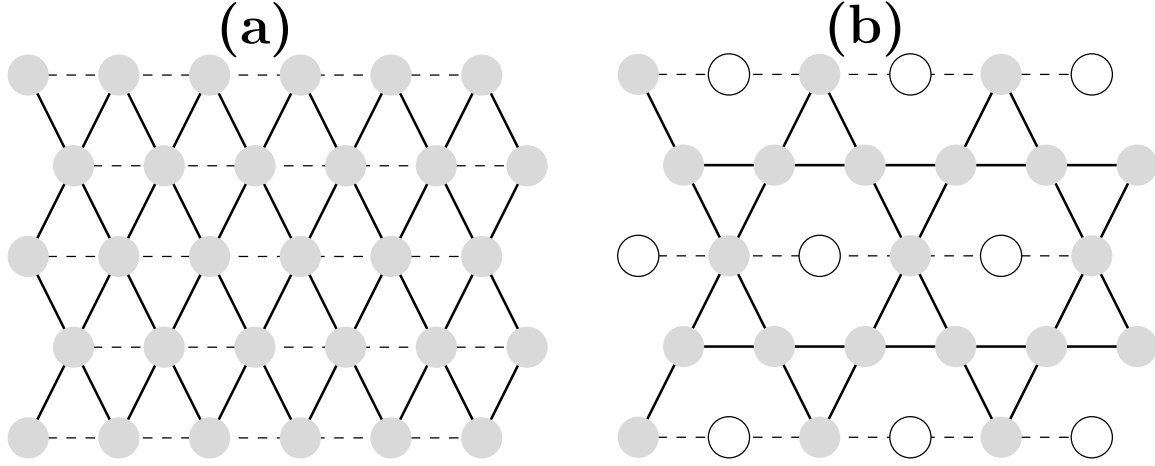


Figure 2.2 Examples of a configuration for the HDL (a) and LDL (b) phases for the Associating Lattice Gas (ALG) model. The solid and dashed lines indicate the bonding and inert arms, respectively.

The gas-LDL and LDL-HDL transition lines are first-order transitions, ending in respective the tricritical points T_{c1}^* and T_{c2}^* , respectively. These two tricritical points are connected by a line of continuous transitions, the λ -line. For the ALG model with no obstacles the tricritical temperatures, $T_{c1}^* = 0.65$ and $T_{c2}^* = 0.65$, respectively. In order to understand the differences between the LDL and HDL phases, the lattice as shown in the Fig. 3.2(a) is divided in four sublattices as illustrated in the Fig. 3.2(b). The LDL phase is characterized by one of the sublattices being empty while all the others are filled, in such a way that the transition to the HDL phase occurs when the empty sublattice is filled. Also, it is signed by a rotation in the inert arms, in which in the HDL phase they are all parallel. In the LDL phase, each particle forms four bonded arms that show a zigzag structure, whereas in the HDL phase each particle also forms four bonded arms but with parallel lines.

The density of bonds, is also an important quantity for characterizing the phase transitions and can be obtained by

$$\rho_{hb} = \frac{1}{L^2} \sum_{i=1}^{L^2} \sum_{i+\delta} \sigma_i \sigma_{i+\delta} \tau_i \tau_{i+\delta}. \quad (2.2)$$

At $T^* = 0$ the gas, LDL and HDL phases has ρ_{hb} reading 0, 1.5 and 2, respectively. Thus the phase transitions are also signed by changes in the fraction of hydrogen bonds. At very high temperature the system is disordered. The sublattice occupations do not exhibit any

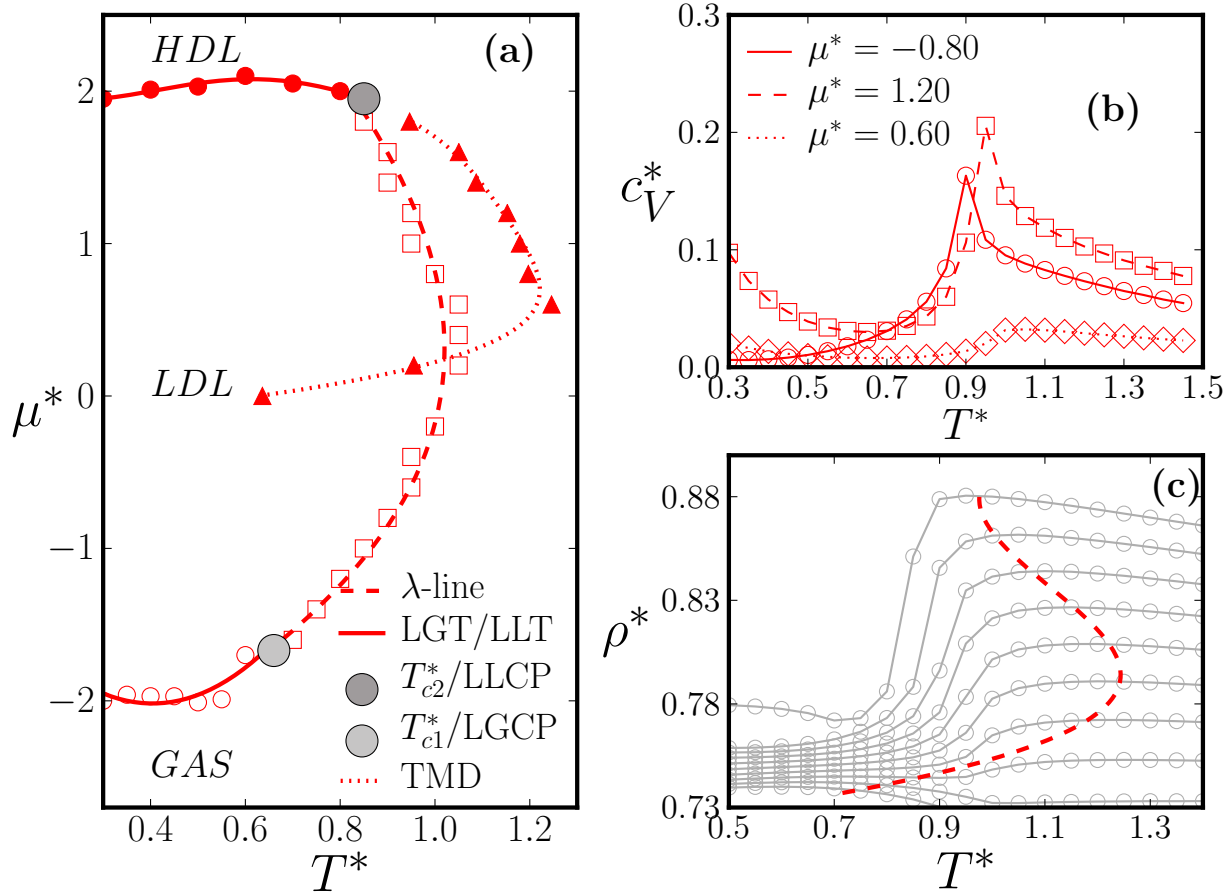


Figure 2.3 For the ALG model, panel (a) shows the phase diagram μ^* vs T^* , illustrating the gas-LDL (empty circles) and the LDL-HDL (filled circles) phase transitions, the λ -line (empty squares) and the TMD line (filled triangles). In panel (b) we plot the c_V^* versus T^* for $\mu^* = -0.80$ (circles), $\mu^* = 0.60$ (diamonds) and $\mu^* = 1.20$ (squares). In (c) the system density ρ versus T^* for fixed μ^* along the TMD line (dashed line).

ordering. By lowering T^* , the λ -line is crossed, which one sublattice is emptied and the others remaining filled with a reorganization of the inert arms that form the above ordered zig-zag structure. This the λ -line transition is identified by the peak of the specific heat at constant volume c_V [51].

In this work the disordered porous media is introduced by considering fixed obstacles that are randomly distributed in the lattice. Each obstacle occupies a single site and interacts with the particles via a “hard core” constraint. The density of obstacles is given by $\rho_o = N_o/L^2$ where N_o is the number of obstacles and L^2 is the system volume. In Fig. 3.2(a), a lattice configuration composed of water, obstacles and empty sites is exemplified.

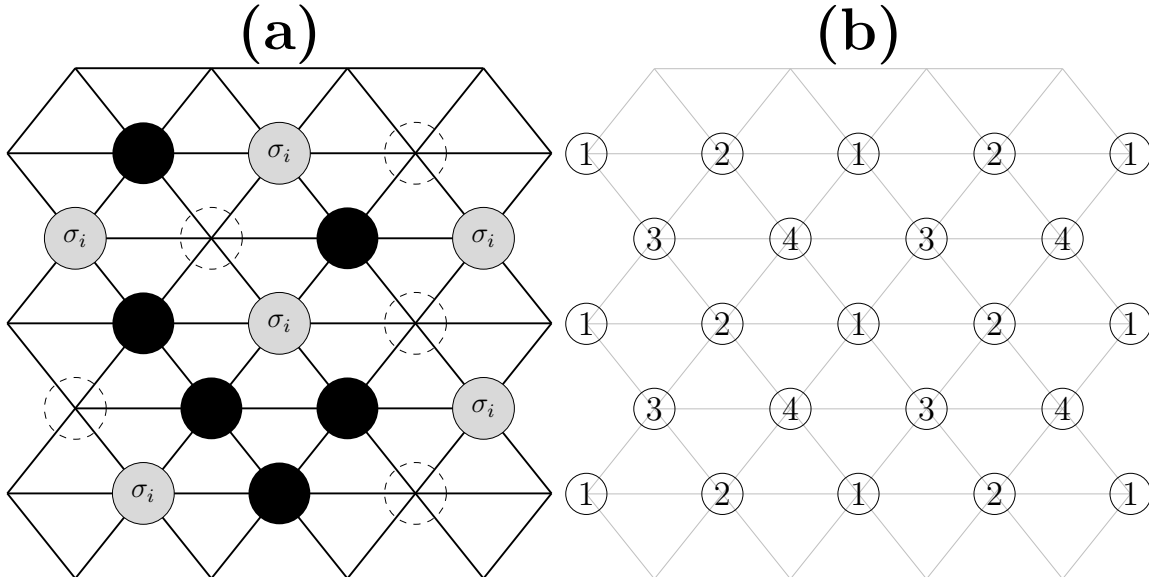


Figure 2.4 (a) shows a lattice configuration where the solid gray, the solid black and the dashed circles describe water molecules, obstacles and empty sites respectively. For clarity, the bonds are not shown. (b) shows a lattice configuration with the subdivision in four sublattices.

2.2 The Methods and Simulation Details

Numerical simulations have been performed for the triangular lattices of size $L = 35$ and periodic boundary conditions. Three representative values for the density of obstacles $\rho_o = 0.08, 0.24$ and 0.40 have been considered.

In all cases, we have used 10^6 Monte Carlo (MC) steps to equilibrate the system and 10^6 MC steps for evaluating the relevant quantities. Each Monte Carlo step is defined as the number of L^2 trials for generating new configurations, including the choice of empty sites and water molecules. Additional simulations for $L = 24, 35, 40, 56$ and 80 and finite size scaling analysis were performed in order to study the critical lines and to test size effects in the porosity.

All the thermodynamic properties have been obtained by performing grand canonical Monte Carlo (MC) simulations for fixed $T^*, \mu^* \equiv \mu/v$ and ρ_0 [47]. Microscopic configurations are generated according to the Metropolis algorithm [83] described as follows. First, the obstacles are randomly distributed. Then, a site k not occupied by an obstacle is randomly selected. If the site k is not occupied, an attempt to occupy the site with a water molecule in a randomly selected arm orientation is made. If the site k is already occupied by a water molecule one of the following actions are tried: to empty the site or to change

the arm configuration of the water molecule to one of the other two possible states. Next, to accept or not the attempts to change the site occupation, the energy difference $\Delta\mathcal{H}$ between the original and the new configuration is computed. The configuration change is accepted according to the Metropolis prescription $\min\{1, e^{-\beta\Delta\mathcal{H}}\}$, where $\beta = 1/k_B T$. As mentioned previously, this process is first repeated 10^6 times without computing and after this, thermodynamic quantities are averaged over 10^6 Monte Carlo steps.

Some remarks over the obstacles distributions are required. In principle, a random distribution might lead to statistical problems. According to some works [84,85], systems with random disorder lose the self-averaging and averages over many distributions of obstacles are required. However, this affects mainly the computation of critical temperatures and exponents. In the present case, by performing tests with different random distributions of obstacles, we have verified that the tested temperatures and chemical potentials led to results not sensitive to the specific distribution of obstacles. Then, for simplicity only one random distribution was employed. For calculating the critical λ -line, we considered the peak of the specific heat at constant volume, given by

$$c_V = \frac{1}{VT^2} \left[\langle \delta\mathcal{H}^2 \rangle_{\text{gcan}} - \frac{\langle \delta\mathcal{H}\delta N \rangle_{\text{gcan}}^2}{\langle \delta N^2 \rangle_{\text{gcan}}} \right] + \frac{3Nk_B}{2V} \quad (2.3)$$

where $\delta X = X - \langle X \rangle$ with $X = \mathcal{H}$ and N and averages are evaluated in the ensemble of T, μ fixed. The chemical potentials and temperatures of the λ -line were obtained through the finite size scaling analysis of c_V employing $L = 24, 35, 40, 56$ and 80 .

In addition to the thermodynamic quantities, the influence of obstacles in the dynamic properties was also investigated. Since we perform Monte Carlo simulations, the dynamics is characterized through the diffusion coefficient D given by Einstein's relation

$$D = \lim_{t \rightarrow \infty} \frac{\langle \Delta r(t)^2 \rangle}{4t}, \quad (2.4)$$

where $\langle \Delta r(t)^2 \rangle = \langle (r(t) - r(0))^2 \rangle$ is the mean square displacement per particle and time is measured in Monte Carlo steps. Although the diffusion coefficient (measured under Monte Carlo simulations) is a stochastic dynamics and not a real space mobility, it is possible to associate the former with the concept of diffusion anomalous like the behavior observed in liquid water [52]. The numerical MC procedure for calculating the diffusion is described as follows. First, the system is equilibrated by employing the previous Metropolis dynamics for fixed T^* and μ^* . After the equilibrium is reached, an occupied site i and its neighbor

j are chosen randomly. In case of neighbor site j be empty, the molecule moves to the empty site also following the above Metropolis prescription $\min\{1, e^{-\beta\Delta\mathcal{H}}\}$, where $\Delta\mathcal{H}$ is the difference of energy due to the movement. A Monte Carlo step t is defined through the number of trials of movement for all system particles. After repeating this algorithm nt times, where n is the number of molecules in the lattice, the diffusion coefficient is calculated from Eq.(2.4). Here we employ $t = 800$ for the evaluations.

2.3 Results

2.3.1 Structural and thermodynamic behavior

First, let us exam what happens with the phases present in the system as the obstacles are introduced. Fig. 2.5 shows the water density ρ , versus the reduced chemical potential μ^* , for distinct porous densities at the fixed temperature $T^* = 0.40$. Figure 2.5 also shows that for $T^* = 0.40$ the gas-LDL phases exhibits a smaller hysteresis loop when compared with the LDL-HDL transition. This indicates that the gas-LDL free-energy barrier is smaller than the LDL-HDL barrier. This also reflects in the difference between the gas-LDL critical temperature, T_{c1}^* , that is smaller than the LDL-HDL tricritical temperature, T_{c2}^* . The size of the hysteresis loops change with the temperature and lattice size but in all the analyzed cases the gas-LDL is much smaller than the LDL-HDL loop.

The inclusion of obstacles changes the temperature and chemical potential locations of the gas-LDL and the LDL-HDL phase transition. In particular, the increase in the number of obstacles leads to the disruption of the hydrogen bonds, decreasing the free-energy barriers separating the coexisting phases. This explains the decrease in the hysteresis loop when obstacles are included. In addition, the density gap between the two liquid phases becomes less abrupt and the inclusion of obstacles moves the transition points to larger chemical potentials.

Figs. 2.6, 2.7 and 2.8 illustrate the chemical potential versus temperature phase diagrams for $\rho_o = 0.08, 0.24$ and 0.40 , respectively. In particular, by increasing ρ_o the tricritical points T_{c1}^* and T_{c2}^* , in which the gas-LDL and LDL-HDL coexistence lines meet the λ -line, decreases as shown in Figs. 2.6 , 2.7 and 2.8. More specifically, while for the system without obstacles the gas-LDL tricritical point is located at $T_{c1} = 0.65$, it moves to $T_{c1}^* = 0.60, 0.55$ and 0.52 for $\rho_o = 0.08, 0.24$ and 0.40 , respectively.

This scenario becomes even more drastic in the case of the LDL-HDL phase transition. The tricritical point not only decreases its value from $T_{c2}^* = 0.825$ (no obstacles) to $T_{c2} =$

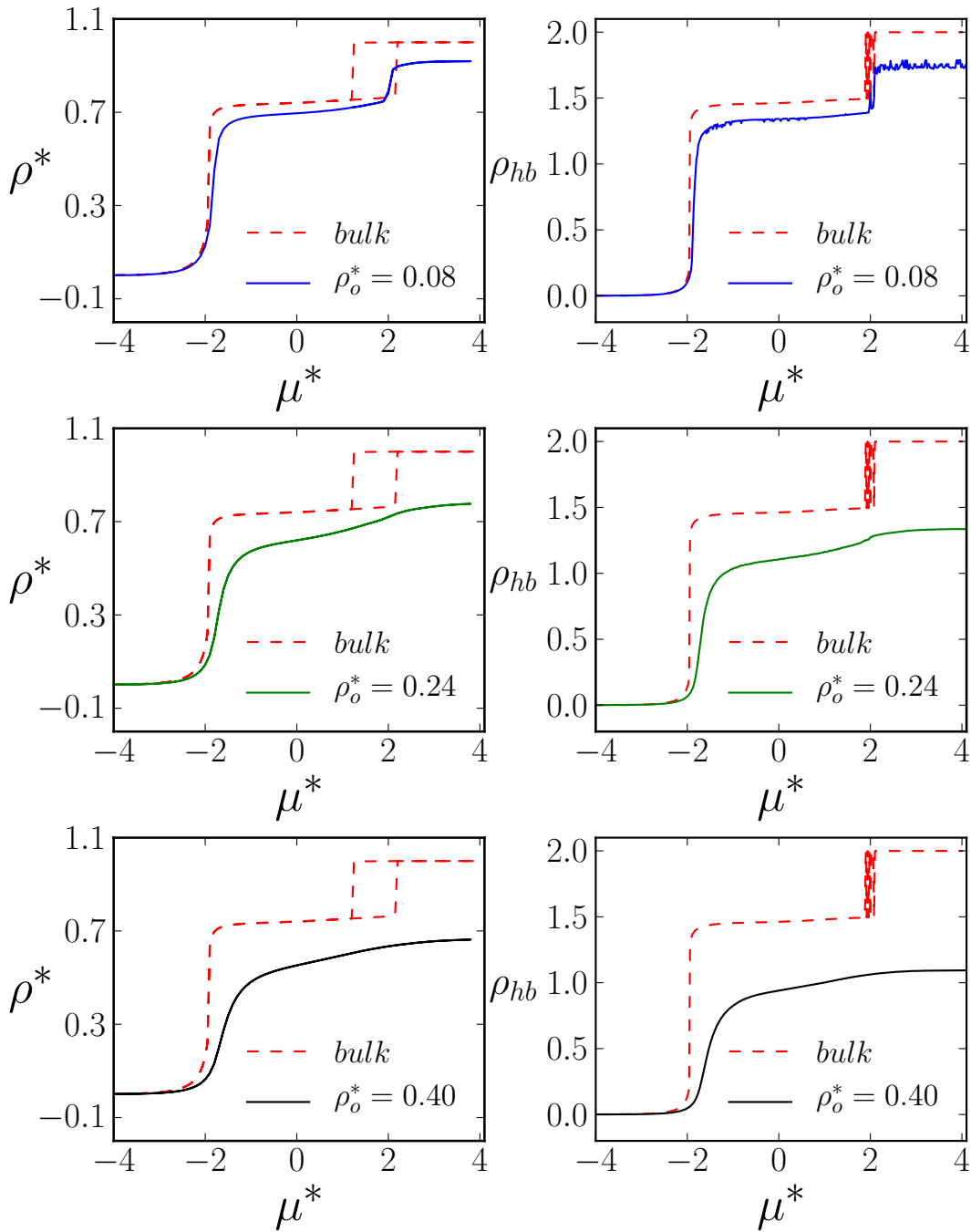


Figure 2.5 ρ vs μ^* for distinct porous densities ρ_o for $T^* = 0.40$.

0.57 and $T_{c2} = 0.52$ for $\rho_o = 0.08$ and 0.24, respectively but the critical line disappears for $\rho_o = 0.40$, implying the absence of liquid-liquid transition line.

The changes in the transition points can be understood by verifying that the inclusion

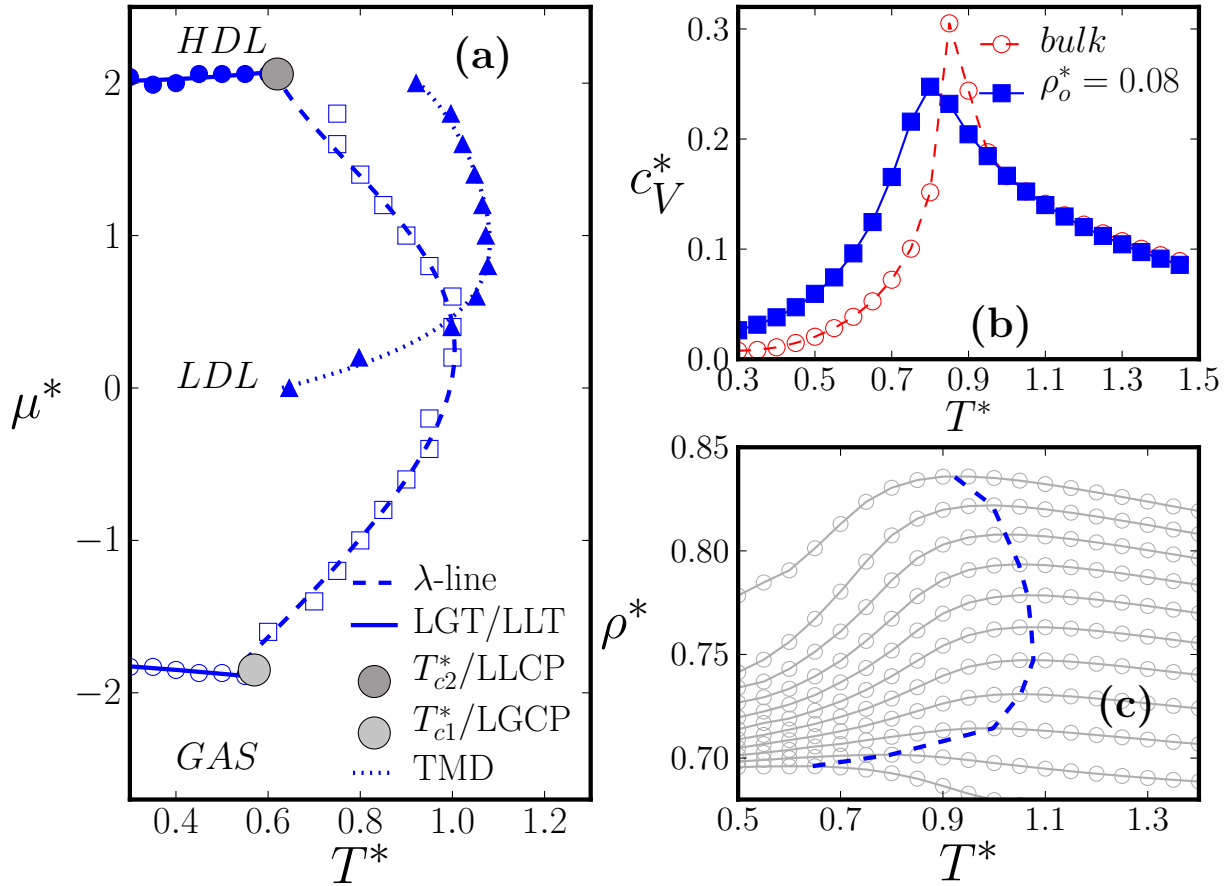


Figure 2.6 For $\rho_o = 0.08$: (a) Chemical potential μ^* versus reduced temperature T^* phase diagram showing the Gas-LDL (empty circles), the LDL-HDL (filled circles) phase transitions, the λ -line (empty squares) and the TMD line (filled triangles). (b) Specific heat at constant volume c_V^* versus T^* for the system with obstacles (filled squares) and system with no obstacles (empty circles) at $\mu^* = -1.00$. Panel (c) ρ versus T^* for $\mu^* = 0.0, \dots, 2.2$ showing the TMD line (dashed line).

of obstacles suppress partially the structured patterns found in the LDL and HDL phases (see e.g Fig. 2.2(a) and (b) for the zero obstacle system). In the case of the LDL phase the ordered structure is distorted as ρ_o increases, as illustrated in the Fig. 2.9 for $\mu^* = -0.5$. For the lowest case $\rho_o = 0.08$, the degree of confinement is low and most occupied sites preserve at least three bonds. As ρ_o is raised (here exemplified for $\rho_o = 0.24$ and 0.40) the fraction of disrupted bonds increases, reaching a limit in which the connectivity of the network is lost. Similar effect is verified in the HDL phase, but the effect is more pronounced in such case. This can be understood by recalling that in the LDL phase, obstacles occupy partially empty sites with neighboring molecules not forming hydrogen

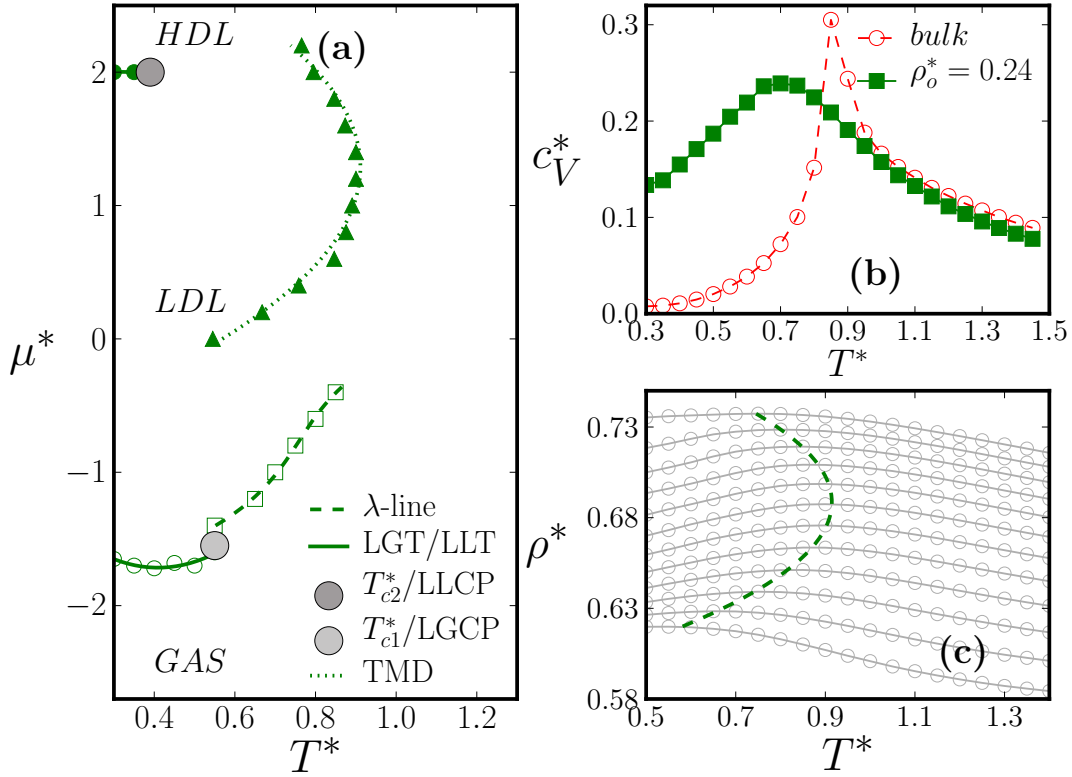


Figure 2.7 For $\rho_o = 0.24$: (a) Chemical potential μ^* versus reduced temperature T^* phase diagram showing the Gas-LDL (empty circles), the LDL-HDL (filled circles) phase transitions, the λ -line (empty squares) and the TMD line (filled triangles). (b) Specific heat at constant volume c_V^* versus T^* for the system with obstacles (filled squares) and system with no obstacles (empty circles) at $\mu^* = -1.00$. Panel (c) ρ versus T^* for $\mu^* = 0.0, \dots, 2.0$ showing the TMD line (dashed line).

bonds. Thus, the disruption of hydrogen bonds is more relevant in the HDL phase.

This lost of connectivity also explains why the transition from the disordered structure to the LDL through the λ -line occurs for lower temperatures when compared with the temperatures obtained for the system with no obstacles. For example, for $\mu = -1$ and distinct obstacle densities $\rho_o = 0.08$ and $\rho_o = 0.24$, analysis of the peak of c_V^* show (in all cases) a scaling with L^{-1} , from which we obtain the critical temperatures $T_c^* = 0.795(1)$ and $0.717(1)$, respectively. These estimates are lower than $0.866(1)$, obtained for the unconfined system. This transition is a order-disorder transition in which one of the sublattices becomes empty while the others are filled, consequently the increase of number of obstacles increases the entropy by breaking bonds what favors disordered phase.

Thus, all transition points, move for lower temperatures as a way for "compensating"

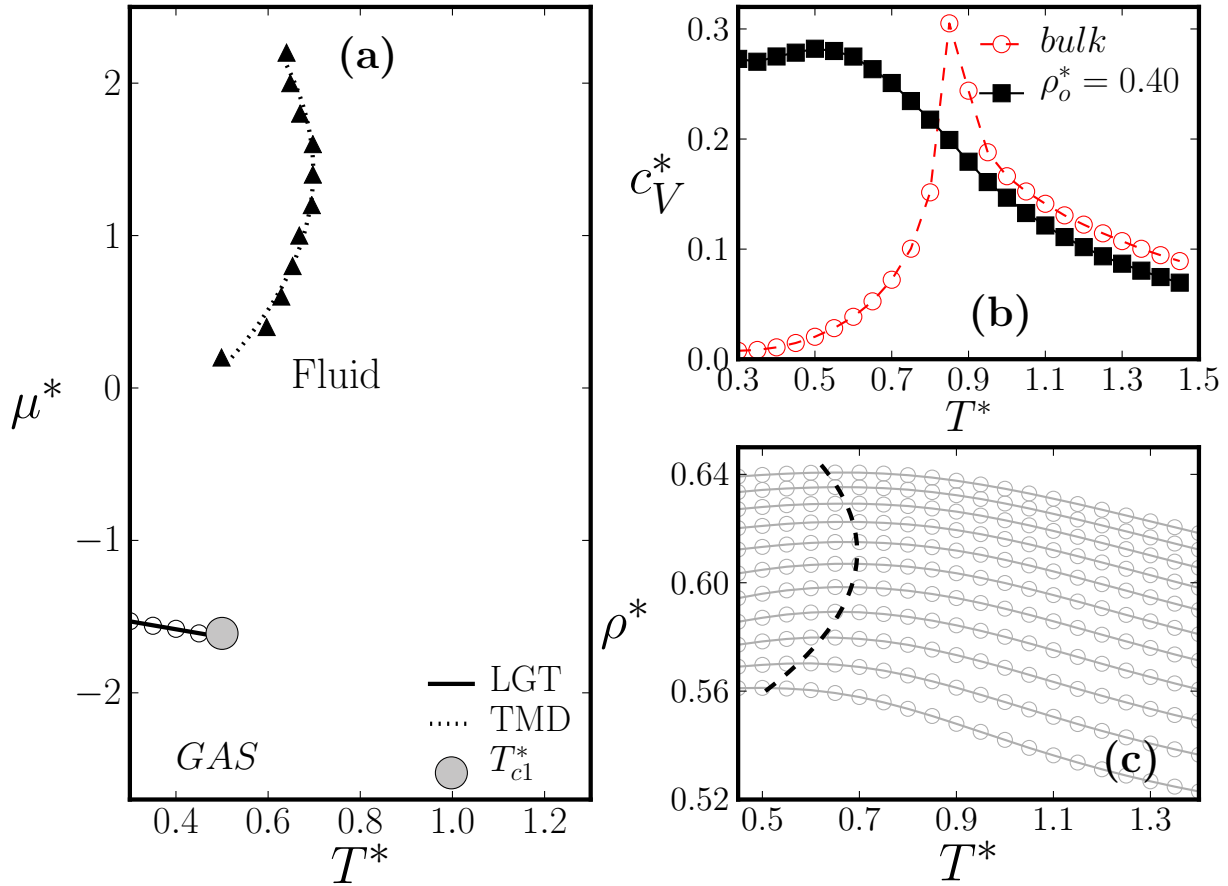


Figure 2.8 For $\rho_o = 0.40$: (a) Chemical potential μ^* versus reduced temperature T^* phase diagram showing the Gas-LDL (empty circles), the LDL-HDL (filled circles) phase transitions, the λ -line (empty squares) and the TMD line (filled triangles). (b) Specific heat at constant volume c_V versus T^* for the system with obstacles (filled squares) and system with no obstacles (empty circles) at $\mu^* = -1.00$. Panel (c) ρ versus T^* for $\mu^* = 0.0, \dots, 2.0$ showing the TMD line (dashed line).

the above increase of disorder. In other words, due to the inclusion of obstacles, the structured phases exist only for lower temperatures than in the unconfined system, whose decreasing become more pronounced as ρ_0 increases. Finally, for high density of obstacles the λ -line transition is destroyed by destroyed of fluctuations. The last comment concerns in the comparison between the TMD as ρ_0 increases, as shown in Fig. 2.10. As for the transition lines, the TMD shortens and move for lower temperatures (with maximum ρ decreasing) as ρ_0 increases. However, in contrast with previous results, for $\rho_0 = 0.40$ a tiny TMD (ranged from $T^* = 0.50$ to 0.70 with $\rho = 0.56$ to 0.64) is verified.

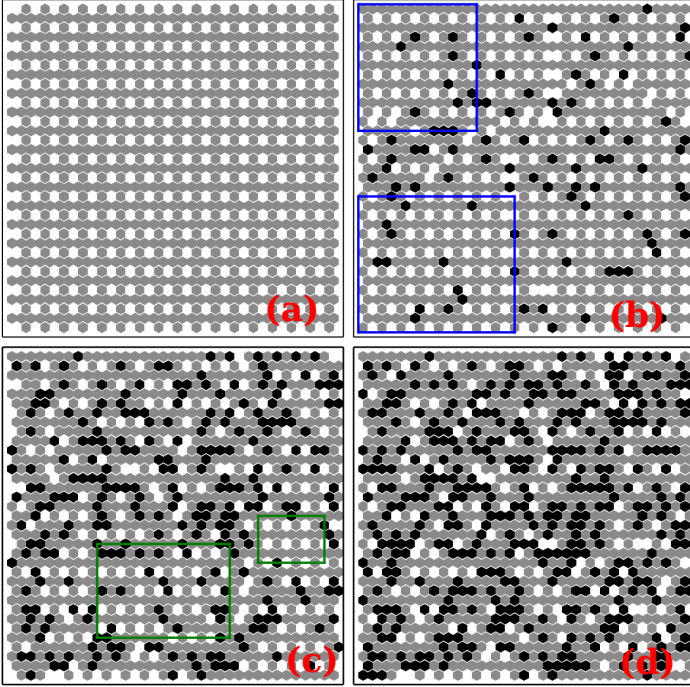


Figure 2.9 Spatial snapshot (35×35 sites) of triangular lattice. Each site is represented by hexagon, with its six nearest-neighbor sites. White hexagons represent vacancies, black hexagons represent obstacles and gray represent water-like particles. The snapshots exhibit character configurations of system with chemical potential $\mu^* = -0.5$ and temperature $T^* = 0.3$. In (a) we present the unconfined system. In (b) the system submitted at low degree of confinement $\rho_o = 0.08$ and the blue rectangles denote the regions where the characteristic geometry of LDL of ALG is preserved. In (c), intermediate degree of confinement $\rho = 0.24$, and green rectangles denote the LDL structure. The highest degree of confinement $\rho = 0.40$ is shown in (d).

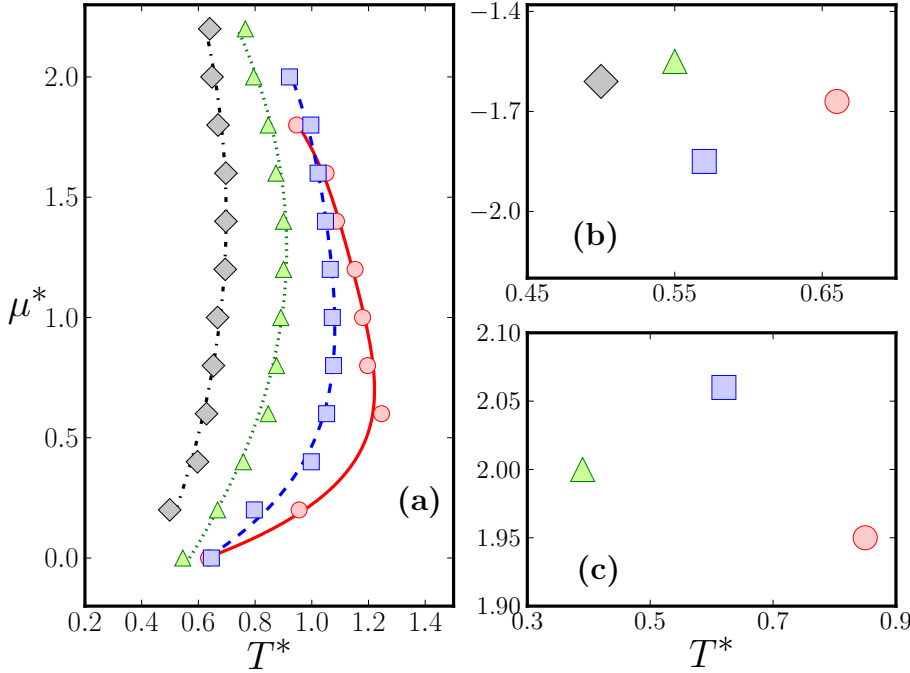


Figure 2.10 Chemical potential versus temperature illustrating (a) the TMD lines (b) the gas-LDL tricritical point (c) the LDL-HDL critical point values for the unconfined (circles) and the system with different concentrations of obstacles. The symbols squares, triangles and diamonds correspond to the $\rho_o = 0.08, 0.24$ and 0.40 , respectively.

2.3.2 Diffusion and dynamic anomaly

Besides the influence of the immobile obstacles in the thermodynamic quantities, another relevant question concerns what happens with the water mobility as the density of obstacles increases.

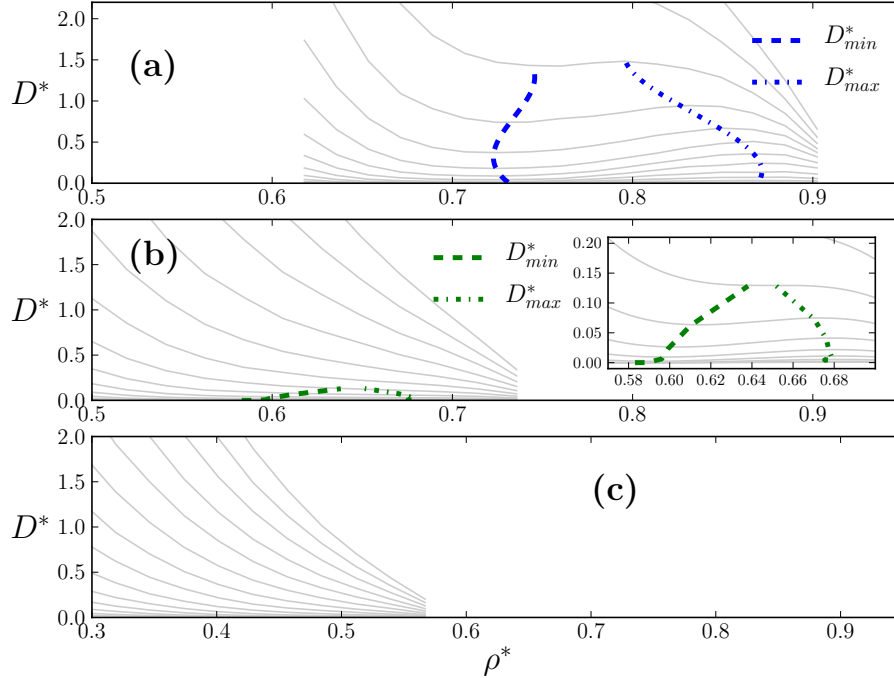


Figure 2.11 Diffusion coefficient versus density at fixed temperatures for: (A) $\rho_o = 0.08$, (B) $\rho_o = 0.24$ and (C) $\rho_o = 0.40$. The solid gray lines are the values of the diffusion coefficient for $T^* = 0.30 \dots 1.00$ with $\Delta T^* = 0.05$ (from bottom to top), the blue dashed and dot-dashed lines connect the minimum and maximum in D respectively.

Fig. 2.11 shows the diffusion coefficient computed using Eq. (2.4) for different T^* 's and ρ_0 's. Similarly with what happens for the ALG model with no obstacles, the diffusion coefficient presents a region in densities in which D increases with ρ . This is the so called diffusion anomaly also present in water. The addition of obstacles shrinks the region in temperatures and pressures in which the diffusion anomaly is present and for $\rho_o = 0.40$ no diffusion anomaly is observed.

The dynamic anomaly depends crucially of the presence of a high number of neighbor sites occupied by the fluid [86]. The obstacles make this difficult and for a very high number of obstacles, the mobility becomes even impossible.

Since for water-like systems, typically the region in the μ^*-T^* phase diagram in which the density anomaly is present is close to the region where the diffusion anomaly appears. Therefore one expects that the suppression of the first is directly related to the disappearance of the other.

2.4 Conclusion

The effects of fixed obstacles in thermodynamic and dynamic properties of an simplified water-like model have been investigated. For low degree of confinement, the thermodynamic, structural and dynamic properties of model are almost totally preserved due to the low steric effects. For intermediate case, $\rho_o = 0.24$, the system suffers significant changes such as, the decrease of the critical and tricritical points to lower temperatures, resulting in a reduction of coexistence regions. This effect is more dramatic for the liquid-liquid coexistence that disappear for $\rho_o = 0.40$. The density and diffusion anomalous regions are also shifted to lower temperature, keeping the reduction in temperature-chemical potential phase diagram. The disappearance of the liquid-liquid temperature also reflects in the absence of density and diffusion anomalous regions in the limit of large density of obstacles. Both effects are related to both the entropy increase due to the presence of the obstacles and the disruption of the bonds network.

This work is published at : [Phys. Rev. E **92**, 032404 \(2015\)](#)

Chapter 3

Lattice Model for water-solute mixtures

This chapter is dedicated to N. G. Almarza

In memoriam

A lattice model for the study of mixtures of associating liquids is proposed. Solvent and solute are modeled by adapting the associating lattice gas (ALG) model. The nature of interaction solute/solvent is controlled by tuning the energy interactions between the patches of ALG model. We have studied three set of parameters, resulting on, hydrophilic, inert and hydrophobic interactions. Extensive Monte Carlo simulations were carried out and the behavior of pure components and the excess properties of the mixtures have been studied. The pure components: water (solvent) and solute, have quite similar phase diagrams, presenting: gas, low density liquid, and high density liquid phases. In the case of solute, the regions of coexistence are substantially reduced when compared with both the water and the standard ALG models. A numerical procedure has been developed in order to attain series of results at constant pressure from simulations of the lattice gas model in the grand canonical ensemble. The excess properties of the mixtures: volume and enthalpy as the function of the solute fraction have been studied for different interaction parameters of the model. Our model is able to reproduce qualitatively well the excess volume and enthalpy for different aqueous solutions. For the hydrophilic case, we show that the model is able to reproduce the excess volume and enthalpy of mixtures of small alcohols and amines. The inert case reproduces the behavior of large alcohols such as, propanol, butanol and pentanol. For the last case (hydrophobic), the excess properties reproduce the behavior of ionic liquids in aqueous solution.

3.1 The Model

We consider three systems: pure water, pure solute and water-solute mixture. In the three cases, the system is defined on a body-centered cubic (BCC) lattice. The use of the same model for describing the solvent and the solute aims to: identify that the anomalous properties of these systems are related to the presence of hydrogen bonding and to identify the differences in the behavior of the excess properties with the solute-solvent interaction. In our model sites on the lattice can be either empty or occupied by a water or by a solute molecule. Particles representing both water and solute molecules carry four arms that point to four of the nearest neighbor (NN) sites on the BCC lattice as illustrated by the figure 3.1. The interactions between NN molecules are described in the framework of the lattice patchy models [87]. The particles carry eight patches (four of them corresponding to the arms in the ALG model), and each of the patches points to one of the NN sites in the BCC lattice as illustrated in the figure 3.1. The water molecules have two patches of the type *A* (donors), two patches of the type *B* (acceptors) and four patches of the type *D* (which do not participate in bonding interactions). The patch *D* represents the non-bonding interactions that are usually represented by the short-range van der Waals interaction. Since the patches of the types *A* and *B* participate in the hydrogen bonding, a water molecule can participate in up to four hydrogen bonds. The structure of the solute is similar to the structure of the water, but it has only one patch of type *A*, the other patch *A* is replaced by a patch of the type *C* that represents the anisotropic group which makes water and the solute different. In the case in which the solute is the methanol *C* is the methyl group while for other alcohols and ionic liquids it does represent larger chains.

The distinction between patches implies 12 possible orientations for the water molecules and 24 possible orientations for the solute molecules.

The potential energy is defined as a sum of interactions between pairs of particles located at sites which are NN on the BCC lattice. The interaction between particles *i* and *j*, which are NN, only depends on the type of patch of particle *i* that points to particle *j*, and on the type of patch of particle *j* that points to particle *i*. The values of the interaction as a function of the types of the two interacting patches are summarized in the Table 3.1. The interaction between occupied neighbor sites is repulsive with an increase of energy by $\epsilon_{ij} = \epsilon$ with the exception of three cases. For patch-patch interaction of type *A* – *B* the energy interaction is taken as: $\epsilon_{ij} = -\epsilon$. If the interaction is of type *B* – *C*, with the *B* patch belonging to a solute molecule there is also an attractive interaction $\epsilon_{ij} = -\lambda_S \epsilon$ (with $\lambda_S > 0$), whereas if the patch *B* belongs to a water molecule the interaction energy

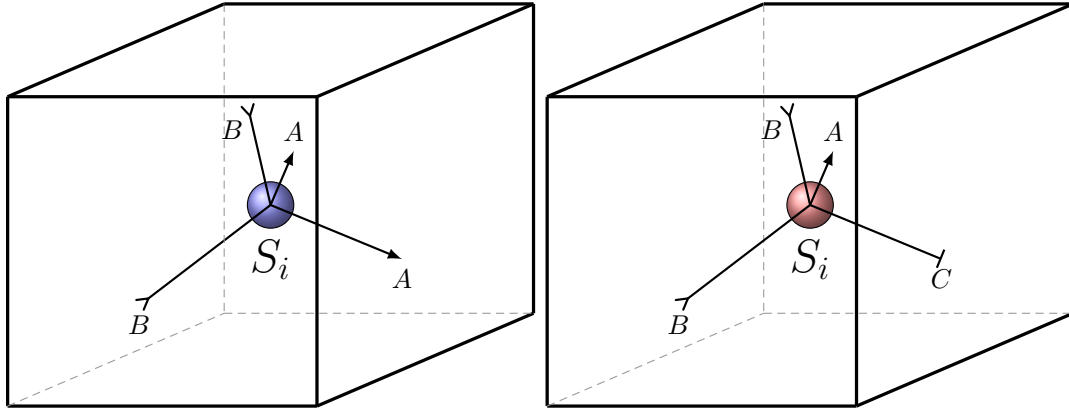


Figure 3.1 Representation of lattice for pure components. The blue sphere represents the water and the patches A and B represent the donors and acceptors arms respectively. The red sphere represent the solute particle and the arms A and B represent the donor and acceptors, and the patch C represents the anisotropic group

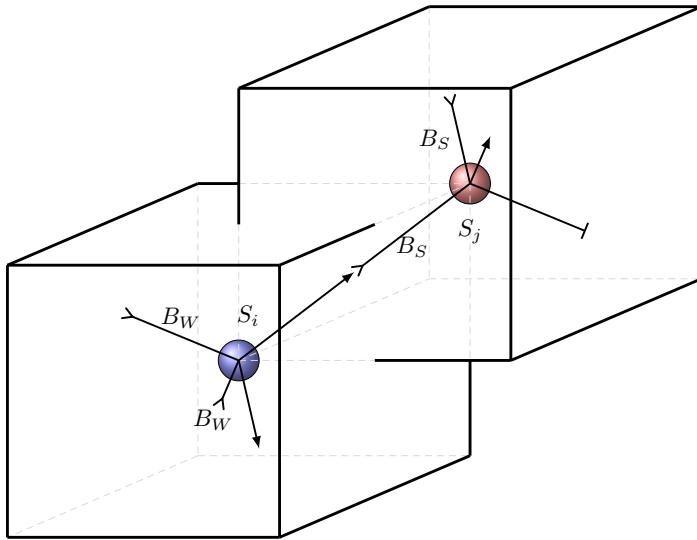


Figure 3.2 Representation of lattice. S_i and S_j represent particle on its respective positions i and j . Blue sphere represent a water and red, a solute particle. B_W and B_S represent the patches B of water and solute respectively. The patch D is not represented here for the clarity of the image.

is given by $\epsilon_{ij} = -\lambda_W \epsilon$.

We have considered $\lambda_S = 0.25$, and three cases for the B - C water-solute interaction: attraction with $\lambda_W = \lambda_S$, non-interacting with $\lambda_W = 0$ and repulsion with $\lambda_W < 0$. The first case represents systems dominated by the water-solute attraction. This is the case of the methanol in which it is assumed that the methyl group shows a small but attractive interaction with the water. This also represents the ionic liquids in which the anions groups are hydrophilic and the cationic chains are not too long [9, 88]. The second case represents alcohols with larger non-polar alkyl substituents [15]. The third case represents the ionic liquids in which the combination of the anions and cations lead to an hydrophobic

$p(S)$	D	A	B _W	B _S	C
D	ϵ	ϵ	ϵ	ϵ	ϵ
A	ϵ	ϵ	$-\epsilon$	$-\epsilon$	ϵ
B _W	ϵ	$-\epsilon$	ϵ	ϵ	$-\lambda_W\epsilon$
B _S	ϵ	$-\epsilon$	ϵ	ϵ	$-\lambda_S\epsilon$
C	ϵ	ϵ	$-\lambda_W\epsilon$	$-\lambda_S\epsilon$	ϵ

Table 3.1 Interactions between NN particles of the same type (solute or water). The interaction depends on the patches of both particles involved in the interparticle bond. The interaction between patches of type C and B depends on the type of molecule: water (W) or solute (S) that provides the patch B. We consider $0 < \lambda_S \leq 1$; and $\epsilon > 0$. Patches of types A, B, and C correspond to the four arms of the standard ALG model.

interaction [9, 88]. Due to the simplicity of our model solute, size and hydrophobicity effects are not taken into account independently, but both are considered through the λ_W parameter.

At zero temperature for the cases of the pure water and the pure solute systems three possible thermodynamic phases can appear in the model: For low values of the chemical potential, μ , the stable phase is the empty lattice representing the gas phase at reduced density, $\rho^* = N/N_L = 0$, with N being the number of particles (occupied sites) and N_L the number of sites of the lattice. Increasing μ a low density liquid phase (LDL) appears [89–92], where half of the sites of the lattice are occupied by particles ($\rho^* = 1/2$). These sites are those belonging to one of the diamond sublattices [93] that can be defined on the BCC lattice. Every patch of the type A is pointing to a patch of the type B , and vice versa as shown in the Fig. 3.3(A). In the case of water only pair interactions AB occur. In the case of the solute both AB and CB interactions occur. At higher values of the chemical potential, the stable phase is the high density liquid (HDL), where all the sites are occupied, and as for the LDL phase, in the case of water, every patch of type A is bonded to a patch of type B and *vice versa*, as shown in the Fig. 3.3(B). In the case of the solute every patch of type A is bonded to a patch of type B and every patch of type C is bonded to a patch of type B . The modification of the ALG model by considering different types of arms introduce, at zero temperature, a residual entropy per particle s_0 , that in thermodynamic limit can be written as, $s_0 = k_B \lim_{N \rightarrow \infty} [N^{-1} \ln Q_0(N)]$, where k_B is Boltzmann’s constant, and $Q_0(N)$ is the number of configurations of the system, in which every patch of type B is interacting with a patch of type A (or C), and every patch of type A (or C) is interacting with a patch of type B. Using Monte Carlo (MC) simulations and thermodynamic integration techniques [94, 95] we have obtained

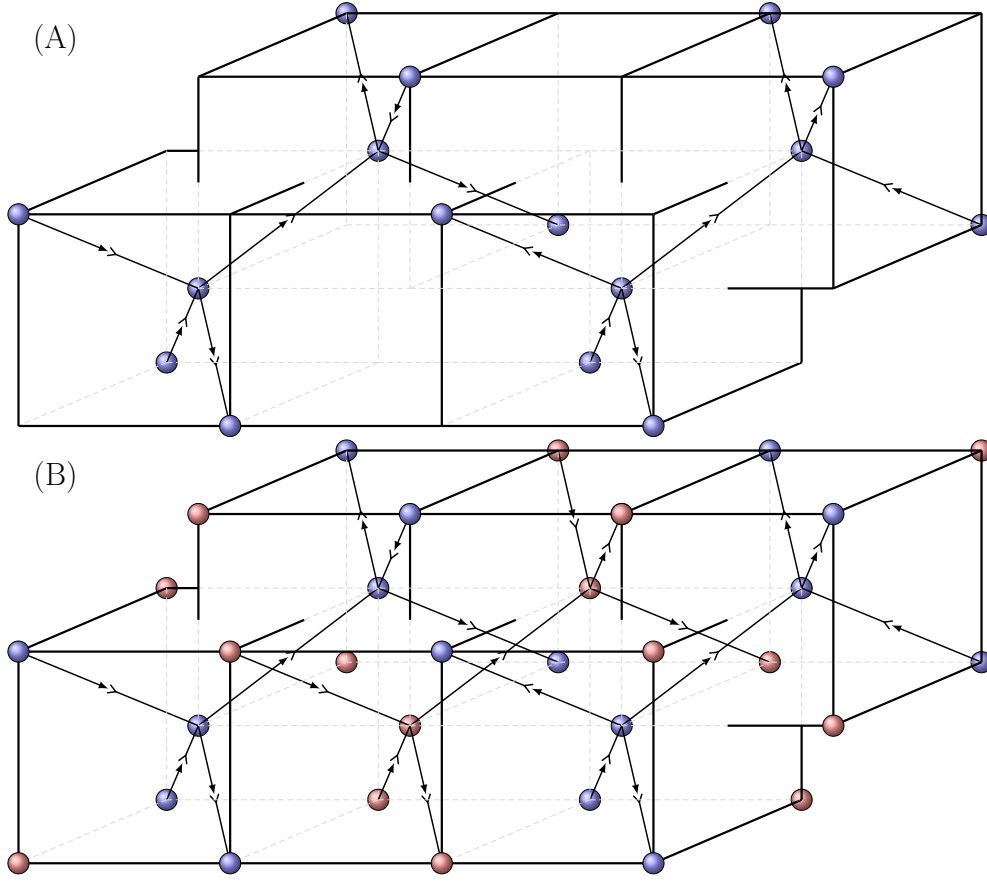


Figure 3.3 (A) LDL (B) HDL phases. At (B), the colors blue and red are used to facilitate the visualization.

the values of residual entropy for the water ($s_0^{(W)}/k_B = 0.41041 \pm 0.00002$) and solute ($s_0^{(S)}/k_B = 1.10356 \pm 0.00002$) models. For more details about the computation of residual entropies, see Appendix A.

From the values of residual entropy we can study the system in ground state. The Grand Canonical thermodynamic potential can be written as:

$$\Phi \equiv -pV = U - TS - \mu N, \quad (3.1)$$

where U is the internal energy, S is the entropy, and N the number of particles (occupied positions). In the Ground State, the stable phase for a given value of μ is the one with the minimum value of Φ . Considering the description of the ordered phases explained above,

for the water model Φ take the values (for $T \rightarrow 0$):

$$\begin{aligned}\Phi_G^{(W)}(V, \mu)/V^* &= 0 & (\rho^* = 0); \\ \Phi_{LDL}^{(W)}(V, \mu)/V^* &= -\epsilon - Ts_0^{(W)}/2 - \mu/2; & (\rho^* = 1/2); \\ \Phi_{HDL}^{(W)}(V, \mu)/V^* &= -Ts_0^{(W)} - \mu; & (\rho^* = 1)\end{aligned}\quad (3.2)$$

with V^* being the reduced volume (equal to the number of sites). Imposing that in coexistence the $\Phi_G^{(W)} = \Phi_{LDL}^{(W)}$ and $\Phi_{LDL}^{(W)} = \Phi_{HDL}^{(W)}$ we obtain the values of the chemical potential and the pressure, at the transitions in the limit of low temperatures

$$\begin{aligned}\mu = -2\epsilon - Ts_0^{(W)}, & \quad pw_0/\epsilon = 0, & \text{G-LDL water} \\ \mu = 2\epsilon - Ts_0^{(W)}, & \quad pw_0/\epsilon = 2, & \text{LDL-HDL water;}\end{aligned}\quad (3.3)$$

where the factor $w_0 = V/N_L$ correspond to the volume per site. For the case of pure solute the thermodynamic potential Φ of the different phases as $T \rightarrow 0$ is given by

$$\begin{aligned}\Phi_G^{(S)}(V, \mu)/V^* &= 0; & (\rho = 0); \\ \Phi_{LDL}^{(S)}(V, \mu)/V^* &= -(1 + \lambda_S)\epsilon/2 - Ts_0^{(S)}/2 - \mu/2; & (\rho = 1/2); \\ \Phi_{HDL}^{(S)}(V, \mu)/V^* &= (1 - \lambda_S)\epsilon - Ts_0^{(S)} - \mu; & (\rho = 1),\end{aligned}\quad (3.4)$$

and for the phase equilibria at low temperature we get:

$$\begin{aligned}\mu = -(1 + \lambda_S)\epsilon - Ts_0^{(S)}, & \quad pw_0/\epsilon = 0, & \text{G-LDL solute,} \\ \mu = (3 - \lambda_S)\epsilon - Ts_0^{(S)}, & \quad pw_0/\epsilon = 2, & \text{LDL-HDL solute}\end{aligned}\quad (3.5)$$

All the relevant quantities will be expressed in reduced units, such as:

$$\mu^* = \frac{\mu}{\epsilon}, \quad T^* = \frac{k_B T}{\epsilon}, \quad c_V^* = \frac{c_V}{k_B}, \quad p^* = \frac{pw_0}{\epsilon}, \quad s^* = \frac{s}{k_B}\quad (3.6)$$

3.2 Simulation and Numerical Details

In order to obtain the phase diagrams and compute the thermodynamic and structural properties of one-component systems, we have performed MC simulations in the grand canonical ensemble (GCE) for system sizes $512 \leq N_L \leq 65536$ where $N_L = 2L^3$. The simulations have used $\sim 8 \times 10^6$ MC sweeps for equilibration and $\sim 4 \times 10^6$ sweeps for evaluating the relevant quantities. Each MC sweep is defined as N_L one-site attempts to generate a new configuration. Each attempt is carried out as follows: i) A site i on the

lattice is chosen at random; this site can adopt n_s possible states, $S_i = 0, 1, 2, \dots, n_s - 1$ ($n_s = 13$ for pure water; $n_s = 25$ for pure solute, and $n_s = 37$ for the mixtures); $S_i = 0$ represents an empty site, and the remaining values stand for the different species that can occupy the site and their respective orientations. ii) For the selected site, one of its possible n_s states is selected at random, with probabilities given by:

$$P(S_i) \propto \exp \left[-\frac{U_i(S_i) - \mu(S_i)}{k_B T} \right], \quad S_i = 0, 1, 2, \dots, n_s; \quad (3.7)$$

where $U_i(S_i)$ contains the potential energy interactions between site i at state S_i with its NN, and $\mu(S_i)$ is the chemical potential of the component associated with state S_i . Notice that for an empty site $S_i = 0$, both $U_i(S_i)$ and $\mu(S_i)$ are zero, and that for $S_i \neq 0$, the value of U_i depends on the states of the sites which are NN of i .

We have combined the one-site sampling procedure with different advanced techniques in order to enhance the simulation efficiency: In the regions close to continuous transitions, where critical slowing down may be present [96], we have made use of the Parallel Tempering (PT) method [97,98]. The Gibbs-Duhem integration [99] technique adapted for working in the GCE [87,93] was employed in the location of the discontinuous phase transitions of the system. In order to study the excess properties of the mixtures as functions of the pressure and temperature we have developed methods to build up isobars for one-component systems (See Subsection 3.2.1), and lines at constant pressure and temperature with varying composition for the binary mixtures (See Subsection 3.2.2).

3.2.1 Computation of isobars for pure components

The excess properties of binary mixtures are usually measured experimentally at fixed conditions of temperature and pressure [15,16]. For lattice gas models it is neither straightforward nor practical the use of simulation in the NPT ensemble. The usual alternative is to carry out simulations in the grand canonical ensemble and compute the pressure by means of thermodynamic integration. Since we are interested in analyzing the excess properties at fixed pressure, we have developed a procedure to build up the lines $\mu(T|p)$ for pure components, i.e. we fix the pressure and compute the chemical potential as a function of temperature at fixed pressure. The objective is to apply this to the ordered phases: LDL and HDL. The pressure at (very) low temperature for these phases can be computed from the ground state analysis. In the GCE the change of the pressure for transformations at constant T and V , is given by $dp = \rho d\mu$. The density of the condensed phases at very low

temperature hardly changes with μ , therefore, we can integrate the pressure to get.

$$p = p_0 + (\mu - \mu_0) \rho_0 \quad (3.8)$$

where the values of p_0 , μ_0 , and ρ_0 can be taken as those corresponding to the phase coexistence at low temperature (Eqs. 3.2-3.5). Once we now how to compute the chemical potential for a given pressure p at a (low) temperature T_1 , we will develop the integration scheme to move on the (μ, T) plane at the fixed pressure p . Imposing $dp = 0$ in the differential form for the thermodynamic potential of the GCE we get:

$$d\mu = -\frac{U + pV - N\mu}{NT} dT = -\frac{\tilde{u} - p + \mu\rho}{\rho T} dT \quad (3.9)$$

We typically considered systems with $N_L = 2 \times 16^3$.

3.2.2 The properties of mixtures at fixed T and p

The excess properties of mixing are usually defined as the differences between the values of the property of the mixture at a given composition, x , and the value of the same property for an *ideal* mixture of the components at the same conditions of x , T , and p . It is, therefore, desirable to develop simulation strategies to sample in an efficient way different compositions of a given mixture for fixed conditions of temperature and pressure. In order to achieve this aim for our lattice model we have borrowed ideas to form the Gibbs-Duhem integration procedures, as we did for computing isobars of pure components.

The differential form for the grand canonical potential of a binary mixture can be written as:

$$-d\left(\frac{pV}{T}\right) = U d\left(\frac{1}{T}\right) - \frac{p}{T} dV - \sum_{i=1}^2 N_i d\left(\frac{\mu_i}{T}\right); \quad (3.10)$$

where N_i is the number of molecules of component i , and μ_i is the chemical potential of component i . If we fix T , p , and V , the chemical potential of the two components can not vary independently when modifying the composition. It should be fulfilled:

$$N_1 d\mu_1 + N_2 d\mu_2 = 0. \quad (3.11)$$

Using activities $z_i \equiv \exp[\mu_i/(k_B T)]$ to carry out the integration of Eq. (3.11) we get:

$$\frac{N_1}{z_1} dz_1 + \frac{N_2}{z_2} dz_2 = 0. \quad (3.12)$$

Let us assume that for some values of T , and p , we know the values of the activities of the pure components $z_1^{(0)}$, and $z_2^{(0)}$. We can integrate numerically (using simulation results) the differential equation:

$$dz_2 = -\frac{N_1 z_2}{N_2 z_1} dz_1. \quad (3.13)$$

For instance, using as starting point $(z_1 = z_1^{(0)}, z_2 = 0)$ and considering z_1 as the independent variable and integrating Eq. (3.13) up to $z_1 = 0$, we should reach $z_2(z_1 = 0) = z_2^{(0)}$. This condition provides a powerful consistency check of the thermodynamic integration schemes at constant pressure. The numerical integration of (3.13) can be carried out using the same numerical procedures as in Sec. 3.2.1. There is still, a minor technical problem, that appears in the limits $z_i \rightarrow 0$; where $N_i \rightarrow 0$, and therefore the ratio (N_i/z_i) can not be directly computed from the simulation. This problem can be solved by applying the Widom-insertion test technique [95] to compute the activity of the minority component (which actually has mole fraction $x = 0$) as a function of its density. The result can be written as:

$$\lim_{z_i \rightarrow 0^+} \frac{\rho_i^*}{z_i} = q_i \langle \exp[-\Delta u_i/(k_B T)] \rangle; \quad (3.14)$$

where $\langle \exp[-\Delta u_i/(k_B T)] \rangle$ represents the average of the Boltzmann exponential over attempts of insertion of a test particle of type i with random position and random orientation on a pure component system of the other component and q_i is the number of possible orientations for molecules of type i . Results were obtained from simulations of systems with $N_L = 2 \times 16^3$.

3.3 Numerical Results

3.3.1 The phase diagram for pure components

The chemical potential *vs.* temperature phase diagrams are shown in the Fig. 3.4 for the pure water and for the pure solute. Three different phases, G, LDL, and HDL appear, as expected. At low temperature, there are two, G-LDL and LDL-HDL first-order transitions, as shown in the figure 3.5 and 3.6.

The first order LDL-HDL transition finishes, both for water and solute, in a liquid-liquid tricritical point (LLTCP). The LLTCPs occur at $T_{tc}^* \simeq 0.59$ and $\mu_{tc}^* \simeq 1.67$ for water and at $T_{tc}^* = 0.25$ $\mu_{tc}^* = 2.42$ the solute. Above T_{tc} the LDL-HDL transition becomes continuous and defines the λ -line (See Fig. 3.4). At high temperature, it appears a continuous transition between G and HDL phases (τ -line in Fig. 3.4). A liquid-liquid transition (LLT) as shown in the figure 3.4 is also observed in molecular liquids. Experimental evidences suggest the existence of two liquid phases in the triphenyl-phosphite [100–102] and in the n-butanol [103]. In addition, Monte Carlo simulations, Hus *et al.* [78] showed that this type of transition is observed in isotropic models for methanol.

The coexistence line between the G and LDL phases for water extends up to a bicritical point (LGBCP) [104] located at $T_{bc}^* \simeq 1.00$ and $\mu_{bc}^* \simeq -0.22$. At this LGBCP the G-LDL transition meets the lines for the critical G-HDL (τ -line) and LDL-HDL (λ -line) transitions. In the case of solute, the G-LDL first order transition meets the λ -line at an end point located at $T_t^* \simeq 0.74$, $\mu_t^* \simeq 0.86$. Above this temperature there is a G-HDL first order transition up to a tricritical point (LGTCP) located at $T_{tc}'^* \simeq 0.85$, $\mu_{tc}'^* = 0.84$. Above this temperature the G-HDL transition becomes continuous and defines the τ -line. The details of the calculation of the critical lines are explained in the Appendix 3.3.2.

Gas-liquid transition in patchy associative lattice models is nothing a new. Tavares *et al.* [105], showed that systems of this nature not only have this kind of coexistence but, depending on the ratio between the interactions of the patches (we are above this ratio), the coexistence line can present a reentrant behavior, and closed miscibility loop. Papaioannou *et al.* [106] showed that for the case of water and methanol, the gas-liquid coexistence can be obtained through the SAFT- γ Mie group with excellent accuracy in relation to the experimental data.

3.3.2 Critical lines and order parameters

The λ -line

The continuous τ and λ transitions, illustrated in the figure 3.4 are represented by thin lines and circles. The values of the temperatures and chemical potentials for the critical lines were obtained by computing appropriated order parameters and their associated moments or cumulants.

In the case of the λ line, the θ_λ order parameter is defined as follows. The system is divided into eight sublattices [91]. The figure 3.7 illustrates the behavior of the eight

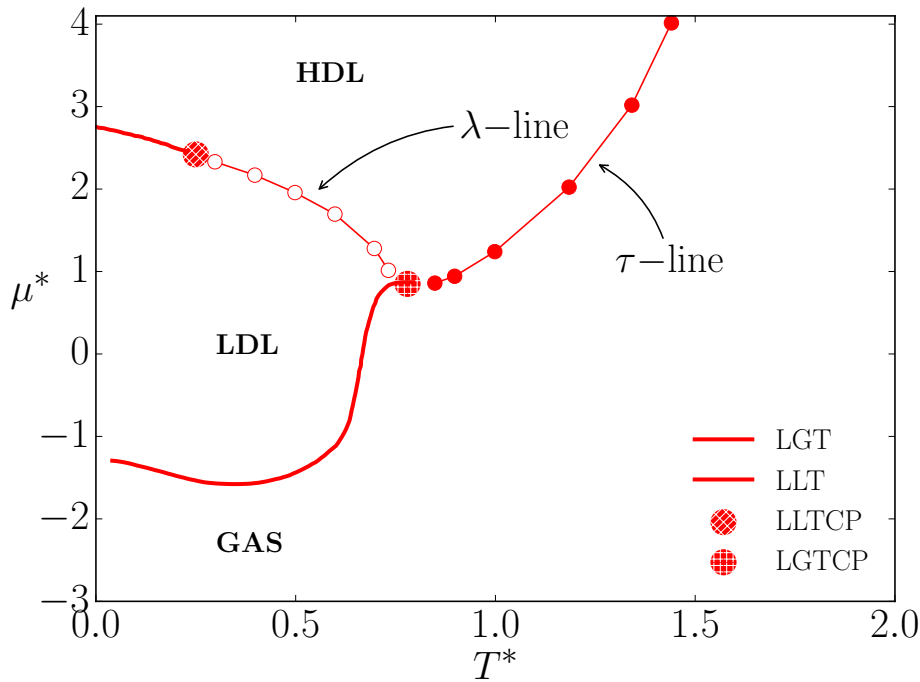
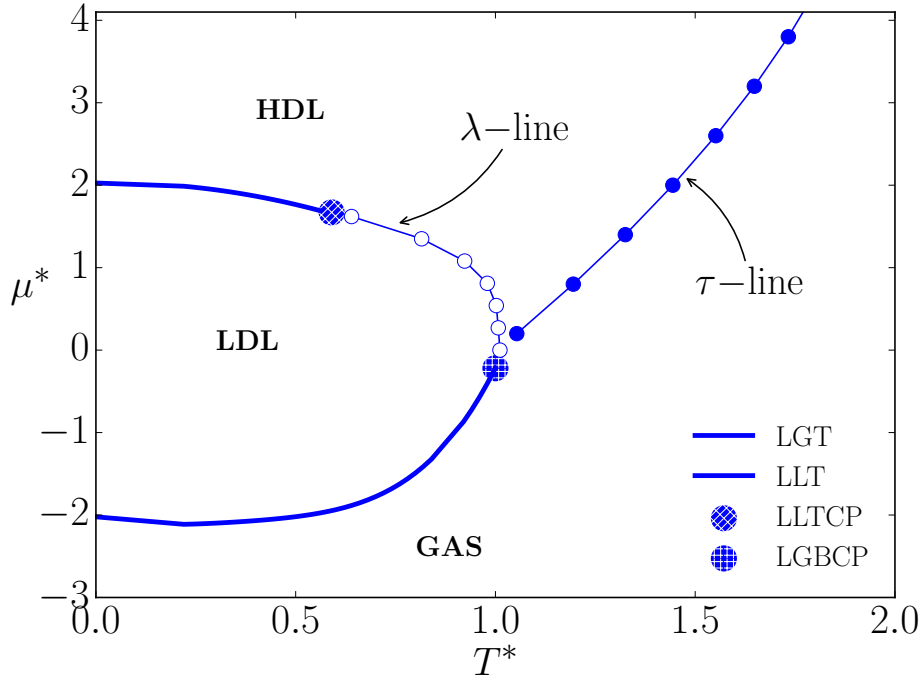


Figure 3.4 Reduced chemical potential versus reduced temperature phase diagram for (up) pure water (down) pure solute. Solid thick lines represent first-order phase transitions, liquid-gas (LGT) and liquid-liquid (LLT). Thin lines represent continuous (second-order) transition, the empty circles show the λ -line and the filled circles are the τ -line. The big patterned circles represent the multi-critical points of the model. (See the text for details).

sublattices as a function of the temperature at the λ -line. As the temperature is decreased four sublattices become full while other four stay empty. Then, from the density of these

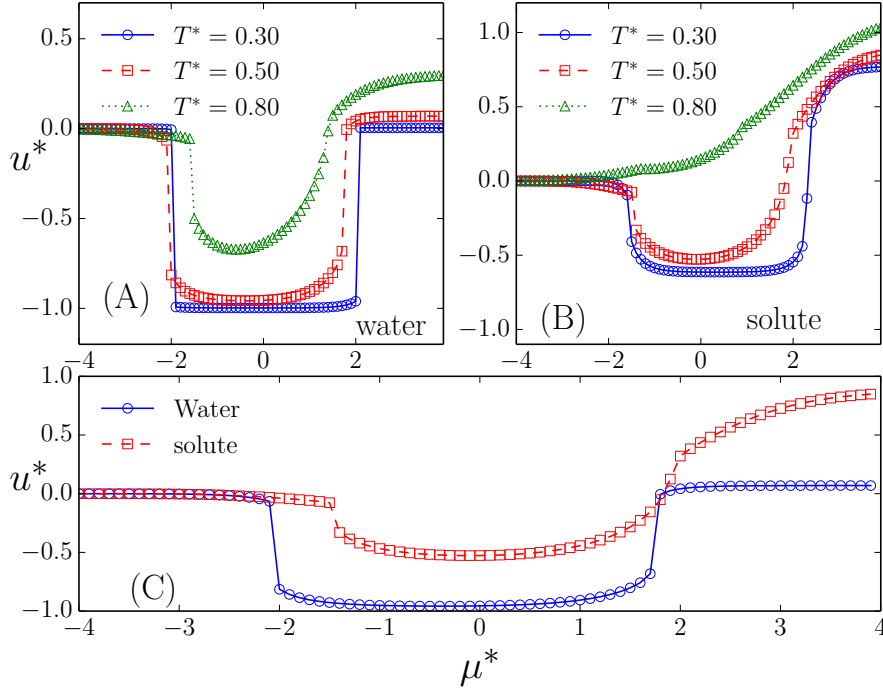


Figure 3.5 In (A) $u^* = U/L^3$ vs chemical potential for (A) water model for three different temperatures $T^* = 0.30, 0.50, 0.80$. and (B) for the solute model. In (C) the energy per site for the different models at $T^* = 0.5$ are compared.

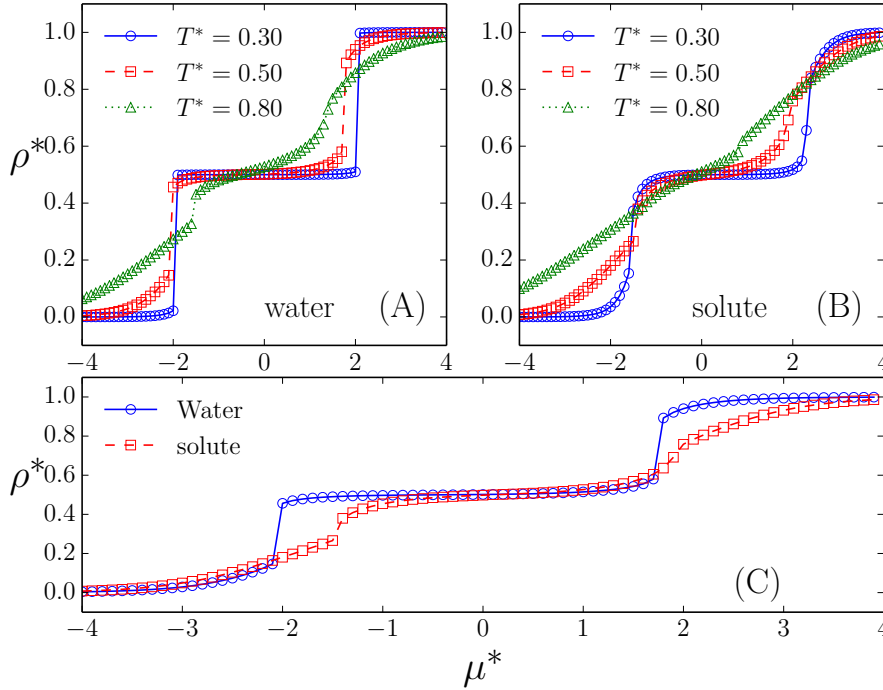


Figure 3.6 In (A) we plot the density $\rho^* = N/L^3$ vs chemical potential for water model for three different temperatures $T^* = 0.30, 0.50, 0.80$. In (B) the same plot of (A) for the methanol model. In (C) the density for the different models for $T^* = 0.5$ are computed.

sublattices, the order parameter is defined by

$$\theta_\lambda = \frac{2}{V} \left[\sum_{i=1}^{\text{full}} \rho_i - \sum_{j=1}^{\text{empty}} \rho_j \right], \quad (3.15)$$

where the index i runs over the four sublattices which become full at the LDL phase while the subindex j runs over the four sublattices which remain empty at the LDL phase. The figure 3.7 illustrates the value of this order parameter as a function of the temperature for fixed chemical potentials for both the pure water and the pure solute cases showing the transition from all the sublattices equally populated to a preferential occupation in four sublattices.

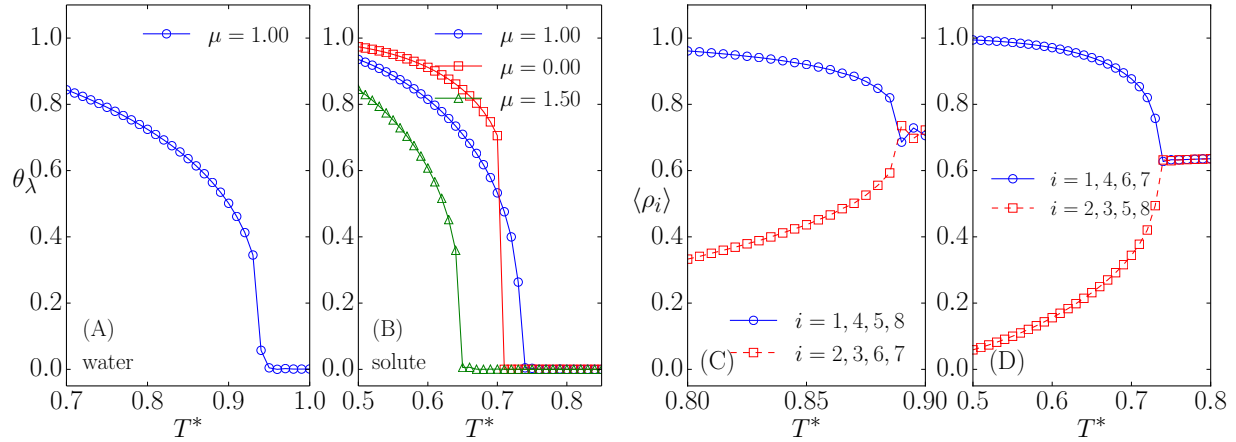


Figure 3.7 Order parameter θ_λ versus reduced temperature for (A) water and (B) solute for various chemical potentials. Average density of the empty (red) and full (blue) sublattices for (C) water and for (D) the solute.

This transition can also be described by taking into account that for the ALG model there are four possible realizations of the LDL structure (with diamond structure) on the BCC lattice. The occupancy of the sites and orientations of the arms (patches of types A, B and C) is well defined for each LDL realization. The realizations of the lattice are obtained by a union of even/odd sites belonging to a BCC lattice. The sites are represented by $(2i, 2j, 2k)$ and $(2i + 1, 2j + i, 2k + 1)$ with $i, j,$ and k integers. An example of the subsets \mathcal{S}_i can be: $\mathcal{S}_1 = \{(000), (022), (202), (220)\}$, $\mathcal{S}_2 = \{(002), (020), (200), (222)\}$, $\mathcal{S}_3 = \{(111), (331), (133), (313)\}$ and $\mathcal{S}_4 = \{(131), (311), (113), (333)\}$. The realizations \mathcal{D}_i ($i = 1, 2, 3, 4$) are then obtained by union of the subsets \mathcal{S}_i ,

$$\mathcal{D}_1 \equiv \mathcal{S}_1 \cup \mathcal{S}_3 \quad , \quad \mathcal{D}_2 \equiv \mathcal{S}_1 \cup \mathcal{S}_4 \quad ,$$

$$\mathcal{D}_3 \equiv \mathcal{S}_2 \cup \mathcal{S}_3 \quad , \quad \mathcal{D}_4 \equiv \mathcal{S}_2 \cup \mathcal{S}_4 \quad .$$

resulting in four possible realizations.

Taking into account the orientation of the occupied sites on a given configuration, we

can compute the number of particles in the system compatible with each of the four LDL realizations. Let n_i , with $i = 1, 2, 3, 4$ be those numbers. From each configuration, we can sort the n_i values so that $n_a \geq n_b \geq n_c \geq n_d$, and compute their corresponding densities $\rho_a = n_a/N_L, \rho_b = n_b/N_L \dots$. In the thermodynamic limit ($N_L \rightarrow \infty$), we expect for the G phase: $\rho_a \simeq \rho_b \simeq \rho_c \simeq \rho_d \simeq \rho/4$. For the HDL phase $\rho_a \simeq \rho_b \gg \rho_c \simeq \rho_d$, and finally for the LDL phase $\rho_a \gg \rho_b$. Accordingly the presence of the LDL phase can be detected by an order parameter, O_λ , given by

$$O_\lambda = \rho_a - \rho_b; \quad (3.16)$$

The system size dependence of the shape the O_λ distribution can be analyzed by looking at the ratio [96]:

$$g_{4\lambda} = \frac{\langle O_\lambda^4 \rangle}{\langle O_\lambda^2 \rangle^2}; \quad (3.17)$$

where the angular brackets represent average values. In figure 3.8, we show the results for $\langle O_\lambda \rangle$ and $g_{4\lambda}$ as functions of the chemical potential for various lattice sizes and at $T^* = 0.80$. The crossing of the lines of $g_{4\lambda}$ for different values of L locate the critical chemical potential at that temperature, i.e, the corresponding point of the λ -line.

Complementary to the study of the θ_λ and O_λ order parameters described above, the behavior of the specific heat at constant volume for different system sizes were analyzed.

At criticality, it is expected that the specific heat would show a divergence as the thermodynamic limit is approached. The finite-size scaling behavior of the critical exponent of the specific heat, α , gives the critical behavior at the infinite system [96]. The heat capacity at constant volume (per lattice site) $c_V = (\partial U / \partial T)_{N,V} / V$ is computed from the data obtained from simulations at constant chemical potential through the expression [94],

$$c_V = \frac{1}{k_B T^2 V} \left[\langle \delta U^2 \rangle - \frac{\langle \delta U \delta N \rangle^2}{\langle \delta N^2 \rangle} \right]. \quad (3.18)$$

Here U is the interaction energy of model described in the Table 3.1, and N is the number of particles. The averages in Eq. (3.18) are carried out on the grand canonical ensemble.

The figure 3.9 shows the specific heat at constant volume *versus* temperature at constant μ , illustrating the diverging peak at $T^* \simeq 0.9$ for the pure water system and at $T^* \simeq 0.6$ for the pure solute, as L increases. The peak in the heat capacity c_V in addition to the O_λ and θ_λ behavior is employed to locate the λ -line.

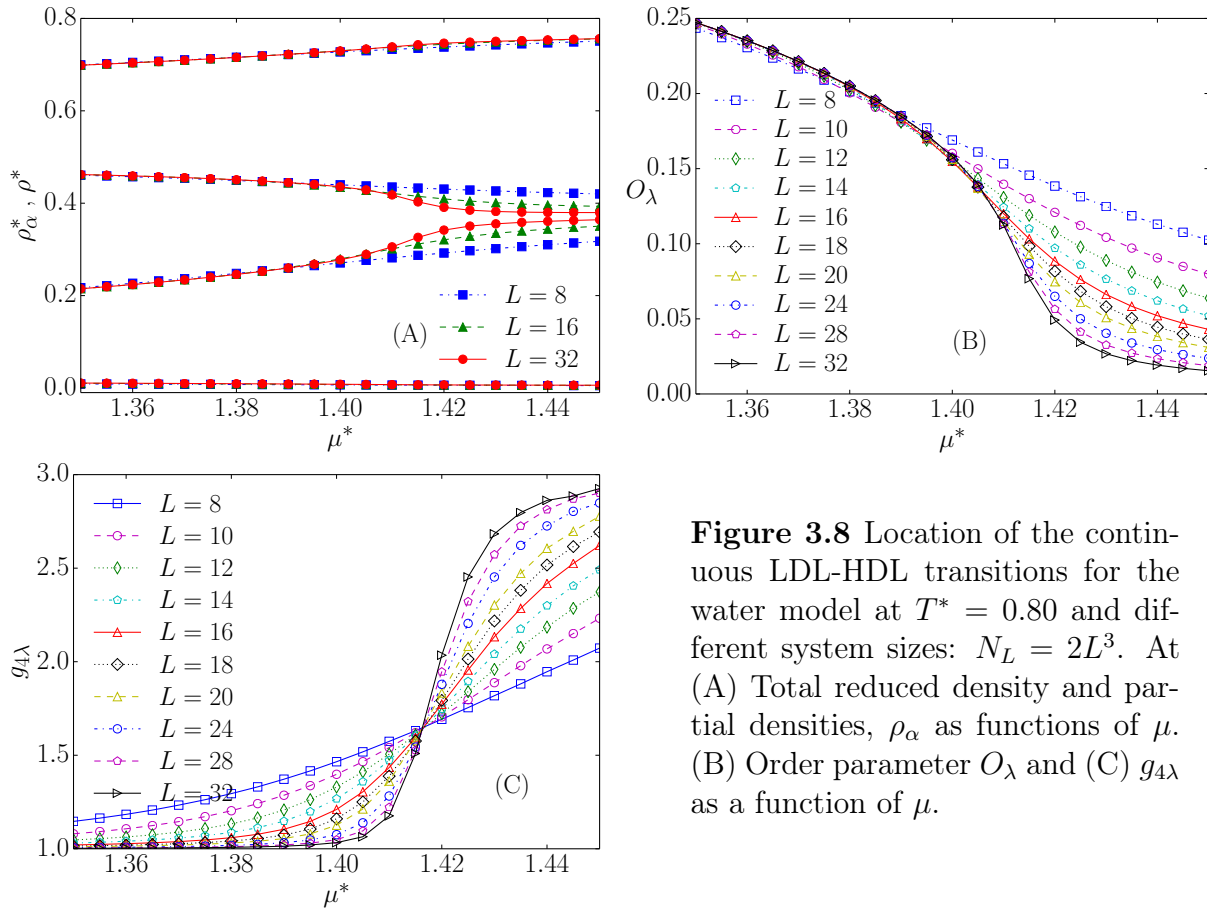


Figure 3.8 Location of the continuous LDL-HDL transitions for the water model at $T^* = 0.80$ and different system sizes: $N_L = 2L^3$. At (A) Total reduced density and partial densities, ρ_α as functions of μ . (B) Order parameter O_λ and (C) $g_{4\lambda}$ as a function of μ .

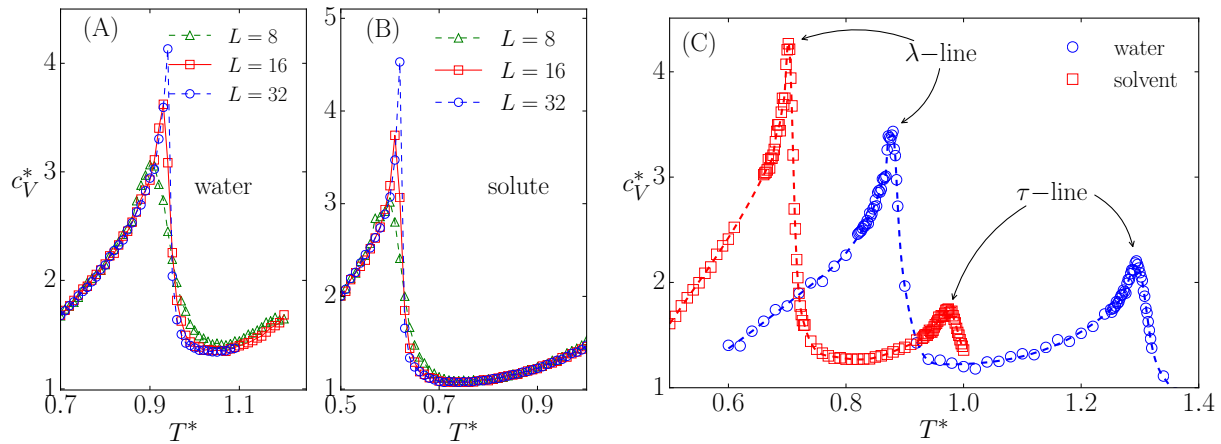


Figure 3.9 Heat capacity versus reduced temperature for the reduced chemical potentials (A) $\mu^* = 1.0$ and (B) $\mu^* = 1.6$ for water and solute respectively for different L values for the λ -line. The same for $\mu^* = 1.2$ showing both the λ and the τ -lines.

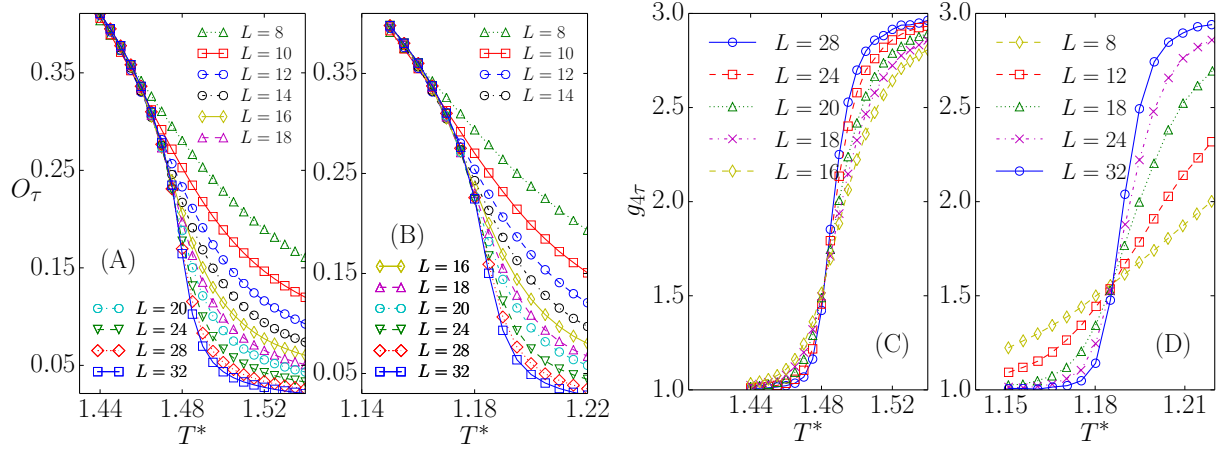


Figure 3.10 O_τ versus reduced temperature for different systems sizes at chemical potential $\mu = 2.0$ for water (A) and solute (B) models. $g_{4\tau}$ versus reduced temperature for different systems sizes at chemical potential $\mu = 2.0$ for water (C) and solute (D) models.

The τ -line

The τ -line corresponds to the transition between G and HDL phases. An order parameter based on the symmetry of the ALG model can be defined to quantify the HDL ordering of the configurations. The BCC lattice can be splitted into two interpenetrated cubic sublattices. In the HDL structure, each sublattice adopts a different but complementary orientation. The appropriate order parameter for the τ -line is given by

$$O_\tau = \frac{1}{N_L} \left| \sum_{i=1}^{N_L} l(i)s(i) \right|, \quad (3.19)$$

where $l(i)$ assumes $+1$ if a sublattice is formed by even sites and -1 if it is formed by a odd sites. $s(i)$ represents the orientation of the particles in the site i . Particles with arms orientated to, $(i, j, k) = \{(1, 1, 1); (-1, -1, 1); (-1, 1, -1); (1, -1, -1)\}$ receive $s = +1$, to $(i, j, k) = \{(-1, 1, 1); (1, -1, 1); (1, 1, -1); (-1, -1, -1)\}$ receive $s = -1$, and empty sites receive $s(i) = 0$. This order parameter is analogous to that for antiferromagnetic Ising models in bipartite lattices. In the figure 3.10 we show the shape of the order parameter at the HDL-G transition (top panels). For the G phase O_τ vanishes in the thermodynamic limit while for the HDL it remains finite. The approximate location of the transition is obtained by the crossing of the curves for different sizes. Even though the behavior of the order parameter illustrates how the structure of the phases change at the phase transition, it does not provide the precise temperature and chemical potential. The precise location

of the transitions can be achieved by looking at the system size dependence of the ratio, $g_{4\tau}$:

$$g_{4\tau} = \frac{\langle O_\tau^4 \rangle}{\langle O_\tau^2 \rangle^2}, \quad (3.20)$$

where the brackets indicate average over grand canonical simulations. At the τ -line transition, it is expected that the values of $g_{4\tau}$ become independent of the system size. The figure 3.10, examples for water and solute of the behavior of $g_{4\tau}(T, N_L)$ for fixed μ , at the $G - HDL$ transition (λ - line) are presented. The value of $g_{4\tau}$ at the crossing region, together with the form of the order parameter suggest three-dimensional Ising criticality. In addition the location of the τ -line can be confirmed by the divergence of the heat capacity.

3.3.3 The excess properties of the water-solute mixtures

Next, we explore the mixture of water and solute. The thermodynamic excess properties of the mixture are defined by comparing the values of a given extensive property per mol (or per molecule) with the values of this quantity for an ideal mixture. In the case of the excess volume we have:

$$\bar{V}^E(x, p, T) = \bar{V}(x, p, T) - [(1 - x)\bar{V}_1^0(p, T) + x\bar{V}_2^0(p, T)]; \quad (3.21)$$

where $\bar{V}(x, p, T)$ is the volume per molecule of the mixture at molecular fraction x of the solute (component 2) x (i.e. $x \equiv x_2$), $\bar{V}_1^0(p, T)$ and $\bar{V}_2^0(p, T)$ are the volumes per molecule of the pure solvent (component 1) and pure solute respectively.

The thermodynamic properties for different compositions at constant T and p were computed using GCE simulations coupled to the integration schemes explained in Appendices 3.2.1 and 3.2.2. In practice, for one component systems we apply an integration scheme to find the line, $\mu(T|p)$ in the plane $\mu - T$ that corresponds to a fixed value, p of the pressure, and for the mixtures we calculate the line $\mu_1(\mu_2|T, p)$ in the plane $\mu_1 - \mu_2$ that keep fixed the values of T and p .

The volumes per molecule were estimated from the simulations as: $\bar{V} = V/\langle N \rangle$. The enthalpy, H of a given system is given by $H = U + pV$, where U is the internal energy (given for the patch-patch interactions). The enthalpy per molecule can be estimated as: $\bar{H} = [\langle U \rangle + pV]/\langle N \rangle$. Whereas the mole fraction for given values of the activities $z_i = \exp[-\mu_i/(k_B T)]$, is computed as: $\langle x \rangle \simeq \langle N_2 \rangle / \langle N \rangle$.

The integration procedure provides the results for the different properties at equally

spaced discrete values of the activity, z , of one of the components, (say component 1) which span from $z_1 = z_1^{(0)}$ (pure solvent) to $z_1 = 0$ (pure solute). For each of these cases the properties of interest, $x(z_1)$, $\bar{V}(z_1)$, $\bar{H}(z_1)$, \dots are computed. Then, to estimate the dependence of the molar properties with the composition these properties are fitted to polynomials of x as:

$$\bar{Y}_f(x, T, p) = \sum_{j=0}^{j_{max}} a_j^{(Y)}(T, p)x^j. \quad (3.22)$$

The degree of the polynomial, j_{max} , is chosen according to statistical criteria, ensuring that the fitted function provides a good description of the values of the property in the whole range $x \in [0, 1]$. Using the functions given in Eq. (3.22) the excess properties for the volume or the enthalpy are computed as a function of x as:

$$\bar{Y}^E(x, T, p) = \bar{Y}_f(x, T, p) - x\bar{Y}_f(1, T, p) - (1-x)\bar{Y}_f(0, T, p). \quad (3.23)$$

The $\lambda_W = \lambda_S = 0.25$ case

First, we analyze the case in which the B - C solvent-solute and solute-solute interactions are both attractive and they have the same value namely $\lambda_W = \lambda_S = 0.25$. This represents a system in which in addition the solvent interacts with the solute in two different ways, B - A and B - C , both attractive. In principle this would be the case of the water - alcohol mixture where water forms hydrogen bonds with the alcohol and shows an effective attraction with the alkyl group.

The figure 3.11 illustrates the excess volume for the pressure and temperature $p^* = 0.10$ and $T^* \simeq 0.3$. For the pure solvent, this point is at a temperature below the temperature of maximum density. As the fraction of the solute increases, the excess volume decreases until it reaches a minimum. The presence of this minimum in a water-solute system is observed in the water-methanol [16, 71, 107–109], in the water-ethanol [110], in the water-alkanolamines [111, 112] and in the water-hydrophilic ionic liquids [113] solutions.

The negative value of the excess volume can be understood as follows. The excess volume for mixtures originates from the competition between energy and entropy [80, 114]. Since the solvent-solvent is more attractive than the solute-solvent, the energetic balance favors the solution to occupy a larger volume [80, 114]. However, the excess volume has a contribution from the entropy. As solute is added to the system the phase diagram shrinks and the phases are shifted to lower temperatures and higher densities [92, 115]. In the case of non anomalous systems, described by a Lennard-Jones potential, this shift in the phase

diagram is not relevant and in the case of $\lambda_W = \lambda_S$ the excess volume is positive [80]. In our system due to the different orientations of the solute, the entropic effect is more relevant and the excess volume is negative.

The figure 3.11 also shows the excess enthalpy for our model as a function of the fraction of the solute. The minimum observed in H^E is also present in the in water-methanol [116], water-ethanol [117], water-alkanolamines- [118] and in water with hydrophilic ionic liquids [113] solutions.

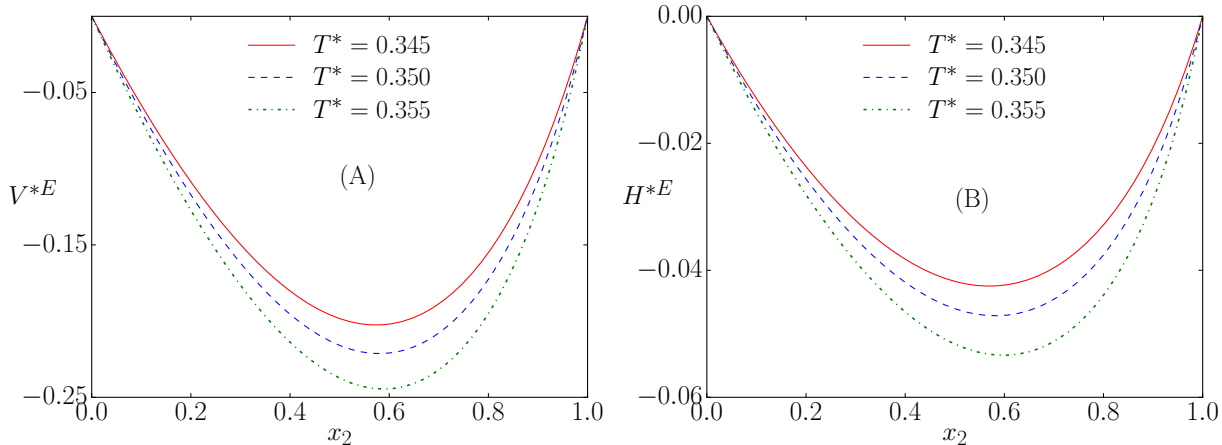


Figure 3.11 (A) excess volume and (B) excess enthalpy per particle as a function of solute concentration for $\lambda_S = 0.25, \lambda_W = 0.25, p^* = 0.10$ and several temperatures.

The figure 3.12 illustrates snapshots of the system as the concentration of the solute is increased. Since the system is in the LDL phase of the solvent, there is one sublattice empty while the other is filled. In the case in which the solute is a hard sphere, as the solute is added to the system it enters in the empty sublattice not competing with the solvent occupation [92]. Here this is not the case. The solute enters in the same sublattice occupied by the solvent.

The excess enthalpy is a combination of the excess internal energy and the excess volume ($H^E = U^E + pV^E$). The excess volume is negative as explained above. The excess internal energy of the mixture is positive due to the solvent-solute less attractive interaction when compared with the solvent-solvent interaction. The balance between these two competing terms for the $\lambda_W = 0.25$ leads to a small but negative excess enthalpy.

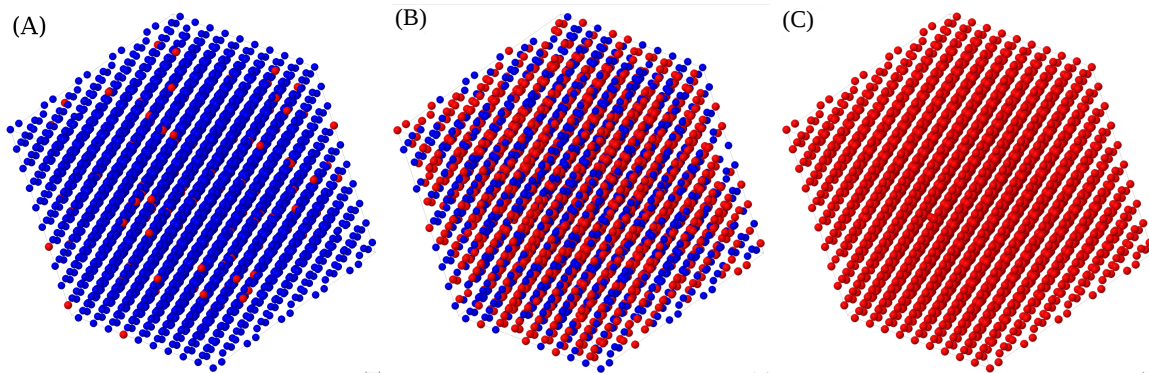


Figure 3.12 The snapshot of system for $\lambda_W = 0.25$ and $T^* = 0.350$. The blue and red spheres represent the water and solute respectively. At (A)- $x_2 = 0.024105$, (B)- $x_2 = 0.704341$ and (C)- $x_2 = 1$.

The $\lambda_W = 0$ and $\lambda_S = 0.25$ case

Next, we analyze the case in which the $B-C$ solute-solute patch is attractive but the $B-C$ solvent-solute patch has no interaction. In this case $\lambda_W = 0$ while the solute-solute $B-C$ is attractive namely $\lambda_S = 0.25$. This represents a system in which in addition the solvent interacts with the solute only through the $B-A$ patch. In principle, this would be the case of the water-alcohol mixture in which the alkyl group is larger than the preceding case and therefore the molecule is less hydrophilic.

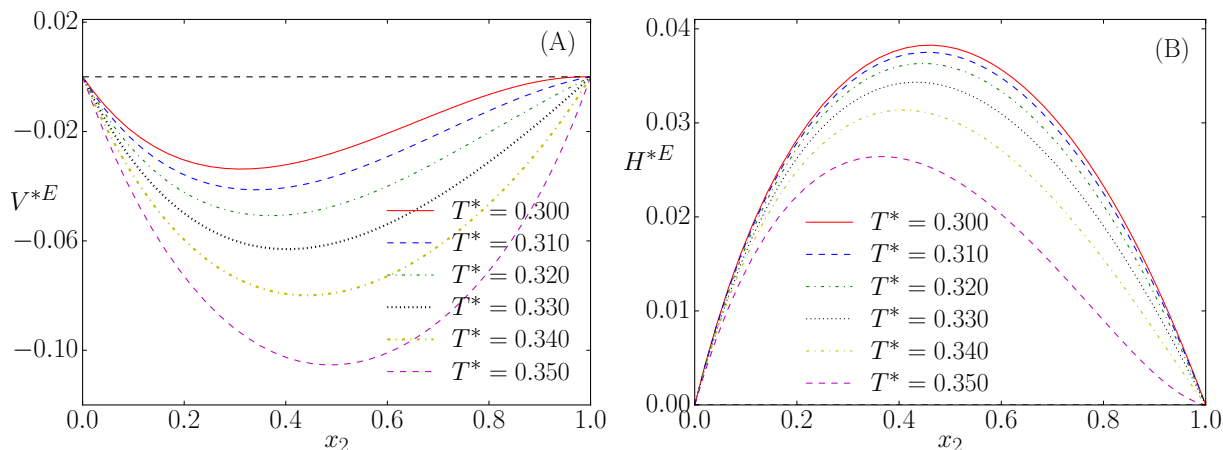


Figure 3.13 (A) Excess volume and (B) Excess enthalpy *versus* fraction of solute for various temperatures, $\lambda_W = 0$, $\lambda_M = 0.25$ and $p^* = 0.10$.

The figure 3.13 illustrates the excess volume and the excess enthalpy as a function of

the fraction of the solute for various temperatures.

The excess volume here as in the previous case, is a combination of energy and entropy. The energy of the mixture is much higher than the entropy of each pure system what contributes to a positive excess volume. The entropy is still more relevant and the excess entropy is larger than in the previous case but it is still negative.

The excess enthalpy ($H^E = U^E + pV^E$) is composed of a small negative excess volume and a excess energy that is positive because both the solvent-solvent and solute-solute interaction are more attractive than the solute-solvent interaction. So, in this case the excess enthalpy is positive.

This behavior is consistent with the excess volume and enthalpy of mixtures of water and large alcohol molecules such as propanol, butanol and pentanol [15, 119].

The $\lambda_W = -0.25$ and $\lambda_S = 0.25$ case

Finally, we analyze the case in which the $B-C$ solute-solute patch is attractive but the $B-C$ solvent-solute patch is repulsive. In this case, $\lambda_W = -0.25$ is repulsive while the solute-solute $B-C$ is attractive namely $\lambda_M = 0.25$. This represents a system in which in addition the solvent interacts with the solute through the $B-A$ with attraction probably forming hydrogen bonds while show repulsion through the $B-C$ patch. In principle, this would be the case of the water mixing with molecules that exhibit a hydrophilic region, and eventually, can form a hydrogen bond, but the overall water-solute interaction is repulsive.

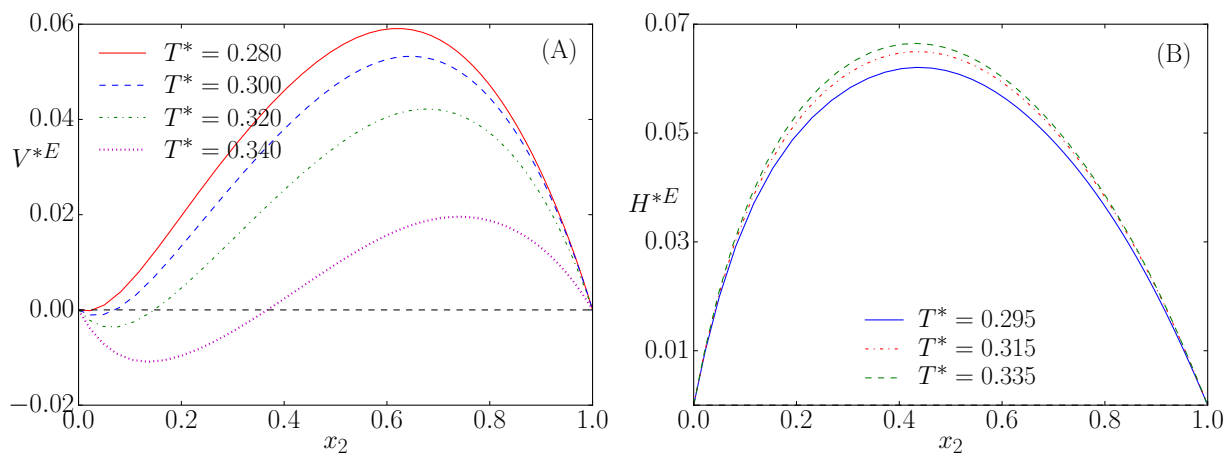


Figure 3.14 (A) Excess volume and (B) excess enthalpy *versus* fraction of methanol for various temperatures. $\lambda_W = -0.25$, $\lambda_M = 0.25$ and $p^* = 0.10$.

The figure 3.14 illustrates the excess volume and the excess enthalpy as a function of the fraction of the solute for various temperatures. This behavior is found in hydrophobic ionic liquids [113, 120].

In this last case, the solute-solvent energy is much larger than the solute-solute and solvent-solvent interaction, so the entropic effect is not enough and the excess volume is positive. Similarly the enthalpy that is a combination of this positive excess energy and excess volume is also positive.

It is important to notice that these three effects of both negative excess functions, one negative and one positive and both negative by controlling the solvent-solute from mildly attractive to repulsive would not be obtained in a Lennard-Jones type of fluid in which the orientational degrees of freedom is not present.

3.4 Conclusions

In this paper, a combination of two Associating Lattice Models is employed to represent a mixture of solute and solvent. The idea is to explore the effect of the orientational degrees of freedom present in the model and of the solute-solvent energy in the excess properties of the mixture.

The ALG model in the range of parameters employed for describing the solvent exhibits the density and diffusion anomalous behavior present in water. The solute is modeled by molecules that form two types of bonds with water: one attractive hydrogen bond-like, the $A-B$ interaction, plus an additional, tunable, $B-C$ interaction.

The pure components, by construction, present very similar phase diagrams. Both present, first (G-LDL/LDL-HDL) and second order (λ -line/ τ -line) transitions, as well as some multicritical points. The phases in coexistence are also the same. The difference between solute and solvent is in the critical temperatures and the location of the temperature of maximum density, at extremely low temperatures for the case of the solute.

For the mixture, by tuning only one parameter, the $B-C$ patch, from attractive to repulsive the model qualitatively reproduce the behavior of the excess volume and enthalpy of different types of mixtures that represent solutes ranging from hydrophilic to hydrophobic.

The mapping of the relative hydrophobicity of the solutes through the λ_W parameter of the model, allows us to explain the trends of the excess properties of the mixtures as function of the intermolecular effective interaction.

Our results indicate that when the balance between the solute-solute plus the solvent-solvent energies are lower than the solvent-solute energy but solute-solvent is hydrophilic, the entropic contribution for the excess volume makes it negative and the excess enthalpy also negative.

When the solute-solvent is hydrophobic the excess energy is very positive so the excess volume becomes positive. The same applies to the excess enthalpy.

Our result even though based on a very simple model reproduce a mechanism that seems to be present in a large variety aqueous solutions.

This work is published at : [J. Chem. Phys. 145, 144501 \(2016\)](#)

Chapter 4

Temperature of maximum density and excess properties of short-chain alcohol aqueous solutions: A simplified model simulation study

We perform an extensive computational study of binary mixtures of water and short-chain alcohols resorting to two-scale potential models to account for the singularities of hydrogen bonded liquids. Water molecules are represented by a well studied core softened potential which is known to qualitatively account for a large number of water's characteristic anomalies. Along the same lines, alcohol molecules are idealized by dimers in which the hydroxyl groups interact with each other and with water with a core softened potential as well. Interactions involving non-polar groups are all deemed purely repulsive. We find that the qualitative behavior of excess properties (excess volume, enthalpy and constant pressure heat capacity) agrees with that found experimentally for alcohols such as t-butanol in water. Moreover, we observe that our simple solute under certain conditions acts as an "structure-maker", in the sense that the temperature of maximum density of the bulk water model increases as the solute is added, i.e. the anomalous behavior of the solvent is enhanced by the solute.

4.1 The Model

As mentioned above, we will have spherical particles representing water-like molecules, together with an amphiphilic solute with a purely repulsive site accounting for the apolar tail, R, in addition to an OH site, characterized by OH-OH and OH-water interactions with two length scales [44]. A short range repulsion accounts for the high density liquid phase, and a much longer range repulsion and attraction attempts to roughly model the more open structures due to hydrogen bonding. To make matters simpler, we will use the same the softened-core potential both for water-water, OH-OH and OH-water interactions, defined by,

$$U_{sc}(r_{ij}) = 4\epsilon_{sc} \left[\left(\frac{\sigma}{r_{ij}} \right)^{12} - \left(\frac{\sigma}{r_{ij}} \right)^6 \right] + \sum_{\ell=0}^1 u_{\ell} \epsilon_{sc} \exp \left[-\frac{1}{c_{\ell}^2} \left(\frac{r_{ij} - r_{\ell}}{\sigma} \right)^2 \right]. \quad (4.1)$$

Here, r_{ij} represents the separation between sites i and j . The first term on the r.h.s. of Equation (4.1), is the standard 12-6 Lennard-Jones (LJ) potential [94], whereas the second term is the summation of two Gaussians, centered at $r_0 = 0.7\sigma$ and $r_1 = 3\sigma$, with depths $u_0 = 5$ and $u_1 = -0.75$ and widths $c_0 = 1$ and $c_1 = 0.5$ respectively. The potential of Eq. (4.1), displays two different length scales, an attractive scale at $r \approx 3\sigma$ and a repulsive shoulder at $r \approx \sigma$. Of the many possible choices of two-scale potentials, ours has been motivated by its ability to account for many of the anomalous features of fluid water [5, 44, 121], displaying the characteristic cascade ordering of anomalies [30]. For the parameters chosen in this work, the model is known to display a density anomaly with a TMD curve in the supercritical region [44]. The attractive well that can be seen in Figure 4.1 is not sufficient to place the anomalous region within the stable liquid phase, in contrast with the situation in real water. Despite these limitations, as already mentioned, this model potential is an excellent candidate to reproduce water anomalies [44].

The non-polar site-site interactions (R-R, R-OH, and R-water) are represented by a purely repulsive Weeks-Chandler-Andersen potential (WCA) [122] of the form

$$U_r(r_{ij}) = \begin{cases} U_{LJ}(r_{ij}) - U_{LJ}(r_c) & \text{if } r \leq r_m \\ 0 & \text{if } r > r_m \end{cases} \quad (4.2)$$

where, $U_{LJ}(r)$ is the standard 12-6 LJ potential with parameters (ϵ_r, σ_r) , and $U_{LJ}(r_m)$ is the LJ potential computed at cutoff distance given by the position of the minimum of the LJ interaction, $r_m = 2^{1/6}\sigma_r$.

In what follows we have used as unit length, $\sigma = \sigma_{ww} = \sigma_{w-OH} = \sigma_{OH-OH}$, and as energy unit, ϵ_{sc} . Reduced pressure and temperature are defined as $P^* = P\sigma^3/\epsilon_{sc}$ and $T^* = k_B T/\epsilon_{sc}$, where k_B is Boltzmann's constant. The simulation time step is given in reduced units of $\tau = \sigma\sqrt{m/\epsilon_{sc}}$, where m is one of the particle masses. Since here we are not interested in dynamic properties, we have considered all particle masses identical.

As mentioned, we have considered an heteronuclear model, in which $\sigma_r/\sigma = 5/3$ (a rough model for tert-butanol), and a homonuclear model in which $\sigma_r/\sigma = 1$.

The energy parameter of the repulsive interaction was set to $\epsilon_r/\epsilon_{sc} = 1.21$, and the dimer bond length to $d_{R-OH} = 0.48\sigma$. This choice of parameters was to some extent inspired by the OPLS force field widely used to simulate alcohols [123]. Cross interaction parameters were computed using Lorentz-Berthelot mixing rules [94]. A graphical representation of our molecular models and the corresponding interactions is depicted in Figure 4.1.

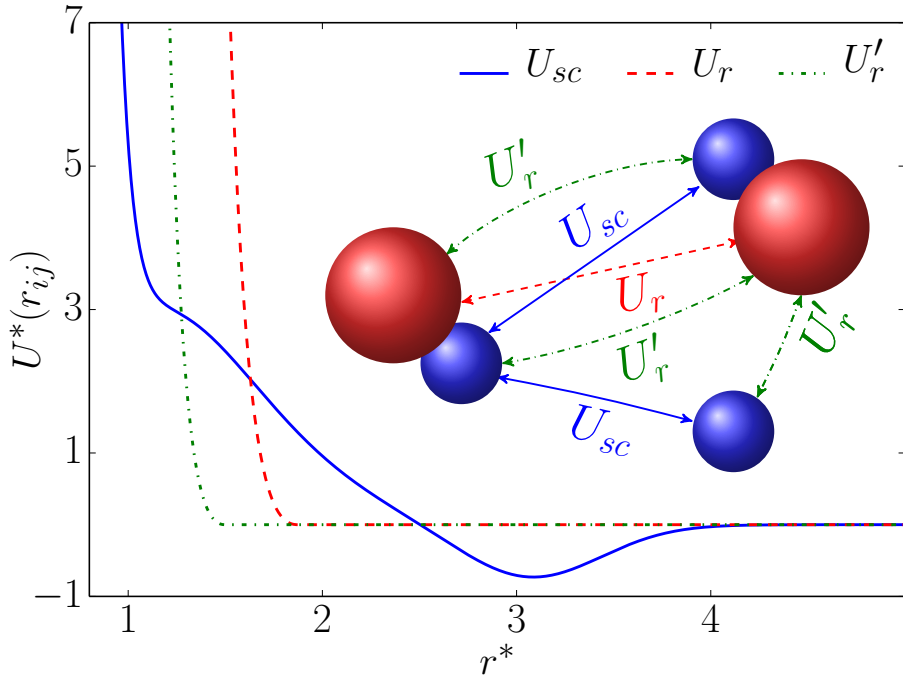


Figure 4.1 Interaction potential *versus* distance. The solid blue line represents the softened-core interaction potential U_{sc} (equation 4.1) between OH-OH, OH-water and water-water sites. The dashed red line and green dot-dashed line represent the R-R, R-OH and R-water repulsive interactions.

4.2 Simulation details

Using the LAMMPS package [124], we have performed MD simulations for a system with a number of particles ranging from 2000 to 4000 for various compositions.

The simulations were performed in the *NPT* ensemble with a Nosée-Hoover thermostat and barostat [125, 126] and particles were placed in a cubic box with standard periodic

boundary condition. The dimer bonds were kept fixed using a SHAKE algorithm [127], with a tolerance factor of 10^{-5} . Since the system can undergo a demixing transition, we have systematically checked that the thermodynamic conditions under consideration were away from instability by inspection of the small wave vector behavior of the concentration-concentration structure factor [128, 129]. For our mixture this quantity is defined by

$$S_{cc}(Q) = x_{ROH}^2 S_{ww}(Q) + x_w^2 S_{ROH-ROH}(Q) - 2x_{ROH}x_w S_{w-ROH}(Q), \quad (4.3)$$

where x_w and $x_{ROH} = 1 - x_w$ are the mole fractions of water and alcohol respectively. For the partial structure factors, we have approximated $S_{ROH-ROH} = S_{RR}$ and $S_{w-ROH} = S_{wR}$, i.e. we have neglected the contribution of the OH-sites of the dimer. In the study of demixing, this approximation is harmless, since the positions of R and OH sites within the same molecule are obviously tightly bound. The site-site structure factors are numerically determined from the spatial configurations generated during additional NVT simulation runs (in order to keep the box size constant for the binning procedure in Q-space) using standard procedures [129].

The signature of concentration fluctuations associated with demixing is typically a low-Q diverging concentration-concentration structure factor. By monitoring this quantity along our simulations we have ruled out the presence of inhomogeneities due to demixing.

Our simulations started from a compositionally disordered mixture of ROH and water particles, which was equilibrated at the chosen pressure and temperature for 1×10^7 steps in the NPT-ensemble. Production runs were 8×10^7 step long. The time step was set to $5 \times 10^{-6} \tau$ in reduced units.

4.3 Results

In what follows we will present our results both for the hetero- and homonuclear ROH models in a solution of our water-like fluid, first focusing on the ROH influence on the temperature of the maximum density curve of water (which was already determined in Ref. Si10). We will analyze the influence of the alkyl-group size on the changes of the TMD, comparing the results of our heteronuclear and homonuclear models. Finally, we will analyze the behavior of the excess thermodynamics of the mixture just for the heteronuclear model.

4.3.1 The temperature of maximum density (TMD)

The density anomaly in water and ROH aqueous solutions can be easily detected representing the temperature dependence of the density along isobars. This can be done studying a series of state points along various isobars by means of NPT simulations. These results are presented in Figure 4.2 for various ROH mole fractions, namely $x_{ROH} = 0.00, 0.01, \dots, 0.04$, first for our heteronuclear model. Note that the apparent low values of the reduced density are due to the fact that densities are scaled with the inner core of the potential. If scaled with the range of the second repulsive range ($\approx 2.5\sigma$), which is a more appropriate measure of the molecular size, we will have reduced densities in line with what one should expect for a liquid ($\rho^* \approx 0.5 \sim 0.9$).

At a certain concentration of ROH the TMD disappears, since our ROH model lacks a density anomaly. A relatively accurate numerical estimate of the TMDs was obtained by a polynomial fit to the simulated densities. These points (denoted by solid squares) are connected in Figure 4.2 with short-dashed lines, that constitute the TMD curve in the $T - \rho$ plane. We observe that the region on the left of the TMD points is characterized by the typical density anomaly, namely a density increase upon heating. Note that for all compositions the TMD increases with pressure, to reach a maximum and then decreases. This decrease of the TMD with pressure corresponds to the experimental behavior found in water [130], and is the result of the destructuring effect of pressure on the open structures (hydrogen bonded network in the case of water) whose interplay with the high density phase gives rise to the density anomaly. The increase of the TMD with pressure at low pressures is not found experimentally, and it is a consequence of the fact that in our model the TMD curve is placed in the supercritical region. This feature is present even in models for which the TMD curve is in a low density liquid region, such as the ramp fluid [131].

The various TMD curves for different mole fractions are represented in Figure 4.3. One readily appreciates that the addition of alcohol reduces the density range and the temperature at which the density anomaly is found, ultimately leading to its disappearance. Points at equal pressure are connected by dashed lines.

The change in the TMD with respect to that of pure water ($\Delta T_{MD}(x_{ROH}) = T_{MD}(x_{ROH}) - T_{MD}(x_{ROH} = 0)$) induced by the presence of solute is represented in 4.4 for various pressures. For pressures below $P^* \approx 10$, and up to a certain concentration, we observe that our solute acts as a “structure-maker”. This means that the presence of solute molecules enhances the anomalous behavior of water, by favoring the build up of open structures and hence increasing the TMD. At $P^* = 9.2$, the curve presents a maximum around

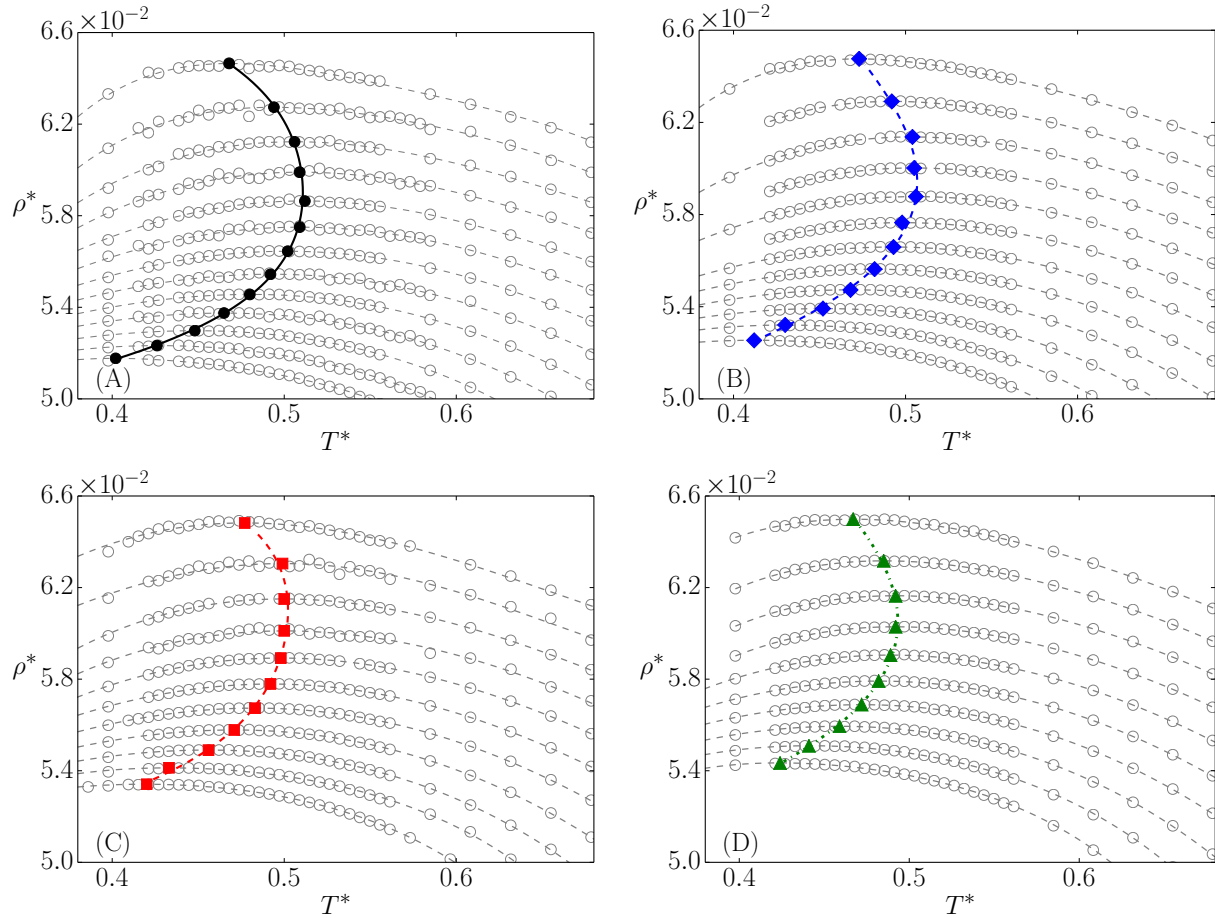


Figure 4.2 Temperature dependence of the density for various solute compositions along isobars with increasing pressure from bottom to top ($P^* = 2.3, \dots, 27.6$). Open circles correspond to simulation data and a dotted line denotes a polynomial fit. (A) $x_{ROH} = 0.0$ (pure water), (B) $x_{ROH} = 0.01$, (C) $x_{ROH} = 0.02$ and (D) $x_{ROH} = 0.03$. The TMD is represented by filled symbols, which are connected with a dashed curve that correspond to a polynomial fit, to represent the TMD curve. Pressure increases from bottom to top.

$x_{ROH} = 0.03$ and then decays, which is the qualitative behavior of the TMD tert-butanol in water [14]. We find that as pressure increases the change in the TMD is lowered, and as a matter of fact for $P^* > 10$, $\Delta T_{MD}(x_{ROH}) < 0$, and the solute behaves as a “structure-breaker”, reducing the range of anomalous behavior of water. This is accordance with the fact that the increase of pressure tends to destroy the low density structures that give rise to the density anomaly, therefore the structuring effect of the solute decreases, to finally turn the “structure-maker” into a “structure-breaker”. For sufficiently high pressures our alcohol-like molecules behave like standard solutes which tend to decrease the TMD [14], i.e. the effect of the two-scale interaction stemming from the OH site is no longer apparent

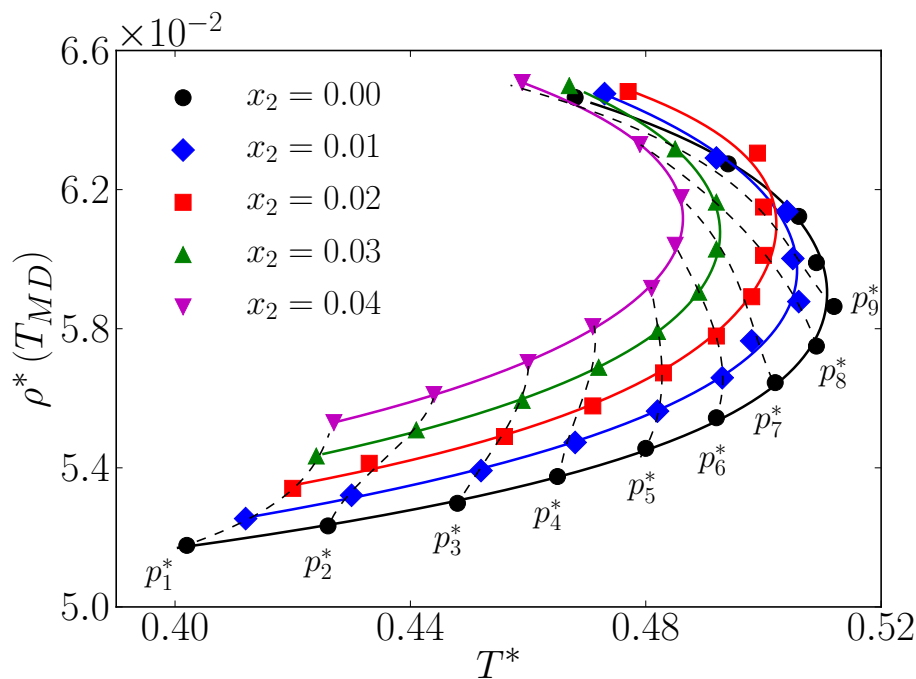


Figure 4.3 Density values at the temperature of maximum density of the heteronuclear alcohol model, for various mole fractions, $x_{ROH} = 0.00$ (black solid lines and filled circles), $x_{ROH} = 0.002$ (red dashed and filled squares) and $x_{ROH} = 0.003$ (green dot-dashed line and filled triangles). In all cases the points are simulation data, and lines correspond to polynomial fits. State points at the same pressure are connected with dotted lines.

for sufficiently high pressures. A parallel situation occurs with the effect of the hydrogen bonds in water when pressure starts to break them.

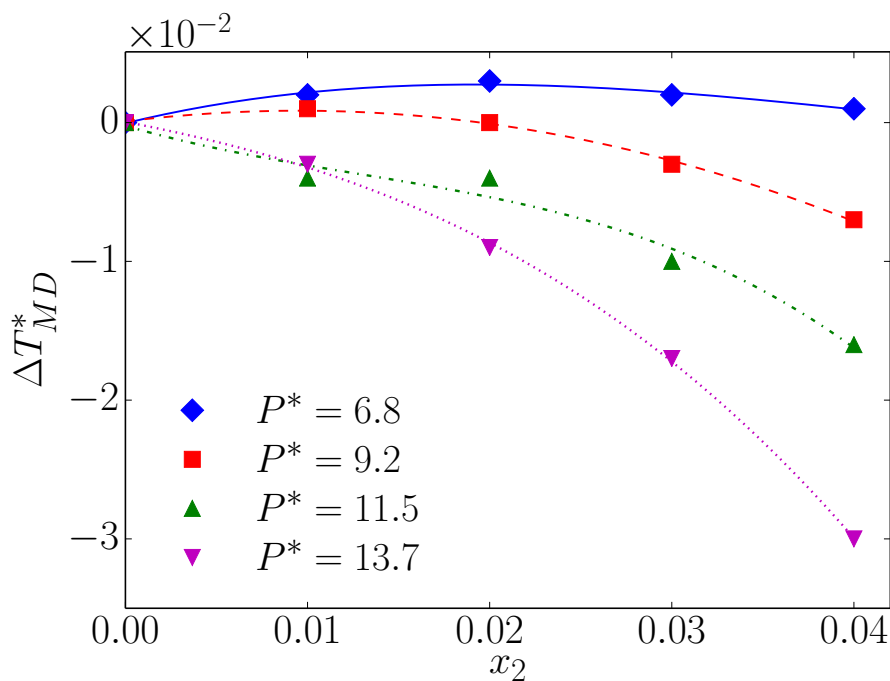


Figure 4.4 Change in the temperature of maximum density with respect to the bulk solvent value vs. alcohol mole fraction for various pressures for the heteronuclear alcohol model.

Now in Figure 4.5 we present the corresponding $\rho - T$ TMD curves for the homonuclear model of alcohol in solution. The first effect one can observe is the shift of the TMD curves as a function of solute concentration is minimized with respect to that observed in Figure 4.3 for the heteronuclear case. This is a clear indication that the larger the size of the apolar tail of the ROH, the more significant the effect of the solute on the TMD. The size dependency of the anomalous behavior is more clearly illustrated in Figure 4.6,

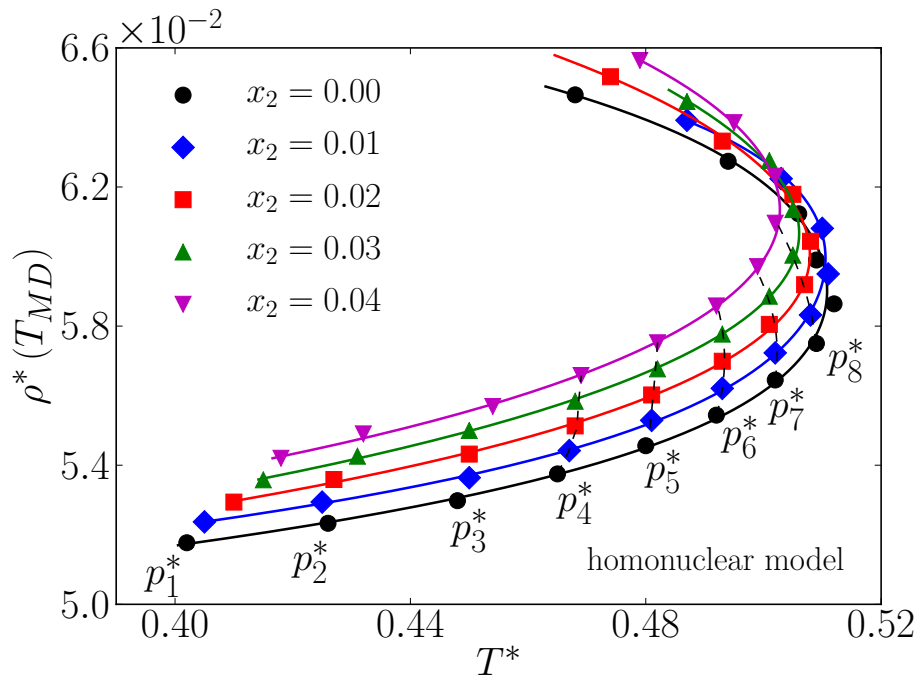


Figure 4.5 Same as Figure 4.3 for the homonuclear alcohol model

where change in the TMD, $\Delta T_{MD}(x_{ROH})$ for the homonuclear model is represented as a function of alcohol concentration, x_{ROH} for various pressures. Note that the same scale as in Figure 4.4 is used. Comparison of both figures shows that the increase in size of the apolar tail of the alcohol increases the changes in the TMD. On one hand, for pressures below $P^* \approx 10$ the maximum in $\Delta T_{MD}(x_{ROH})$ (a characteristic of t-butanol and ethanol in dilution [14]), practically disappears for the homonuclear model. Interestingly, this model displays a behavior resembling that of methanol [14], for which the maximum is hardly visible. For this values of the pressure, the “structure-maker” character of the model alcohol is enhanced when the apolar chain is larger. This is in agreement with the experimental data, and with the theoretical predictions of Chatterjee et al. [132] statistical mechanical model for solutions of apolar solvents in water. Now, as pressure increases above, $P^* \approx 10$ the solute behaves as a “structure breaker”, and interestingly, its effect on the T_{MD} is also more significant as the size of the R-site increases, to the point that the drop of the

TMD for the largest concentration considered is three times larger for the heteronuclear model. Unfortunately, we are not aware of any experimental investigation of the pressure dependence of $\Delta T_{MD}(x_{ROH})$, but since the net effect of pressure is to reduce the range of anomalous behavior (in real fluid by breaking the hydrogen bond network, in our model by displacing particles towards to first range of the potential), that fact that the effect is maximized when the volume of the solute is larger is understandable from an enthalpic point of view.

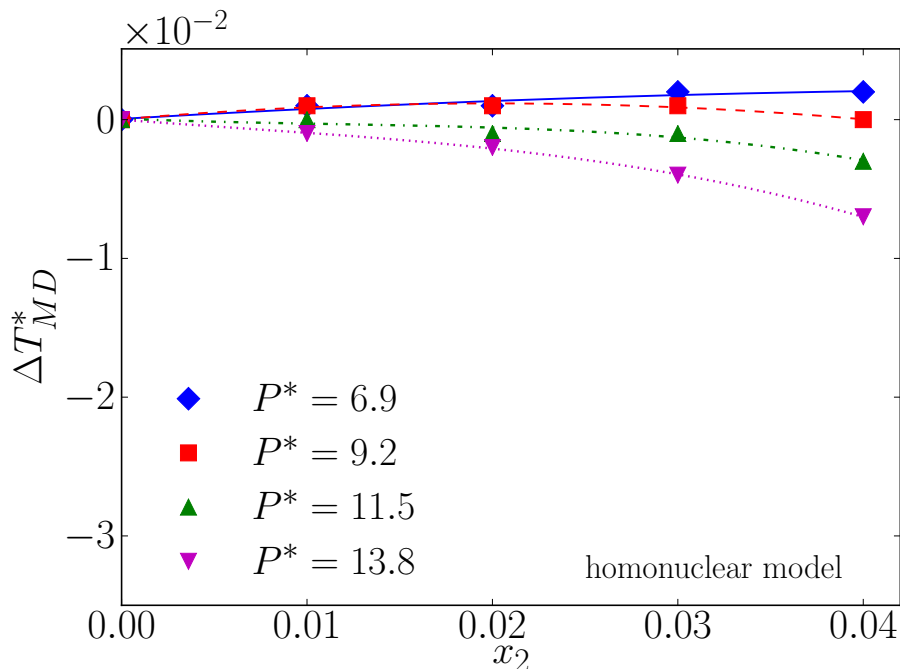


Figure 4.6 Change in the temperature of maximum density with respect to the bulk solvent value vs. alcohol mole fraction for various pressures for the homonuclear alcohol model.

From a microscopic point of view, structural effects of the addition of solute should be visible in the water-water and water-OH pair distribution functions. These are plotted in Figures 4.7 for $P^* = 6.8$ and $T^* = 0.4$. One observes that a small number water particles move into the first scale of the potential (more compact structures), but at the same time, the area corresponding to the second repulsive range of the potential ($r \approx 2\sigma$) becomes more populated, which is particularly visible in the evolution of the second maximum of the g_{wOH} site-site function. In this way, the addition of solute molecules leads to an increase of open structures and more compact ones. The balance between these open and compact structures is correlated with the subtle change from $\Delta T_{MD} > 0$ to $\Delta T_{MD} < 0$ as x_{ROH} grows.

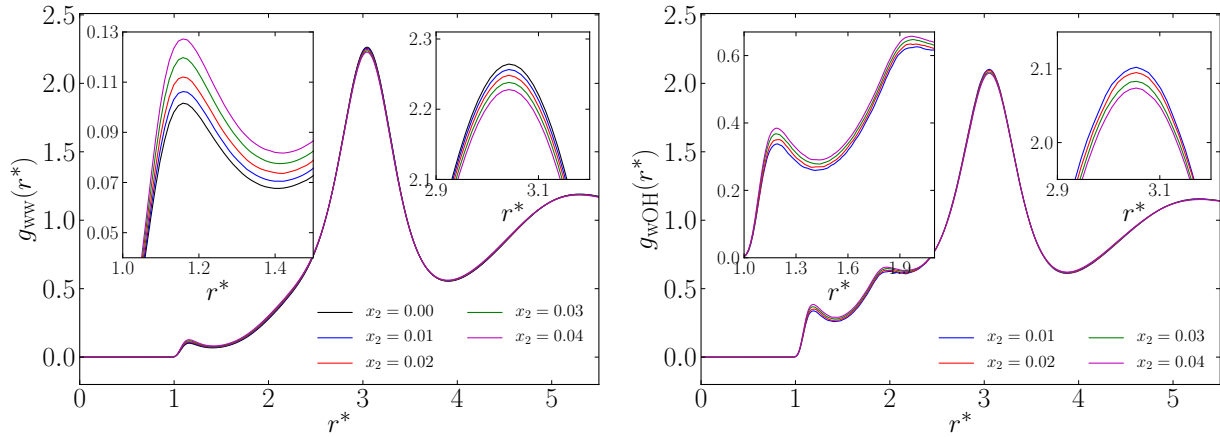


Figure 4.7 Water-water (left) and Water-OH (right) radial distribution functions for $P^* = 6.8$ and $T^* = 0.4$ for various solute concentrations. The insets show zoom of the regions around the first two maxima.

4.3.2 Excess thermodynamic properties

Excess thermodynamic properties of a mixture are defined as the difference between the values of a given thermodynamic quantity and those that would be obtained in an ideal mixture. For a given quantity, A , the corresponding excess property is defined by

$$A^E(x_2, p, T) = A(x_2, p, T) - [x_2 A_2^0(p, T) + (1 - x_2) A_1^0(p, T)] \quad (4.4)$$

where $A(x_2, p, T)$ is the value A in binary mixture of a given composition defined by mole fractions (x_1, x_2) . A_1^0 and A_2^0 are the values of A for the pure components at the same thermodynamic state. Quantities of interest in binary mixtures are the excess volume V^E , enthalpy, H^E , and specific heat at constant pressure c_p^E . Excess entropy is also of interest, but it is not directly accessible in MD calculation. Excess volumes, V^E , are determined from the average volume values obtained along NPT simulations for the mixtures and pure components. Similarly, excess enthalpy is obtained from the usual expression

$$H^E(x_2, p, T) = U^E(x_2, p, T) + PV^E(x_2, p, T), \quad (4.5)$$

and the excess internal energy, U^E , is also directly evaluated from the MD runs for the mixture and pure components. The fluctuation of the enthalpy provides a direct path for

the calculation of the specific heat at constant pressure, c_p^E ,

$$c_p(x_2, p, T) = \left(\frac{\partial H(x_2, p, T)}{\partial T} \right)_P \simeq \langle (H(x_2, p, T) - \langle H(x_2, p, T) \rangle)^2 \rangle_{NpT}. \quad (4.6)$$

and therefore,

$$c_p^E(x_2, p, T) = c_P(x_2, p, T) - [x_2 c_{p,2}^0(p, T) + (1 - x_2) c_{p,1}^0(p, T)]. \quad (4.7)$$

This property requires extremely long simulation runs, and we have assessed the validity of our results comparing the results of the fluctuation approach to those obtained by numerical differentiation of the enthalpy with respect to temperature, for specific points.

Our results for the excess thermodynamics of our mixture system (heteronuclear model) are collected in Figure 4.8. The excess volume exhibits the typical volume contraction of

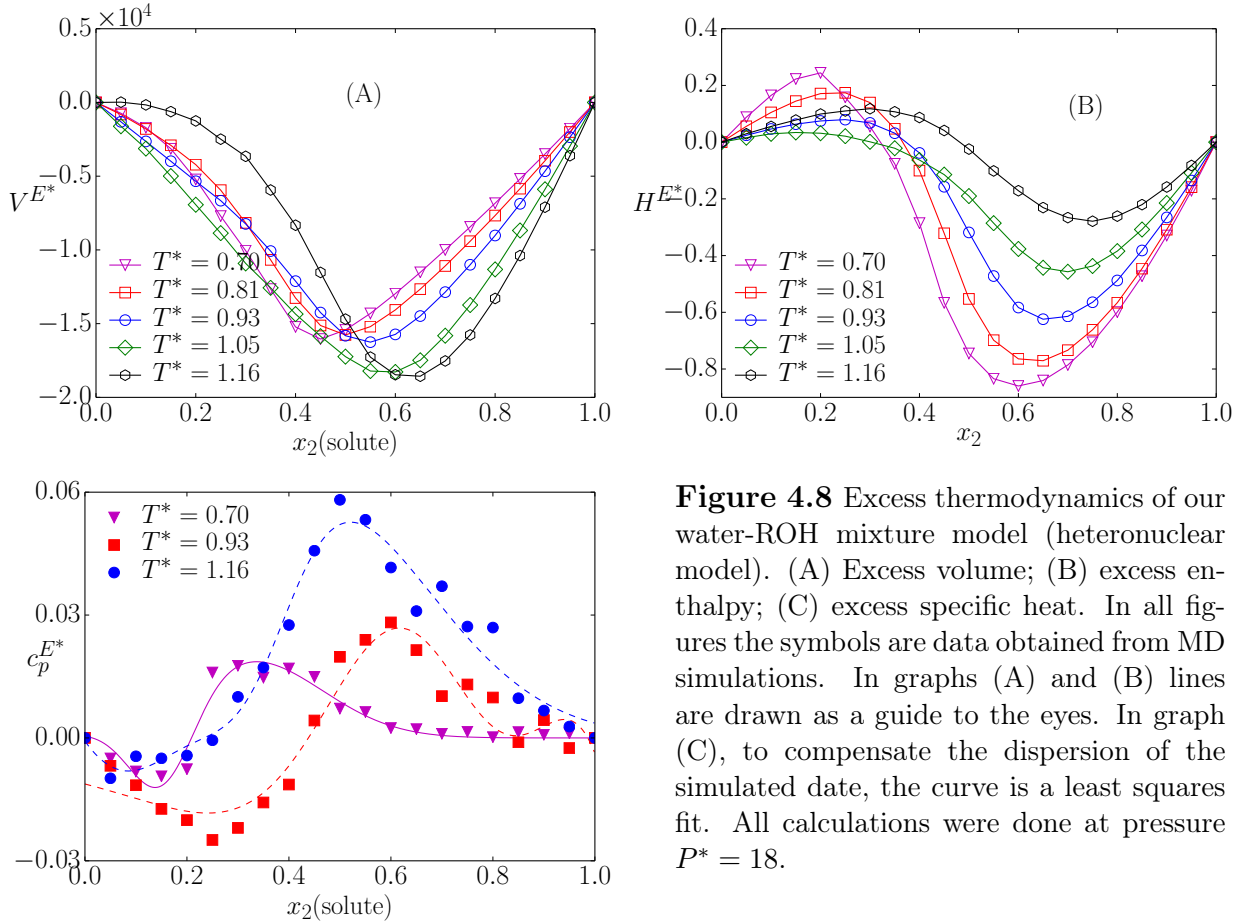


Figure 4.8 Excess thermodynamics of our water-ROH mixture model (heteronuclear model). (A) Excess volume; (B) excess enthalpy; (C) excess specific heat. In all figures the symbols are data obtained from MD simulations. In graphs (A) and (B) lines are drawn as a guide to the eyes. In graph (C), to compensate the dispersion of the simulated data, the curve is a least squares fit. All calculations were done at pressure $P^* = 18$.

the mixture, characteristic of short chain alcohols [19, 133, 134]. This is in agreement with

the observed behavior in $g(r)$ (Figure 4.7), in which is seen that water particles move closer to each other when solute is incorporated.

The situation is somewhat different for the excess enthalpy. Here our model exhibits a minimum for alcohol-rich solutions, in contrast with the experimental situation for methanol [19], ethanol [134] and tert-butanol [133]. In these cases the minimum occurs for water-rich conditions. Moreover, tert-butanol [133] excess enthalpies change sign as the concentration of alcohol increases but, contrary to our model’s behavior, positive values occur at high alcohol concentrations. As shown by González-Salgado and coworkers [19] these discrepancies could be cured by a simple tuning of the cross interaction parameters. Even with more or less sophisticated models for the pure alcohol and water, excess properties can be even qualitatively wrong when Lorentz-Berthelot mixing rules are used [19, 134].

Finally, in the lower graph of Figure 4.8 we have the excess constant pressure heat capacity, as obtained from Eq. 4.7. The model performance for the excess heat capacity is correlated with that of the excess enthalpy. Again here we observe the presence of a maximum in agreement with experimental results for methanol [19] and tert-butanol [133], but the model predicts its position at somewhat higher concentrations of alcohol. Nonetheless, we can say that at relatively low temperature the increase of the heat capacity reflects the structure-making character of our solvent, in accordance with the experimental findings. Again, discrepancies such as the presence of negative values of the excess heat capacity or the shift of the maxima to regions of higher alcohol concentration can be tuned by a careful choice of the cross interaction parameters.

4.4 Conclusions

In summary, we have presented a detailed computer simulation study of a simple model for diluted alcohol-water mixtures, in which the interactions involving hydrogen bonding are represented by a two-scale potential which is known to reproduce a good number of water anomalies. Our results for the dependence of the temperature of maximum density on the solute concentration, are in qualitative agreement with the experimental behavior of methanol and t-butanol solutions, whose molecules are modeled by a homonuclear and heteronuclear dimer respectively. These results indicate that for a small range of concentrations and up to certain values of pressure, these hydrogen-bonding-like solutes tend to enhance the open structures of water and hence increase the TMD, behaving as “structure-makers”.

As pressure increases the “structure-breaker” character of the solutes is enhanced, being larger as the size of the alkyl group grows. This is understandable as the presence of the apolar group as pressure increases makes more unfavorable the open structures which are responsible for the anomalous behavior of the model. This enthalpic effect increases with the size of the solute molecule.

Future work will focus on the dynamic anomalies (e.g. the increase of the diffusion constant with pressure) which are known to be influenced in a similar fashion when diluted hydrogen bonded solutes are present, in marked contrast with the effect of other solutes, either polar or apolar.

This work was submitted at Journal Chemical Physics. At this moment this work is available on: [arXiv:1701.08670](https://arxiv.org/abs/1701.08670)

Chapter 5

General Conclusions

In this thesis, we have studied the problems of confinement/disorder and mixtures in water-like models. In the first chapter, we addressed the effect of a porous media on the anomalous properties of a two-dimensional lattice water-like model. We have shown that the coverage of the low-density liquid phase decreases gradually as the increasing of the degree of confinement, and as consequence of the entropic effects, the temperature of maximum density shifts to lower temperatures. For the anomalous behavior, we observe that the TMD is present for all degree of confinement but the anomaly in the diffusion remains only to intermediate degrees. Interesting features observed here is the suppression of the fluctuations that prevents the estimation of the critical line for the intermediate and higher degree of confinement.

In relation to the mixtures, we studied the excess properties of the aqueous solution through a lattice model. Initially, we proposed a variation of the associating lattice gas (3D) in order to represent both, solute and solvent. The results for pure components was performed through a detailed study of the different order parameters and showed that structure of the phase diagrams are quite similar, with gas and liquid phases, critical points and critical lines. For the study of the mixture, we propose a method to simulate lattice model at a constant pressure. Using it, we obtained the excess properties at a liquid region of solute and solvent. Our model is able to reproduce the excess properties of different types of solute like, short-chain alcohols and ionic liquids. When the cross interaction is attractive, the excess volume and enthalpy are negative, since the “distance” between solute-solvent are lower than the distance solute-solute/solvent-solvent in bulk. This kind of behavior is observed in the water-alcohol mixture as, water-methanol and water-ethanol. The inert case, the excess enthalpy is positive while the excess volume is still negative.

For the case repulsive (hydrophobic) the system show a positive excess volume since the mixture has higher density than the pure componentes due to the cross interactions. In general lines, we show through a very simple model, with only two free parameters, that the complex behavior of aqueous alcohol solutions can be reproduced.

In the last chapter, we addressed on the dependence of the temperature of maximum density with the solute concentration and the excess properties. Our results show that the TMD increase at low solute fractions similar observed experimentally for alcohol aqueous solution. The excess volume shows the contraction effect as the introduction of solute. This behavior is evidenced by the radial distribution function. The excess enthalpy of our model, diverge of the experimental behavior. The fractions in which the experimental excess enthalpy is positive, our model shows negative values and *vice – versa*. The specific heat shows a maximum similar experimental results for methanol, however, in our model, the fraction of maximum is slightly higher than the experimental results.

Chapter 6

Published articles

1. A. P. Furlan, Carlos E. Fiore, and M. C. Barbosa, “*Influence of disordered porous media on the anomalous properties of a simple water model*”, *Phys. Rev. E* **92**, 032404 (2015)
2. A. P. Furlan, N. G. Almarza and M. C. Barbosa “*Lattice model for water-solute mixtures*”, *J. Chem. Phys.* **145**, 144501 (2016)
3. L. Pinheiro, A. P. Furlan, L. B. Krott, A. Diehl, M. C. Barbosa, “*Critical points, phase transitions and water-like anomalies for an isotropic two length scale potential with increasing attractive well*”, *Physica A* **145**, 144501 (2017)
4. A. P. Furlan, E. Lomba and M. C. Barbosa, “*Temperature of maximum density and excess properties of short-chain alcohol aqueous solutions: A simplified model simulation study*”, Submitted to Journal Chemical Physics. Available on [arXiv:1701.08670](https://arxiv.org/abs/1701.08670)

Appendix A

Computation of the residual entropy

We consider a model defined over the diamond lattice with full occupancy. Each particle (site) carries four arms which point to the four NN sites. In order to compute the residual entropy of the lattice model for water we consider two arms of type A (or $+1$) and two arms of type B (or -1). A given particle on the lattice can present $q_W = 4!/(2!2!) = 6$ possible configurations. For the lattice model of solute, we consider two arms of type A , two of type B and one of type C , which leads to $q_M = 4!/2! = 12$ possible orientations of the particle. We set interactions between NN particles, so that the interaction energy is equal to zero for configurations compatible with the ground state of the full model, and greater than zero another case. The pair interactions between NN particles are therefore $u = 0$ when are due to the interactions between pair of arms AB or CB , and $u = \epsilon > 0$ for the other cases (AA , BB , AC , and CC).

The partition function of the system can be written as:

$$Q = \sum_{i=1}^{q^N} \exp \left[-\frac{U(\{\mathbf{S}\}_i)}{k_B T} \right] \quad (\text{A.1})$$

where N being the number of particles (sites) of the system, U the interaction energy and q the number of possible orientations of each particle. $\{\mathbf{S}\}_i$ represent the different configurations of the system. The Helmholtz energy, A , is related with the partition function through:

$$\frac{A}{k_B T} = -\ln Q \quad (\text{A.2})$$

In the limit of infinite temperature, all the possible configurations have the same probability and we get: $A/(k_B T) = -N \ln q$. We are interested in the limit at low temperature. Given

the fact that we know the partition function at high temperature, we can make use of thermodynamic integration [94, 95] to get:

$$A(T)/(k_B T) = -N \ln q + \int_0^{1/(k_B T)} U(T') d\left(\frac{1}{k_B T'}\right); \quad (\text{A.3})$$

Taking into account the thermodynamic relation $A = U - TS$, S being the entropy, and defining reduced quantities $U^* = U/\epsilon$, and $T^* = k_B T/\epsilon$, we can get:

$$\frac{S(T)}{k_B} = N \ln q_1 + \frac{U^*(T)}{T^*} - \int_0^{1/T^*} U^*(T') d(1/T'^*). \quad (\text{A.4})$$

In the limit of low temperature the potential energy of the model vanishes, and it is also fulfilled $\lim_{T \rightarrow 0}(U/T) = 0$, therefore we get:

$$\frac{S(T)}{k_B} \simeq N \ln q - \int_0^{1/T^*} U^*(T') d(1/T'^*); \quad (T^* \rightarrow 0) \quad (\text{A.5})$$

The residual entropy per particle $s_0(N)$ (as a function of the system size) can be computed as:

$$\frac{s_0(N)}{k_B} = \ln q - \lim_{T^* \rightarrow 0} \int_0^{1/T^*} \frac{U^*(N, T')}{N} d(1/T'^*) \quad (\text{A.6})$$

The determination of $s_0(N)$ has been carried out using Monte Carlo simulation, in combination with thermodynamic integration, and parallel tempering techniques. Different system sizes were considered in order to carry out a finite-size scaling analysis to determine s_0 in the thermodynamic limit. Parallel tempering facilitates the equilibration of the systems at low temperature, where the systems reach the ground state (except for some elementary excitations). For the lattice model for water, we have considered different system sizes: $N = 8\ell^3$, with $\ell = 2, 3, 4, \dots, 14$. In each case we considered 257 values of $(1/T^*)$; $1/T_i^* = i \times \Delta(1/T^*)$; $i = 0, 1, \dots, 256$; with $\Delta(1/T^*) = 0.050$. The averaged reduced potential energy per particle $u^* = U/(N\epsilon)$ is 1 for $T \rightarrow \infty$, and it almost vanishes for the lowest values of T considered in the integration $u^* \ll 10^{-6}$ (for the largest system sizes). It decays rapidly as $T \rightarrow 0$, making possible a reliable cut-off of the integration for a given level of accuracy in the results. In TABLE A.1 we present the estimates for $s_0(N)$. In order to estimate the value of s_0 in the thermodynamic limit we have considered the scaling relations used by Berg *et al.* [135],

$$s_0(N)/k_B = s_0/k_B + a_1 N^{-\theta}; \quad (\text{A.7})$$

ℓ	2	3	4	5	6
$s_0(8\ell^3)/k_B$	0.435774(13)	0.418939(18)	0.414306(18)	0.412543(16)	0.411693(18)
ℓ	7	8	9	10	11
$s_0(8\ell^3)/k_B$	0.411271(19)	0.410988(22)	0.410823(21)	0.410737(24)	0.410645(21)
ℓ	12	13	14		
$s_0(8\ell^3)/k_B$	0.410619(14)	0.410574(13)	0.410549(8)		

Table A.1 System-size dependent estimates for the residual entropy presented as $s_0^*(N)/k_B$

The fitting of the simulation results given in TABLE A.1 to Eq. (A.7), with (s_0/k_B) , a_1 , and θ being adjustable parameters leads to:

$$s_0^{(W)}/k_B = 0.410\,41 \pm 0.000\,02; \quad \theta = 0.899 \pm 0.005, \quad (\text{A.8})$$

where the label (W) refers to water. Considering the quantities $\Omega(N_L) = \exp[s_0(N_L)/k_B]$, and fitting the results to

$$\Omega(N) = \Omega + a_\Omega N^{-\theta}, \quad (\text{A.9})$$

we get

$$\Omega = 1.507\,44 \pm 0.000\,04; \quad \theta = 0.905 \pm 0.005. \quad (\text{A.10})$$

The values of the exponent θ agree within statistical uncertainty with the results of Berg et al. [135]. For the residual entropy of the ordinary ice. Interestingly, our estimate of Ω for our model defined over a system with cubic symmetry and the estimate of for the ordinary ice of Berg et al. [135]: $\Omega^{\text{Ice}} = 1.507\,38 \pm 0.000\,16$; $\theta = 0.923(23)$, seem to coincide (at least within error bars) in spite of the different structures of the underlying lattices.

In principle, we could apply the same simulation techniques used for the water in the determination of the residual entropy of the lattice gas model of the solute. However, the value of s_0 for methanol can be deduced directly from the water results. Given a ground state, the configuration of the water for a system with N molecules (occupied positions) one can build up 2^N directly related ground states for the methanol model, since the two (undistinguishable) A patches of each particle in the water model corresponds to two distinguishable (A and C) patches in the methanol model. Therefore, we get:

$$s_0^{(S)} = s_0^{(W)} + k_B \ln 2. \quad (\text{A.11})$$

Bibliography

- [1] CHAPLIN, M. Water: structure and science. <http://www.lsbu.ac.uk/water>. Acesso em: 15/05/2015. [iii](#), [1](#), [2](#), [4](#), [5](#), [6](#), [7](#)
- [2] STANLEY, H. E.; BULDYREV, S. V.; FRANZESE, G.; GIOVAMBATTISTA, N.; STARR, F. W. Static and dynamic heterogeneities in water. *Philosophical Transactions of the Royal Society A: Mathematical, Physical and Engineering Sciences*, v. 363, n. 1827, p. 509–523, 2005. [iii](#), [3](#)
- [3] H., P. P.; SCIORTINO, F.; ESSMANN, U.; STANLEY, H. E. Phase behaviour of metastable water. *Nature*, London, v. 360, p. 324–328, 1992. [iii](#), [2](#), [3](#)
- [4] KELL, G. S. Density, thermal expansivity, and compressibility of liquid water from 0°C to 150°C. correlations and tables for atmospheric pressure and saturation reviewed and expressed on 1968 temperature scale. *Journal of Chemical and Engineering Data*, v. 20, n. 1, p. 97–105, 1975. [iii](#), [1](#), [4](#), [6](#)
- [5] ANGELL, C. A.; FINCH, E. D.; BACH, P. Spin–echo diffusion coefficients of water to 2380 bar and -20°C. *The Journal of Chemical Physics*, v. 65, n. 8, p. 3063–3066, 1976. [iii](#), [1](#), [4](#), [6](#), [7](#), [64](#)
- [6] STELL, G.; HEMMER, P. C. Phase transitions due to softness of the potential core. *The Journal of Chemical Physics*, v. 56, n. 9, 1972. [iii](#), [8](#), [9](#)
- [7] JAGLA, E. A. Core-softened potentials and the anomalous properties of water. *The Journal of Chemical Physics*, v. 111, n. 19, p. 8980–8986, 1999. [iii](#), [8](#), [9](#), [13](#), [21](#)
- [8] DE OLIVEIRA, A. B.; BARBOSA, M. C.; NETZ, P. A. Interplay between structure and density anomaly for an isotropic core-softened ramp-like potential. *Physica A: Statistical Mechanics and its Applications*, v. 386, n. 2, p. 744 – 747, 2007. [iii](#), [4](#), [8](#), [10](#)

- [9] FRANZESE, G. Differences between discontinuous and continuous soft-core attractive potentials: The appearance of density anomaly. *Journal of Molecular Liquids*, v. 136, n. 3, p. 267 – 273, 2007. EMLG/JMLG 2006. [iii](#), [9](#), [10](#), [13](#), [41](#), [42](#)
- [10] XU, L.; KUMAR, P.; BULDYREV, S. V.; CHEN, S.-H.; POOLE, P. H.; SCIORTINO, F.; STANLEY, H. E. Relation between the widom line and the dynamic crossover in systems with a liquid–liquid phase transition. *Proceedings of the National Academy of Sciences of the United States of America*, Washington, v. 102, n. 46, p. 16558–16562, 2005. [iv](#), [11](#), [12](#)
- [11] STREKALOVA, E. G.; LUO, J.; STANLEY, H. E.; FRANZESE, G.; BULDYREV, S. V. Confinement of anomalous liquids in nanoporous matrices. *Phys. Rev. Lett.*, v. 109, p. 105701, 2012. [iv](#), [11](#), [13](#), [14](#)
- [12] PAGE, K. S.; MONSON, P. A. Monte carlo calculations of phase diagrams for a fluid confined in a disordered porous material. *Phys. Rev. E*, v. 54, p. 6557–6564, 1996. [iv](#), [14](#)
- [13] STREKALOVA, E. G.; MAZZA, M. G.; STANLEY, H. E.; FRANZESE, G. Hydrophobic nanoconfinement suppresses fluctuations in supercooled water. *Journal of Physics: Condensed Matter*, Bristol, v. 24, n. 6, p. 064111, 2012. [iv](#), [14](#), [15](#)
- [14] WADA, G.; UMEDA, S. Effects of nonelectrolytes on the temperature of the maximum density of water. i. alcohols. *Bulletin of the Chemical Society of Japan*, v. 35, n. 4, p. 646–652, 1962. [iv](#), [15](#), [16](#), [21](#), [68](#), [70](#)
- [15] MARONGIU, B.; FERINO, I.; MONACI, R.; SOLINAS, V.; TORRAZZA, S. Thermodynamic properties of aqueous non-electrolyte mixtures. alkanols + + water systems. *Journal of Molecular Liquids*, v. 28, n. 4, p. 229 – 247, 1984. [iv](#), [17](#), [41](#), [45](#), [59](#)
- [16] PATEL, N. C.; SANDLER, S. I. Excess volumes of the water/methanol, n-heptane/ethyl acetate, n-heptane/n-butyraldehyde, and n-heptane/isobutyraldehyde systems. *Journal of Chemical & Engineering Data*, v. 30, n. 2, p. 218–222, 1985. [iv](#), [17](#), [19](#), [45](#), [56](#)
- [17] BAKO, I.; MEGYES, T.; BALINT, S.; GROSZ, T.; CHIHAIA, V. Water-methanol mixtures: topology of hydrogen bonded network. *Phys. Chem. Chem. Phys.*, v. 10, p. 5004–5011, 2008. [iv](#), [18](#), [19](#)

- [18] ALLISON, S.; FOX, J.; HARGREAVES, R.; BATES, S. Clustering and microimmiscibility in alcohol-water mixtures: Evidence from molecular-dynamics simulations. *Physical Review B*, v. 71, n. 2, p. 024201, Jan. 2005. [iv](#), [18](#), [19](#)
- [19] GONZÁLEZ-SALGADO, D.; ZEMÁNKOVÁ, K.; NOYA, E. G.; LOMBA, E. Temperature of maximum density and excess thermodynamics of aqueous mixtures of methanol. *The Journal of Chemical Physics*, v. 144, n. 18, 2016. [iv](#), [18](#), [19](#), [20](#), [73](#), [74](#)
- [20] STANLEY, H.; BARBOSA, M.; MOSSA, S.; NETZ, P.; SCIORTINO, F.; STARR, F.; YAMADA, M. Statistical physics and liquid water at negative pressures. *Physica A: Statistical Mechanics and its Applications*, v. 315, n. 1–2, p. 281 – 289, 2002. Slow Dynamical Processes in Nature. [1](#), [4](#), [6](#)
- [21] DEBENEDETTI, P. G.; STANLEY, H. E. Supercooled and glassy water. *Print edition*, v. 56, n. 6, 2003. [2](#)
- [22] MISHIMA, O.; STANLEY, H. E. Decompression-induced melting of ice iv and the liquid-liquid transition in water. v. 392, p. 164–198, 1998. [2](#)
- [23] POOLE, P. H.; SCIORTINO, F.; ESSMANN, U.; STANLEY, H. E. Spinodal of liquid water. *Phys. Rev. E*, v. 48, p. 3799–3817, 1993. [2](#)
- [24] KANNO, H.; MIYATA, K. The location of the second critical point of water. *Chemical Physics Letters*, Amsterdam, v. 422, n. 4–6, p. 507 – 512, 2006. [2](#)
- [25] MISHIMA, O. Liquid-liquid critical point in heavy water. *Phys. Rev. Lett.*, v. 85, p. 334–336, 2000. [2](#)
- [26] MISHIMA, O. Reversible first-order transition between two H₂O amorphs at ~ 0.2 GPa and ~ 135 K. *The Journal of Chemical Physics*, v. 100, n. 8, p. 5910–5912, 1994. [2](#)
- [27] SPEEDY, R. J.; ANGELL, C. A. Isothermal compressibility of supercooled water and evidence for a thermodynamic singularity at -45°C . *The Journal of Chemical Physics*, v. 65, n. 3, p. 851–858, 1976. [4](#), [6](#)
- [28] ANGELL, C. A. Insights into phases of liquid water from study of its unusual glass-forming properties. *Science*, Washington, v. 319, n. 5863, p. 582–587, 2008. [4](#)

- [29] SASTRY, S.; DEBENEDETTI, P. G.; SCIORTINO, F.; STANLEY, H. E. Singularity-free interpretation of the thermodynamics of supercooled water. *Phys. Rev. E*, v. 53, p. 6144–6154, 1996. [4](#)
- [30] ERRINGTON, J. R.; DEBENEDETTI, P. G. Relationship between structural order and the anomalies of liquid water. *Nature*, London, v. 409, p. 318–321, 2001. [4](#), [64](#)
- [31] GEIGER, A. Mechanisms of the molecular mobility of water. *Journal of Molecular Liquids*, v. 106, n. 2–3, p. 131 – 146, 2003. Contribution to the Seminar on the Structure of Liquids and Liquid Solutions of the Russian Academy of Sciences in the Honour of Professor O. Ya. Samoilov, Moscow 2001. [4](#)
- [32] SOPER, A. K. Water: Two liquids divided by a common hydrogen bond. *The Journal of Physical Chemistry B*, v. 115, n. 48, p. 14014–14022, 2011. PMID: 21612286. [4](#)
- [33] TOMBARI, E.; FERRARI, C.; SALVETTI, G. Heat capacity anomaly in a large sample of supercooled water. *Chemical Physics Letters*, Amsterdam, v. 300, n. 5–6, p. 749 – 751, 1999. [6](#)
- [34] STILLINGER, F. H.; RAHMAN, A. Improved simulation of liquid water by molecular dynamics. *The Journal of Chemical Physics*, v. 60, n. 4, p. 1545–1557, 1974. [7](#), [8](#)
- [35] TOUKAN, K.; RAHMAN, A. Molecular-dynamics study of atomic motions in water. *Phys. Rev. B*, v. 31, p. 2643–2648, 1985. [7](#)
- [36] KUSALIK, P. G.; SVISHCHEV, I. M. The spatial structure in liquid water. *Science*, Washington, v. 265, n. 5176, p. 1219–1221, 1994. [7](#), [18](#)
- [37] JORGENSEN, W. L.; CHANDRASEKHAR, J.; MADURA, J. D.; IMPEY, R. W.; KLEIN, M. L. Comparison of simple potential functions for simulating liquid water. *The Journal of Chemical Physics*, v. 79, n. 2, p. 926–935, 1983. [7](#), [18](#)
- [38] MAHONEY, M. W.; JORGENSEN, W. L. A five-site model for liquid water and the reproduction of the density anomaly by rigid, nonpolarizable potential functions. *The Journal of Chemical Physics*, v. 112, n. 20, p. 8910–8922, 2000. [7](#)
- [39] SMALLENBURG, F.; POOLE, P. H.; SCIORTINO, F. Phase diagram of the st2 model of water. *Molecular Physics*, v. 113, n. 17-18, p. 2791–2798, 2015. [8](#)

- [40] BROVCHENKO, I.; OLEINIKOVA, A. Multiple phases of liquid water. *ChemPhysChem*, v. 9, n. 18, p. 2660–2675, 2008. [8](#)
- [41] DE OLIVEIRA, A.; NETZ, P.; BARBOSA, M. Which mechanism underlies the water-like anomalies in core-softened potentials? *The European Physical Journal B - Condensed Matter and Complex Systems*, v. 64, p. 481–486, 2008. [10.1140/epjb/e2008-00101-6](#). [8](#), [9](#), [13](#)
- [42] NEY M. BARRAZ, J.; SALCEDO, E.; BARBOSA, M. C. Thermodynamic, dynamic, structural, and excess entropy anomalies for core-softened potentials. *The Journal of Chemical Physics*, v. 135, n. 10, p. 104507, 2011. [8](#)
- [43] DE OLIVEIRA, A. B.; FRANZESE, G.; NETZ, P. A.; BARBOSA, M. C. Waterlike hierarchy of anomalies in a continuous spherical shouldered potential. *The Journal of Chemical Physics*, v. 128, n. 6, p. 064901, 2008. [8](#), [9](#)
- [44] DA SILVA, J. N.; SALCEDO, E.; DE OLIVEIRA, A. B.; BARBOSA, M. C. Effects of the attractive interactions in the thermodynamic, dynamic, and structural anomalies of a two length scale potential. *The Journal of Chemical Physics*, v. 133, n. 24, p. –, 2010. [8](#), [64](#)
- [45] NETZ, P. A.; RAYMUNDI, J. F.; CAMERA, A. S.; BARBOSA, M. C. Dynamic anomalies of fluids with isotropic doubled-ranged potential. *Physica A: Statistical Mechanics and its Applications*, v. 342, p. 48–53, 2004. [8](#)
- [46] BELL, G. M.; LAVIS, D. A. Two-dimensional bonded lattice fluids i. interstitial model. *Journal of Physics A: General Physics*, v. 3, n. 4, p. 427, 1970. [9](#), [10](#)
- [47] G. FRANZESE, G. MALESCIO, A. S. S. B. E. S. Generic mechanism for generating a liquid-liquid phase transition. [9](#), [29](#)
- [48] LAVIS, D. A. The steam-water-ice system: a two-dimensional bonded lattice model. the first-order approximation. *Journal of Physics C: Solid State Physics*, v. 6, n. 9, p. 1530, 1973. [10](#)
- [49] HENRIQUES, V. B.; BARBOSA, M. C. Liquid polymorphism and density anomaly in a lattice gas model. *Phys. Rev. E*, v. 71, p. 031504, 2005. [10](#)

- [50] DE OLIVEIRA, A. B.; BARBOSA, M. C. Density anomaly in a competing interactions lattice gas model. *Journal of Physics: Condensed Matter*, Bristol, v. 17, n. 3, p. 399, 2005. [10](#)
- [51] BALLADARES, A. L.; HENRIQUES, V. B.; BARBOSA, M. C. Liquid polymorphism, density anomaly and h-bond disruption in associating lattice gases. *Journal of Physics: Condensed Matter*, Bristol, v. 19, n. 11, p. 116105, 2007. [10](#), [26](#), [28](#)
- [52] SZORTYKA, M. M.; HENRIQUES, V. B.; GIRARDI, M.; BARBOSA, M. C. Dynamic transitions in a two dimensional associating lattice gas model. *The Journal of Chemical Physics*, v. 130, n. 18, p. 184902, 2009. [10](#), [30](#)
- [53] SZORTYKA, M. M.; BARBOSA, M. C. Diffusion anomaly in an associating lattice gas model. *Physica A: Statistical Mechanics and its Applications*, v. 380, n. 0, p. 27 – 35, 2007. [10](#)
- [54] FRANZESE, G.; STANLEY, H. E. Liquid-liquid critical point in a hamiltonian model for water: analytic solution. *Journal of Physics: Condensed Matter*, Bristol, v. 14, n. 9, p. 2201, 2002. [10](#)
- [55] CIACH, A.; GÓŹDŹ, W.; PERERA, A. Simple three-state lattice model for liquid water. *Phys. Rev. E*, v. 78, p. 021203, Aug 2008. [10](#)
- [56] BLUME, M.; EMERY, V. J.; GRIFFITHS, R. B. Ising model for the λ transition and phase separation in he^3 - he^4 mixtures. *Phys. Rev. A*, v. 4, p. 1071–1077, Sep 1971. [10](#)
- [57] LIU, L.; CHEN, S.-H.; FARAONE, A.; YEN, C.-W.; MOU, C.-Y. Pressure dependence of fragile-to-strong transition and a possible second critical point in supercooled confined water. *Phys. Rev. Lett.*, v. 95, p. 117802, 2005. [11](#)
- [58] FARAONE, A.; LIU, L.; MOU, C.-Y.; YEN, C.-W.; CHEN, S.-H. Fragile-to-strong liquid transition in deeply supercooled confined water. *The Journal of Chemical Physics*, v. 121, n. 22, p. 10843–10846, 2004. [11](#)
- [59] MALLAMACE, F.; BROCCIO, M.; CORSARO, C.; FARAONE, A.; LIU, L.; MOU, C.-Y.; SOW-HSINCHEN. Dynamical properties of confined supercooled water: an nmr study. *Journal of Physics: Condensed Matter*, Bristol, v. 18, n. 36, p. S2285, 2006. [11](#)

- [60] KROTT, L. B.; BARBOSA, M. C. Anomalies in a waterlike model confined between plates. *J. Chem. Phys.*, v. 138, 2013. [11](#)
- [61] ERKO, M.; FINDENEGG, G. H.; CADE, N.; MICHETTE, A. G.; PARIS, O. Confinement-induced structural changes of water studied by raman scattering. *Phys. Rev. B*, v. 84, p. 104205, 2011. [11](#)
- [62] INGÖLFSSON, H. I.; LI, Y.; VOSTRIKOV, V. V.; GU, H.; HINTON, J. F.; KOEPPE, R. E.; ROUX, B.; ANDERSEN, O. S. Gramicidin a backbone and side chain dynamics evaluated by molecular dynamics simulations and nuclear magnetic resonance experiments. i: Molecular dynamics simulations. *The Journal of Physical Chemistry B*, v. 115, n. 22, p. 7417–7426, 2011. PMID: 21574563. [11](#)
- [63] VAN OSS, C. J. Development and applications of the interfacial tension between water and organic or biological surfaces. *Colloids and Surfaces B: Biointerfaces*, v. 54, n. 1, p. 2 – 9, 2007. [11](#)
- [64] GAO, J.; LUEDTKE, W. D.; LANDMAN, U. Layering transitions and dynamics of confined liquid films. *Phys. Rev. Lett.*, v. 79, p. 705–708, 1997. [11](#)
- [65] SCHEIDLER, P.; KOB, W.; BINDER, K. Cooperative motion and growing length scales in supercooled confined liquids. *EPL (Europhysics Letters)*, v. 59, n. 5, p. 701, 2002. [11](#)
- [66] TOLONEN, L. K.; BERGENSTRÄHLE-WOHLERT, M.; SIXTA, H.; WOHLERT, J. Solubility of cellulose in supercritical water studied by molecular dynamics simulations. *The Journal of Physical Chemistry B*, v. 119, n. 13, p. 4739–4748, 2015. PMID: 25756596. [11](#)
- [67] MADDEN, W.; GLANDT, E. Distribution functions for fluids in random media. *Journal of Statistical Physics*, New York, v. 51, n. 3-4, p. 537–558, 1988. [12](#)
- [68] STREKALOVA, E. G.; MAZZA, M. G.; STANLEY, H. E.; FRANZESE, G. Large decrease of fluctuations for supercooled water in hydrophobic nanoconfinement. *Phys. Rev. Lett.*, v. 106, p. 145701, Apr 2011. [13](#)
- [69] DOMINGUEZ, H.; PIZIO, O.; PUSZTAI, L.; SOKOLOWSKI, S. The structural properties and diffusion of a three-dimensional isotropic core-softened model fluid

- in disordered porous media. molecular dynamics simulation. *Adsorption Science & Technology*, v. 25, n. 7, p. 479–491, 2007. [13](#), [14](#)
- [70] KAMINSKY, R. D.; MONSON, P. A. The influence of adsorbent microstructure upon adsorption equilibria: Investigations of a model system. *The Journal of Chemical Physics*, v. 95, n. 4, p. 2936–2948, 1991. [14](#)
- [71] BENSON, G.; D'ARCY, P.; KIYOHARA, O. Thermodynamics of aqueous mixtures of nonelectrolytes ii. isobaric heat capacities of water-n-alcohol mixtures at 25c. *Journal of Solution Chemistry*, v. 9, n. 12, p. 931–938, 1980. [17](#), [56](#)
- [72] BENSON, G. C.; D'ARCY, P. J. Excess isobaric heat capacities of water-n-alcohol mixtures. *Journal of Chemical & Engineering Data*, v. 27, n. 4, p. 439–442, 1982. [17](#)
- [73] BUTLER, J. A. V.; THOMSON, D. W.; MACLENNAN, W. H. 173. the free energy of the normal aliphatic alcohols in aqueous solution. part i. the partial vapour pressures of aqueous solutions of methyl, n-propyl, and n-butyl alcohols. part ii. the solubilities of some normal aliphatic alcohols in water. part iii. the theory of binary solutions, and its application to aqueous-alcoholic solutions. *J. Chem. Soc.*, p. 674–686, 1933. [17](#)
- [74] HEADGORDON, T.; STILLINGER, F. H. An orientational perturbation theory for pure liquid water. *The Journal of Chemical Physics*, v. 98, n. 4, 1993. [18](#)
- [75] DIXIT, S.; CRAIN, J.; POON, W.; FINNEY, J.; SOPER, A. Molecular segregation observed in a concentrated alcohol-water solution. *Nature*, London, v. 416, n. 6883, p. 829–832, 2002. [18](#)
- [76] LAAKSONEN, A, P. G. K. I. M. S. Three-dimensional structure in water-methanol mixtures. *J. Phys. Chem. A*, , n. 101, p. 5910–5918, 1997. [18](#)
- [77] SU, Z.; BULDYREV, S. V.; DEBENEDETTI, P. G.; ROSSKY, P. J.; Eugene Stanley, H. Modeling simple amphiphilic solutes in a Jagla solvent. *The Journal of chemical physics*, v. 136, n. 4, p. 044511, Jan. 2012. [21](#)
- [78] HUŠ, M.; MUNAÒ, G.; URBIC, T. Properties of a soft-core model of methanol: An integral equation theory and computer simulation study. *The Journal of Chemical Physics*, v. 141, n. 16, p. –, 2014. [21](#), [48](#)

- [79] HUŠ, M.; ŽAKELJ, G.; URBIČ, T. Properties of methanol-water mixtures in a coarse-grained model. *Acta Chimica Slovenica*, v. 61, n. 0, 2015. [21](#)
- [80] FUJIHARA, I.; MIYANO, Y.; SAKAMOTO, K.; SATOH, K.; NAKANISHI, K. Excess thermodynamic properties for equal size Lennard–Jones mixtures and the effect of the difference of the potential well depth between components. *Fluid Phase Equilibria*, Amsterdam, v. 336, p. 1–8, 2012. [22](#), [56](#), [57](#)
- [81] FURLAN, A. P.; FIORE, C. E.; BARBOSA, M. C. Influence of disordered porous media on the anomalous properties of a simple water model. *Phys. Rev. E*, v. 92, p. 032404, Sep 2015. [23](#)
- [82] FURLAN, A. P.; ALMARZA, N. G.; BARBOSA, M. C. Lattice model for water-solute mixtures. *The Journal of Chemical Physics*, v. 145, n. 14, p. 144501, 2016. [23](#)
- [83] METROPOLIS, N.; ROSENBLUTH, A. W.; ROSENBLUTH, M. N.; TELLER, A. H.; TELLER, E. Equation of state calculations by fast computing machines. *The Journal of Chemical Physics*, v. 21, n. 6, p. 1087–1092, 1953. [29](#)
- [84] ÁLVAREZ, M.; LEVESQUE, D.; WEIS, J.-J. Monte carlo approach to the gas-liquid transition in porous materials. *Phys. Rev. E*, v. 60, p. 5495–5504, Nov 1999. [30](#)
- [85] FISH, J. M.; VINK, R. L. C. Nematics with quenched disorder: Violation of self-averaging. *Phys. Rev. Lett.*, v. 105, p. 147801, Sep 2010. [30](#)
- [86] NETZ, P.; STARR, F.; BARBOSA, M. C.; STANLEY, H. Relation between structural and dynamical anomalies in supercooled water. *Physica A: Statistical Mechanics and its Applications*, v. 314, n. 1–4, p. 470 – 476, 2002. Horizons in Complex Systems. [37](#)
- [87] ALMARZA, N. G.; TAVARES, J. M.; NOYA, E. G.; TELO DA GAMA, M. M. Three-dimensional patchy lattice model for empty fluids. *The Journal of Chemical Physics*, v. 137, n. 24, p. –, 2012. [40](#), [45](#)
- [88] RANKE, J.; OTHMAN, A.; FAN, P.; MÜLLER, A. Explaining ionic liquid water solubility in terms of cation and anion hydrophobicity. *International Journal of Molecular Sciences*, v. 10, n. 3, p. 1271–1289, 2009. [41](#), [42](#)

- [89] GIRARDI, M.; SZORTYKA, M.; BARBOSA, M. C. Diffusion anomaly in a three-dimensional lattice gas. *Physica A: Statistical Mechanics and its Applications*, v. 386, n. 2, p. 692 – 697, 2007. [42](#)
- [90] BUZANO, C.; De Stefanis, E.; PRETTI, M. Cluster-variation approximation for a network-forming lattice-fluid model. *The Journal of Chemical Physics*, v. 129, n. 2, p. –, 2008. [42](#)
- [91] SZORTYKA, M. M.; GIRARDI, M.; HENRIQUES, V. B.; BARBOSA, M. C. Dynamic transitions in a three dimensional associating lattice gas model. *The Journal of Chemical Physics*, v. 132, n. 13, p. 134904, 2010. [42](#), [48](#)
- [92] SZORTYKA, M. M.; GIRARDI, M.; HENRIQUES, V. B.; BARBOSA, M. C. Structure and anomalous solubility for hard spheres in an associating lattice gas model. *The Journal of Chemical Physics*, v. 137, n. 6, p. 064905, 2012. [42](#), [56](#), [57](#)
- [93] ALMARZA, N.; NOYA, E. Phase transitions of a lattice model for patchy particles with tetrahedral symmetry. *Molecular Physics*, v. 109, n. 1, p. 65–74, 2011. [42](#), [45](#)
- [94] ALLEN, M. P.; TILDESLEY, D. J. *Computer simulation of liquids*. Oxford University Press, 1987. [42](#), [52](#), [64](#), [65](#), [80](#)
- [95] FRENKEL, D.; SMIT, B. *Understanding molecular simulation. from algorithms to applications*. Boston: Academic Press, 1996. [42](#), [47](#), [80](#)
- [96] LANDAU, D. P.; BINDER, K. *A guide to monte carlo simulations in statistical physics, 2nd edition*. Cambridge University Press, 2005. [45](#), [52](#)
- [97] SWENDSEN, R. H.; WANG, J.-S. Replica monte carlo simulation of spin-glasses. *Phys. Rev. Lett.*, v. 57, p. 2607–2609, Nov 1986. [45](#)
- [98] EARL, D. J.; DEEM, M. W. Parallel tempering: Theory, applications, and new perspectives. *Phys. Chem. Chem. Phys.*, v. 7, p. 3910–3916, 2005. [45](#)
- [99] KOFKE, D. A. Gibbs-duhem integration: a new method for direct evaluation of phase coexistence by molecular simulation. *Molecular Physics*, v. 78, n. 6, p. 1331–1336, 1993. [45](#)
- [100] TANAKA, H.; KURITA, R.; MATAKI, H. Liquid-liquid transition in the molecular liquid triphenyl phosphite. *Phys. Rev. Lett.*, v. 92, p. 025701, Jan 2004. [48](#)

- [101] KURITA, R.; TANAKA, H. Critical-like phenomena associated with liquid-liquid transition in a molecular liquid. *Science*, Washington, v. 306, n. 5697, p. 845–848, 2004. [48](#)
- [102] COHEN, I.; HA, A.; ZHAO, X.; LEE, M.; FISCHER, T.; STROUSE, M. J.; KIVELSON, D. A low-temperature amorphous phase in a fragile glass-forming substance. *The Journal of Physical Chemistry*, v. 100, n. 20, p. 8518–8526, 1996. [48](#)
- [103] KURITA, R.; TANAKA, H. On the abundance and general nature of the liquid–liquid phase transition in molecular systems. *Journal of Physics: Condensed Matter*, Bristol, v. 17, n. 27, p. L293, 2005. [48](#)
- [104] LAVIS, D. A. *Equilibrium statistical mechanics of lattice models*. Dordrecht: Springer, 2015. [48](#)
- [105] TAVARES, J. M.; ALMARZA, N. G.; DA GAMA, M. M. T. Three-dimensional patchy lattice model: Ring formation and phase separation. *The Journal of Chemical Physics*, v. 140, n. 4, p. 044905, 2014. [48](#)
- [106] PAPAIOANNOU, V.; CALADO, F.; LAFITTE, T.; DUFAL, S.; SADEQZADEH, M.; JACKSON, G.; ADJIMAN, C. S.; GALINDO, A. Application of the soft-mie group contribution equation of state to fluids of relevance to the oil and gas industry. *Fluid Phase Equilibria*, Amsterdam, v. 416, p. 104 – 119, 2016. Special Issue: {SAFT} 2015. [48](#)
- [107] ABELLO, L. Enthalpies d’excès des systèmes binaires constitués d’hydrocarbures benzeniques et du chloroforme ou du méthylchloroforme. *J. Chim. Phys. Phys.-Chim, Biol.*, v. 70, p. 1355–1359, 1973. [56](#)
- [108] BENSON, G. C. Deuterium isotope effect on the excess enthalpy of methanol water solutions. *J. Phys. Chem.*, v. 67, p. 858–861, 1963. [56](#)
- [109] PANOV, M. Y. Lösungsenthalpie des wassers in den alkoholen,. *Vestn. Leningr. Univ. Fiz. Khim.*, v. 10, p. 149–150, 1976. [56](#)
- [110] OTT, J.; SIPOWSKA, J.; GRUSZKIEWICZ, M.; WOOLLEY, A. Excess volumes for (ethanol+water) at the temperatures (298.15 and 348.15) k and pressures (0.4, 5, and 15) mpa and at the temperature 323.15 k and pressures (5 and 15) mpa. *The Journal of Chemical Thermodynamics*, v. 25, n. 2, p. 307 – 318, 1993. [56](#)

- [111] MAHAM, Y.; TENG, T. T.; HEPLER, L. G.; MATHER, A. E. Densities, excess molar volumes, and partial molar volumes for binary mixtures of water with monoethanolamine, diethanolamine, and triethanolamine from 25 to 80c. *Journal of Solution Chemistry*, v. 23, n. 2, p. 195–205, 1994. [56](#)
- [112] STEC, M.; TATARCZUK, A.; ŚPIEWAK, D.; WILK, A. Densities, excess molar volumes, and thermal expansion coefficients of aqueous aminoethylethanolamine solutions at temperatures from 283.15 to 343.15k. *Journal of Solution Chemistry*, v. 43, n. 5, p. 959–971, 2014. [56](#)
- [113] GARCÍA-MIAJA, G.; TRONCOSO, J.; ROMANÍ, L. Excess enthalpy, density, and heat capacity for binary systems of alkylimidazolium-based ionic liquids + water. *The Journal of Chemical Thermodynamics*, v. 41, n. 2, p. 161 – 166, 2009. [56](#), [57](#), [60](#)
- [114] PRIGOGINE, I.; BELLEMANS, A.; ENGLERTCHWOLES, A. Statistical thermodynamics of solutions. *The Journal of Chemical Physics*, v. 24, n. 3, p. 518–527, 1956. [56](#)
- [115] GIRARDI, M.; SZORTYKA, M. M.; HENRIQUES, V. B.; BARBOSA, M. C. The associating lattice gas in the presence of interacting solutes. *The Journal of Chemical Physics*, v. 142, n. 9, p. 094502, 2015. [56](#)
- [116] TOMASZKIEWICZ, I.; RANDZIO, S.; GIERYCZ, P. Excess enthalpy in the methanol-water system at 278.15, 298.15 and 323.15 k under pressures of 0.1, 20 and 39 mpa. *Thermochimica Acta*, v. 103, n. 2, p. 281 – 289, 1986. [57](#)
- [117] OTT, J.; CORNETT, G.; STOUFFER, C.; WOODFIELD, B.; GUANQUAN, C.; CHRISTENSEN, J. Excess enthalpies of (ethanol+water) at 323.15, 333.15, 348.15, and 373.15 k and from 0.4 to 15 mpa. *The Journal of Chemical Thermodynamics*, v. 18, n. 9, p. 867 – 875, 1986. [57](#)
- [118] MUNDHWA, M.; HENNI, A. Molar excess enthalpy for various alkanolamine (1) + water (2) systems at $t = (298.15, 313.15, \text{ and } 323.15)$ k. *The Journal of Chemical Thermodynamics*, v. 39, n. 11, p. 1439 – 1451, 2007. [57](#)
- [119] BEN-NAIM, A.; NAVARRO, A. M.; LEAL, J. M. A kirkwood-buff analysis of local properties of solutions. *Phys. Chem. Chem. Phys.*, v. 10, p. 2451–2460, 2008. [59](#)

- [120] VATAŠČIN, E.; DOHNAL, V. Thermophysical properties of aqueous solutions of the 1-ethyl-3-methylimidazolium tricyanomethanide ionic liquid. *The Journal of Chemical Thermodynamics*, v. 89, p. 169 – 176, 2015. [60](#)
- [121] KELL, G. S. Precise representation of volume properties of water at one atmosphere. *Journal of Chemical & Engineering Data*, v. 12, n. 1, p. 66–69, 1967. [64](#)
- [122] WEEKS, J. D.; CHANDLER, D.; ANDERSEN, H. C. Role of repulsive forces in determining the equilibrium structure of simple liquids. *The Journal of Chemical Physics*, v. 54, n. 12, p. 5237–5247, 1971. [64](#)
- [123] JORGENSEN, W. L. Optimized intermolecular potential functions of liquid alcohols. *J. Phys. Chem.*, v. 90, p. 1276, 1986. [65](#)
- [124] PLIMPTON, S. Fast parallel algorithms for short-range molecular dynamics. *Journal of Computational Physics*, v. 117, n. 1, p. 1 – 19, 1995. [65](#)
- [125] NOSÉ, S. A unified formulation of the constant temperature molecular dynamics methods. *The Journal of Chemical Physics*, v. 81, n. 1, p. 511–519, 1984. [65](#)
- [126] HOOVER, W. G. Canonical dynamics: Equilibrium phase-space distributions. *Phys. Rev. A*, v. 31, p. 1695–1697, Mar 1985. [65](#)
- [127] RYCKAERT, J.-P.; CICCOTTI, G.; BERENDSEN, H. J. Numerical integration of the cartesian equations of motion of a system with constraints: molecular dynamics of n-alkanes. *Journal of Computational Physics*, v. 23, n. 3, p. 327 – 341, 1977. [66](#)
- [128] HANSEN, J.-P.; MCDONALD, I. *Theory of simple liquids*. 2nd. ed. Academic, London, 1990. [66](#)
- [129] BORES, C.; LOMBA, E.; PERERA, A.; ALMARZA, N. G. Pattern formation in binary fluid mixtures induced by short-range competing interactions. *J. Chem. Phys.*, v. 143, p. 084501, 2015. [66](#)
- [130] PI, H. L.; ARAGONES, J. L.; VEGA, C.; NOYA, E. G.; ABASCAL, J. L.; GONZALEZ, M. A.; MCBRIDE, C. Anomalies in water as obtained from computer simulations of the tip4p 2005 model: density maxima, and density, isothermal compressibility and heat capacity minima. *Mol. Phys.*, v. 107, p. 365 – 374, 2009. [67](#)

- [131] LOMBA, E.; ALMARZA, N. G.; MARTIN, C.; MCBRIDE, C. Phase behavior of attractive and repulsive ramp fluids: Integral equation and computer simulation studies,. *J. Chem. Phys.*, v. 126, p. 244510, 2007. [67](#)
- [132] CHATTERJEE, S.; ASHBAUGH, H. S.; DEBENEDETTI, P. G. Effects of nonpolar solutes on the thermodynamic response functions of aqueous mixtures. *J Chem Phys.*, p. 164503, 2005. [70](#)
- [133] SUBRAMANIAN, D.; KLAUDA, J. B.; LEYS, J.; ANISIMOV, M. A. Thermodynamic anomalies and structural fluctuations in aqueous solutions of tertiary butyl alcohol. *Vestn. S.-Peterb. Univ., Ser. 4: Fiz., Khim.*, v. 4, p. 140 – 153, 2013. [73](#), [74](#)
- [134] MIJAKOVIĆ, M.; POLOK, K. D.; KEŽIĆ, B.; SOKOLIĆ, F.; PERERA, A.; ZORANIĆ, L. A comparison of force fields for ethanol–water mixtures. *Molecular Simulation*, 2014. [73](#), [74](#)
- [135] BERG, B. A.; MUGURUMA, C.; OKAMOTO, Y. Residual entropy of ordinary ice from multicanonical simulations. *Phys. Rev. B*, v. 75, p. 092202, Mar 2007. [80](#), [81](#)